MUTANT LUGDUNIN AND THEIR GNP CONJUGATES: SYNTHESES AND ITS APPLICATION

BY

NATTAMON TRIRATTANAPORN

A THESIS SUBMITTED IN PARTIAL FULFILLMENT OF
THE REQUIREMENTS FOR THE DEGREE OF
MASTER OF SCIENCE (CHEMISTRY)
DEPARTMENT OF CHEMISTRY
FACULTY OF SCIENCE AND TECHNOLOGY
THAMMASAT UNIVERSITY
ACADEMIC YEAR 2023

MUTANT LUGDUNIN AND THEIR GNP CONJUGATES: SYNTHESES AND ITS APPLICATION

BY

NATTAMON TRIRATTANAPORN

A THESIS SUBMITTED IN PARTIAL FULFILLMENT OF
THE REQUIREMENTS FOR THE DEGREE OF
MASTER OF SCIENCE (CHEMISTRY)
DEPARTMENT OF CHEMISTRY
FACULTY OF SCIENCE AND TECHNOLOGY
THAMMASAT UNIVERSITY
ACADEMIC YEAR 2023

THAMMASAT UNIVERSITY
FACULTY OF SCIENCE AND TECHNOLOGY

THESIS

BY

NATTAMON TRIRATTANAPORN

ENTITLED

MUTANT LUGDUNIN AND THEIR GNP CONJUGATES: SYNTHESES AND ITS APPLICATION

was approved as partial fulfillment of the requirements for
the degree of Master of Science (Chemistry)

on December 7, 2023

Chairman _____
(Assistant Professor Jiraporn Arunpanichlert, Ph.D.)

Member and Advisor _____
(Assistant Professor Panumart Thongyoo, Ph.D.)

Member Dumrongkiet Arthan
(Associate Professor Dumrongkiet Arthan, Ph.D.)

Dean _____
(Associate Professor Supet Jirakajohnkool, Ph.D.)

Thesis Title	MUTANT LUGDUNIN AND THEIR GNP CONJUGATES: SYNTHESES AND ITS APPLICATION
Author	Nattamon Trirattanaporn
Degree	Master of Science (Chemistry)
Department/Faculty/University	Chemistry Faculty of Science and Technology Thammasat University
Thesis Advisor	Assistant Professor Panumart Thongyoo Ph.D.
Academic Year	2023

ABSTRACT

The emergence of drug resistant bacteria has now become a serious issue, affecting human health globally. The discovery of novel therapeutic alternatives is urgently necessary. This research represented the exploration of novel strategy to fight against drug resistant bacteria strains by utilizing “Lugdunin” as a promising lead candidate. Lugdunin is a recently isolated novel cyclic peptide, showing highly effective antibacterial activity against methicillin-resistant *Staphylococcus aureus* (MRSA). To this work, two synthetic strategies have been proposed; namely (1) the uses of gold nanoparticle (GNPs) conjugation with thiol-incorporated peptides (both linear and cyclic motifs) derived from lugdunin, (2) syntheses of hybrid lugdunin. Firstly, the design of GNPs-lugdunin conjugates is mainly based on the intrinsic property of GNPs and lugdunin, particularly anti-bacterial activity and its hydrophobic property.

Basically, GNPs demonstrated anti-bacterial activity against both gram-positive and gram-negative bacteria and multidrug-resistant strains. To this work, we proposed the functionalization of gold nanoparticles (GNPs) with thiol-incorporated peptides derived from the lugdunin in order to enhance their potentials as anti-microbial agents. Thiol-incorporated peptides were designed based on the lugdunin scaffold, which covalently bonded with GNPs to afford thiol-incorporated peptides-GNP conjugates. Subsequently, thiol-incorporated peptides-GNP conjugates was further

analyzed by scanning electron microscopy (SEM), showing the average sizes of 134 and 48 nm of linear and cyclic thiol incorporated peptides-GNPs, respectively.

Furthermore, chemical interactions between thiol-incorporated peptides and GNPs *via* Au-S bond were also confirmed by using infrared and X-ray photoelectron spectroscopy (XPS). To determine the loading capacity, UV-Vis spectroscopy was used to evaluate the loading capacity of a thiol-incorporated peptide-GNPs, showing the loading capacities of approximately 77% and 79% for linear and cyclic thiol- incorporated peptide-GNPs, respectively.

The occurrence of drug-resistant *plasmodium* parasites has caused a significant number of deaths annually. To appropriately address the resistance of *plasmodium* parasites, there is a critical need for the discovery of new and effective anti-malarial drugs. Herein, we reported the design and syntheses of re-engineered mortiamide peptides based on the combination of mortiamide A and lugdunin scaffold, consisting of seven amino acid residues with linear and cyclic scaffold. Mortiamide A and lugdunin are generally isolated from *Mortierella sp*. and *Staphylococcus lugdunensis*, respectively. To this synthetic strategy, the sequence of mortiamide A was partly re-engineered with an epitope sequence of lugdunin together with an amino acid replacement by using L-configuration at Phe^{1}, Val^{3}, Val^{4}, Val^{5} and Val^{7} residues. This synthetic approach was carried out *via* Fmoc based SPPS, giving linear and cyclic re-engineered mortiamides (**9**-**12**) in a great yield (>60%). Notably, re-engineered cyclic mortiamide with all-L (**11**) and D/L configuration (**12**) showed very promising anti-malarial activities against *Plasmodium falciparum* sensitive strain (TM4/8) with IC_{50} values of 6.25±0.52 μM, 4.83±0.10 μM and against *Plasmodium falciparum* multidrug resistant strain (V1/S) with IC_{50} values of 5.04±2.60 μM, and 3.75±0.70 μM, respectively. Interestingly, a linear re-engineered mortiamide with D/L configuration (**10**) not only demonstrated a very potent anti-malarial activity against *Plasmodium falciparum* sensitive strain (TM4/8) with IC_{50} value of 3.57±0.52 μM, but it also showed a very promising inhibition against *Plasmodium falciparum* multidrug resistant strain (V1/S) with an IC_{50} value of 2.81±0.70 μM with low cytotoxicity (>50 μM).

(3)

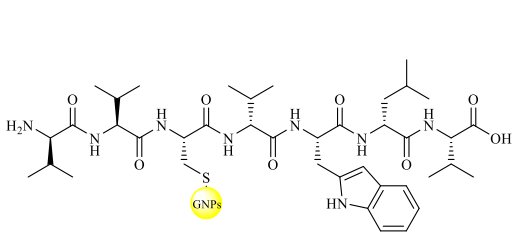

6

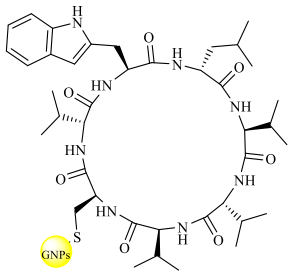

8

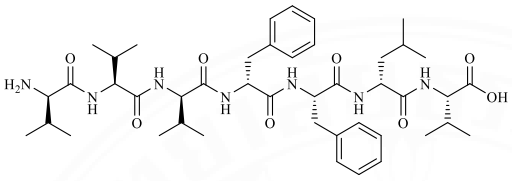

10

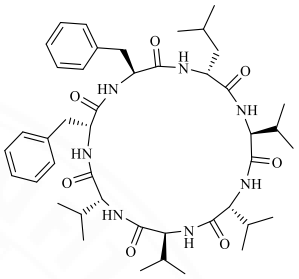

12

Chemical structures of linear and cyclic thiol-incorporated peptides-GNPs conjugates (**6** and **8**) and linear and cyclic re-engineered mortiamide (**10** and **12**)

Keywords: Lugdunin, Mortiamide, Malaria, Macrocyclic peptide

ACKNOWLEDGEMENTS

I am deeply grateful to my advisor, Assistant Professor Dr. Panumart Thongyoo, Department of Chemistry, Faculty of Science and Technology, Thammasat University, for providing valuable advice, encouragement, and support throughout my studies.

I also extend my sincere appreciation to Assistant Professor Dr. Dumrongkiet Arthan and Dr. Dusit Promrug, Department of Tropical Nutrition and Food Science, Faculty of Tropical Medical, Mahidol University, for their support.

Besides my advisor, sincere thanks would like to extent to my thesis committee to Assistant Professor Dr. Jiraporn Arunpanichlert, Department of Chemistry, Faculty of Science and Technology, Thammasat University, and Assistant Professor Dr. Dumrongkiet Arthan, Department of Tropical Nutrition and Food Science, Faculty of Tropical Medical, Mahidol University, for their valuable suggestions and generous advice.

I would like to thank the Medical Chemistry Research Unit, Thammasat University members, for their support and kindness.

Additionally, I am truly grateful for the scholarship for talented students to study the graduate program in the Faculty of Science and Technology, Thammasat University, contract NO. TB 21/2019.

Lastly, my sincere thanks to my family for their unwavering support and encouragement throughout the challenges faced during this research. I am also thankful to my friends, who were always willing to listen to my problems and provided motivation during difficult times in my studies. This work would not have been possible without the collective contribution of everyone involved. Thank you.

Nattamon Trirattanaporn

TABLE OF CONTENTS

LIST OF TABLES

LIST OF FIGURES

LIST OF SCHEMES

LIST OF ABBREVIATIONS

Symbols/Abbreviations	Terms
α	Alpha
β	Beta
δ	Chemical shift (ppm)
μM	Micromolar
Abs.	Absorbance
ACN	Acetonitrile
BOC	*Tert*-butyloxycarbonyl
CD	Circular dichroism
COSY	Homonuclear correlation spectroscopy
Cys	Cysteine
DCC	*N,N'*-dicyclohexylcarbodiimide
DCM	Dichloromethane
DIPEA	*N,N'*-Diisopropylethylamine
DMAP	4-Dimethylaminopyridine
DMF	Dimethylformamide
E. coli	*Escherichia coli*
EDT	Ethane-1,2-dithiol
EDS	Energy-dispersive X-ray spectroscopy
ESI-Q-TOF MS/MS	Electrospray ionization quadrupole time-of-flight mass spectrometry
Fmoc	9-Fluorenylmethyloxycarbonyl
FTIR	Fourier-transform infrared spectroscopy
HATU	1-[Bis(dimethylamino)methylene]-1H-1,2,3-triazolo[4,5-b]pyridinium 3-oxide hexafluorophosphate
HMBC	Heteronuclear multiple bond correlation
HOBt	1-Hydroxybenzotriazole

Symbols/Abbreviations	Terms
HPLC	High-performance liquid chromatography
HSQC	Heteronuclear single quantum correlation
IC_{50}	Half-maximal inhibitory concentration
Int.	Intensity
KB cell	Keratin-forming tumor cell line
LC-MS	Liquid chromatography mass spectroscopy
Leu	Leucine
MeOH	Methanol
mg	Milligram
MIC	Minimum inhibitory concentration
MRSA	Methicillin-resistance *Staphylococcus*
MS	Mass spectroscopy
NMR spectroscopy	Nuclear magnetic resonance spectroscopy
P. falciparum	*Plasmodium falciparum*
Phe	Phenylalanine
SEM	Scanning electron microscope
SPPS	Solid phase peptide synthesis
TFA	Trifluoroacetic acid
TIS	Triisopropylsilane
t_r	Retention time
Trp	Tryptophan
Trt	Triphenylmethane
UV-vis spectroscopy	Ultraviolet visible spectroscopy
Val	Valine
VRE	Vancomycin-resistance *enterococci*
XPS	X-ray photoelectron spectroscopy

CHAPTER 1
INTRODUCTION

1.1 Antimicrobial resistance (AMR)

Antibiotics are widely recognized as chemotherapeutic agents, playing a vital role for the treatment of bacterial infection. Its potent efficacy is regarded as robust tools in the clinical management of bacterial diseases. The discovery of the antibiotics, particularly sulfonamides, marked a significant milestone. However, the development of specific mechanism of resistance has posed challenges to its therapeutic efficacy. Particularly, the discovery of penicillin by Alexander Fleming in 1928 and streptomycin in 1943, marked the initiation of the antibiotic's era. Penicillin is a novel antibiotic, saving innumerable lives by combatting bacterial infections, most notably those caused by *Staphylococcus* and *Streptococci*.

Nonetheless, instances of penicillin resistance began to surface in the 1950s, representing a serious clinical concern about bacterial resistance of β-lactam antibiotics. It was, in 1962 (United Kingdom) and 1968 (United States) that the first case of methicillin-resistant *Staphylococcus aureus* emerged. To combat methicillin-resistant *Staphylococcus aureus* and coagulase-negative *Streptococci* infections, vancomycin was introduced into clinical in 1972.(Bisht, Katiyar, Singh, & Mittal, 2009; Ventola, 2015) Unfortunately, instances of vancomycin resistance were surfaced and initially reported in coagulase-negative *Streptococci* in 1979 and 1983. Since the 1980s, various pharmaceutical enterprises have undertaken initiatives to develop new antibiotic drugs in response to the antibiotic resistance crises, aiming to save human lives over the globe.(Ventola, 2015)

Presently, over 700,000 people individuals globally succumb to illnesses caused by bacteria that have developed antimicrobial resistance (AMR) annually. The World Health Organization (WHO) suggests that if this problem trends to continue, it could claim the lives of 10 million people annually by 2050, exceeding the number of people died from diabetes, tuberculosis, and HIV/AIDS altogether.(Holmberg, Solomon, & Blake, 1987)

1.2 Antimicrobial peptides (AMPs)

Antimicrobial peptides (AMPs) are widely known as a highly promising class of agents with the great capability to inhibit pathogen growth effectively with low risk of resistance. According to its broad-spectrum activity, great potential in overcome drug resistance, including its influence against immune responses, AMPs have attracted of great interest for the discovery of novel AMPs in the fight against pathogens.(Huan, Kong, Mou, & Yi, 2020) AMPs are generally isolated from microorganisms, particularly bacteria and fungi which are recognized as the great natural antibiotics. In addition, AMPs have been discovered to possess a diverse range of biological roles(Mookherjee, Anderson, Haagsman, & Davidson, 2020), namely drosocin, pyrrhocoricin and lugdunin, encompassing immune regulation(Roudi, Syn, & Roudbary, 2017), facilitating of wound healing(Pfalzgraff, Brandenburg, & Weindl, 2018), and exerting of anti-tumor activity. The approach of treating pathogenic bacterial infections has long been primarily reliant on effective antibiotics. However, the rise of drug resistance, attributed to the narrow focus of antibiotics on a single target, prolonged usage, and widespread application, has emerged as a significant obstacle in the field of clinical infection control. In contrast, AMPs offer distinct advantages by engaging multiple targets on both the plasma membrane and intracellular sites of pathogenic bacteria.(Chung & Khanum, 2017; Mwangi, Hao, Lai, & Zhang, 2019) This comprehensive approach confers the potent efficacy even against drug-resistant bacterial strains. Consequently, AMPs present a novel and viable alternative to conventional antibiotic treatment strategies.

1.3 Lugdunin

Lugdunin, a novel antibiotic consisting of thiazolidine-containing macrocyclic peptide with a head-to-tail cyclization of six amino acids. It was isolated from *Staphylococcus lugdunensis*, bacterium identified within human nasal. This discovery represents a rare occurrence of a bioactive compound synthesized through non-ribosomal processes in bacteria associated with humans. Lugdunin has demonstrated a potent antibacterial efficacy against a range of gram-positive bacteria,

most notably including methicillin-resistant *Staphylococcus aureus* (MRSA) and vancomycin-resistant *Enterococcus* (VRE), with MIC of 1.5-3 μg/mL and 3-12 μM, respectively. Notably, lugdunin does not extend its impact to the lysis of primary human neutrophils or erythrocytes. Furthermore, it has no discernible impact on the metabolic activity of the human monocytic cell line HL60 with an IC_{50}>50 μg/mL. The inhibition mechanism of lugdunin involves the disruption of bacterial energy sources by ceasing the incorporation of DNA, RNA, and cell wall precursors. This disruption leads to the break of bacterial cells, and become the evidence of potent anti-bacterial mechanism.(Zipperer et al., 2016)

Recently, great attempts have been devoted to synthesize lugdunin and its synthetic analogue, further including its stereochemical integrity; namely alanine and stereo scanning. Peptides modified thiazolidine rings have been successfully synthesized for structure-activity relationship studies, followed by investigating of its antimicrobial activity. Through these studies, Trp^3 and Leu^4 have been important residues, playing critical roles for the interaction with bacterial cell membranes, as confirmed through the synthetic poly-(Trp-Leu)-octapeptides, showing of ability to disrupt bacterial cell membranes. Intriguingly, alterations in the D and L-amino acid backbone did not impede the lugdunin activity.(Schilling et al., 2019)

More recently, a comprehensive SAR analysis has centered at three key lugdunin residues; D-Val^2, L-Trp^3 and D-Leu^4. The findings revealed that D-Val^2 and D-Leu^4 were reasonably tolerated within the bioactive lugdunin structure, with higher non-polarity groups significantly enhancing its biological activity. Notably, the hydrophobic aromaticity of L-Trp3 is emerged as vital roles for membrane insertion and penetration processes, especially within the interfacial layer of the membrane.(Saur et al., 2021)

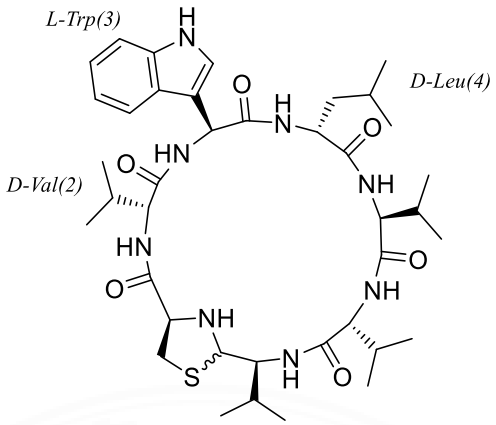

Figure 1.1 Chemical structure of lugdunin

1.4 Gold nanoparticles (GNPs) to combat antimicrobial resistance

1.4.1 Gold nanoparticles (GNPs)

Metal nanoparticles, particularly gold nanoparticles (GNPs), exhibit a broad spectrum of intrinsic properties, namely, a great biocompatibility applicable for using as carriers for drug delivery, cancer radiotherapy and antimicrobial activities. In the early 1950s, Turkevich developed the synthetic method of GNPs(Turkevich, Stevenson, & Hillier, 1951), involving the reduction of hydrogen tetrachloroaurate (III) in water by using trisodium citrate as a reducing agent. GNPs exhibit a unique physical, chemical and optical properties, which could be ascribed as the results of their small dimensions and high surface-to-volume ratio. A noteworthy aspect is their localized surface plasmon resonance (SPR), involving the excitation of an electron on the gold surface by a photon possessing a specific wavelength.(Bai et al., 2020) Additionally, the specific wavelength is intricately linked to GNPs characteristics; such as size, shape, surface, and agglomeration. The aggregation of GNPs results in significant changes, including a red-shift in the SPR frequency, broadening of the surface plasmon band, and the transformation of the color from red to blue due to the coupling of interparticle plasmons.(Su et al., 2003) This aggregation-induced absorption shift facilitates the detection of analytes and quenching of fluorescence intensity. These characteristics have found extensive applications in various areas, including diagnostics, tumor treatment, and cellular imaging.

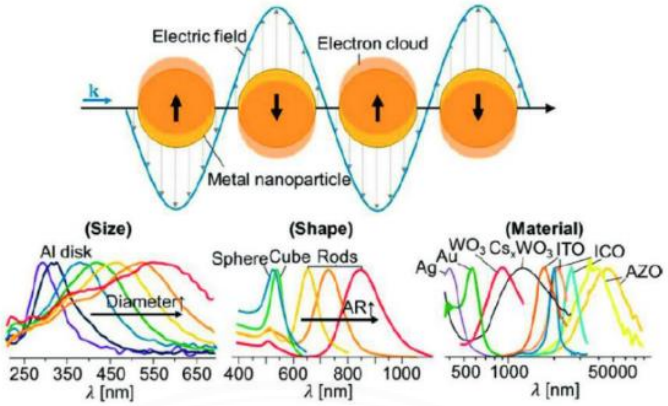

Figure 1.2 Shape, size and agglomeration effect on the refractive index sensitivity at LSPR(Jeong, 2017)

1.4.2 Co-functionalization of GNPs with peptides

The misuse and insufficient utilization of antibiotics constitute significant contributors to the issue of antibiotic resistance.(Jia et al., 2019) One viable approach to mitigate antibiotic misuse and to enhance their effectiveness of antibiotics has been the utilization of structured formations with adaptable antibacterial properties.(Tang, Zhang, Yang, Zheng, & Jiang, 2020) The application of GNPs based mainly on their optical and physicochemical properties has widely expanded within medical field, particularly for improving antibiotics loading to facilitate the internalization of antibiotics. The GNPs can be readily bio-conjugated, facilitating its functionalization with a variety of peptides consisting of thiols, amines, and even phosphine moieties.(Zong, Cobb, & Cameron, 2017) Moreover, GNPs exhibit an ability to interact with lipopolysaccharides (LPS) and proteins presenting at the outer membrane of bacteria, leading to its deposition at the membrane surface.(Verma et al., 2008) Then, these deposited GNPs are subsequently permeated the bacterial membrane by traversing the phospholipid bilayer. This penetration process facilitates enhanced interactions with therapeutic agents, namely antimicrobial peptides. In particular, when these peptides are conjugated to the GNPs. The resulting conjugated peptides with GNPs amplifies its activity compared to their non-conjugated counterparts. Notably, the conjugation of peptides with GNPs has demonstrated increased stability and

heightened its biological activity, surpassing the effectiveness of either antimicrobial peptides or GNPs considered individually.(Pal et al., 2016)

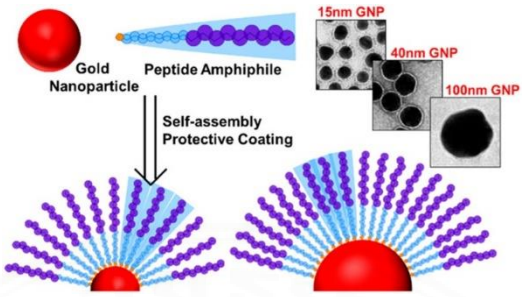

Figure 1.3 The functionalization of gold nanoparticles (GNPs) with peptide moieties(Egorova et al., 2020)

1.5 Malaria

To date, Malaria is extensively recognized as a severe global health concern, particularly impacting populations in developing countries. In 2021, the World Health Organization (WHO) reported 249 million cases of malaria, resulting in 619,000 human fatalities. Particularly, children under the age of five and people from the African subcontinent represent most patients suffering from mosquito-borne diseases like malaria. Typically, five *Plasmodium* parasite species (*P.falciparum, P.malariae, P.vivax, P.ovale* and *P. knowles*) cause malaria in humans in which *P.falciparum,* and *P. vivax* are among the most important *Plasmodium* parasite strains responsible for about half a million deaths annually. Additionally, morbidity and mortality have significantly increased along with the prevalence of infections caused by MDR *Plasmodium* parasite.(Desselberger, 2000) The overuse and misuse of current anti-malarial drugs have greatly promoted the evolution of resistant *Plasmodium* parasites, giving rise of multiple mutations in the transmembrane proteins. This would effectively reduce the accumulation of anti-malarial drugs in its digestive vacuole. The emergence of *Plasmodium* parasite resistance against approved drugs has dramatically increased in the last decades.

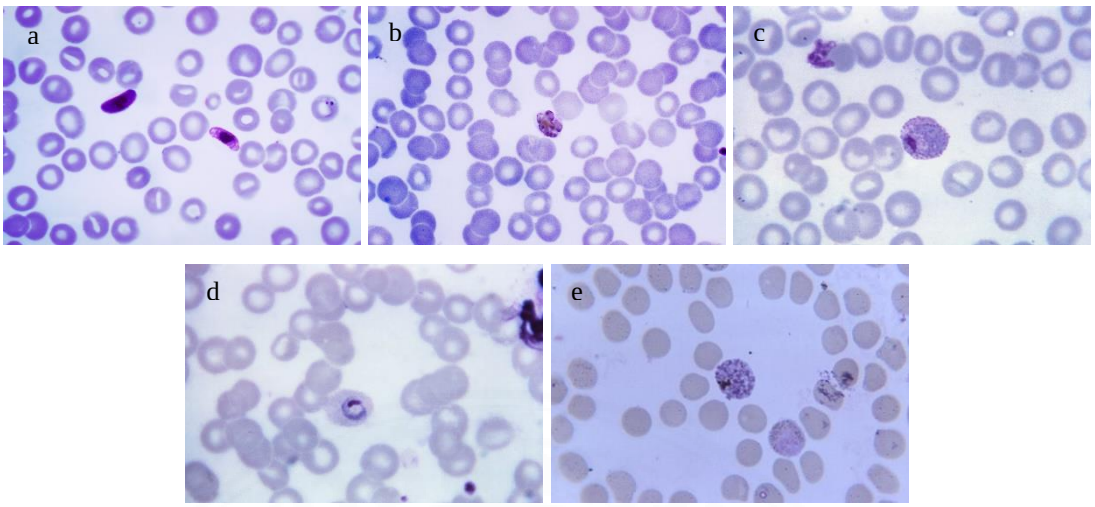

Figure 1.4 This photomicrograph of five *Plasmodium* parasite *Plasmodium* parasite (a) *P.falciparum*, (b) *P.malariae*, (c) *P.vivax*, (d) *P.ovale* and *P. Knowles*

1.6 Mortiamide A-D

In 2017, Alyssa L. Grunwald discovered a novel new class of cyclic heptapeptides with the great anti-malarial activity, denoted as mortiamide A-D. These compounds were firstly isolated from a novel *Mortierella* sp. from marine sediment collected in the intertidal zone of Frobisher Bay, Nunavut, Canada. The structures of mortiamides are cyclic peptides, comprising seven hydrophobic amino acids, five of which consist D-configuration. Mortiamide A-D displayed a negligible efficacy against methicillin-resistance *Staphylococcus aureus*, vancomycin-resistance *Enterococcus faecium*, *Staphylococcus warneri*, *Pseudomonas aeruginosa* and *Candida albicans* or cytotoxicity against keratinocyte fibroblast, HTB-26 and MCF-7 breast cancer cell lines.(Grunwald, Berrue, Robertson, Overy, & Kerr, 2017)

In 2019, Christopher Berube reported the syntheses of mortiamide A-D, classified as a cyclic of heptapeptide. This synthetic procedure was mainly based on a solid support approach, giving the overall yield of up to 48%. Importantly, it demonstrated inhibitory effects against the proliferation of *Plasmodium falciparum* strains 3D7 and Dd2. Mortiamide A, B and D displayed IC_{50} values of 1.31-7.85 µM and 0.94-5.31 µM against the 3D7 and Dd2 strains, respectively. Furthermore, the

observed growth inhibition was not attributed to the lysis of red blood cells. This findings indicated that only mortiamide D induced a mild effect of red blood cell lyses of 19.7% at 25.6 μM and reduced to 4.4% at 12.8 μM compared to the control sample.(Bérubé, Gagnon, Borgia, Richard, & Voyer, 2019)

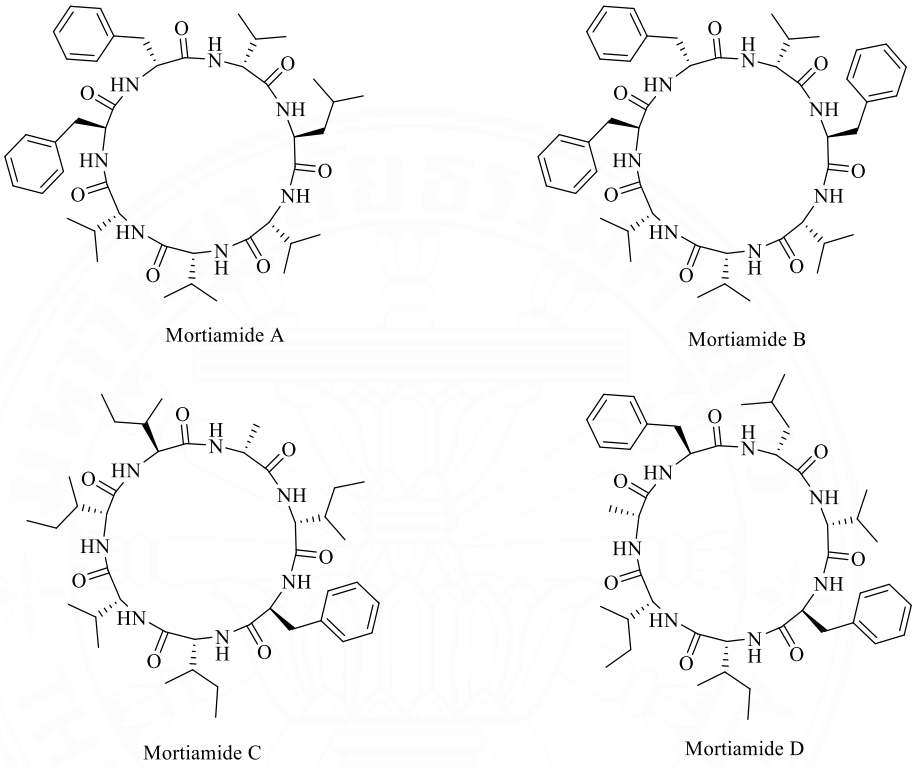

Figure 1.5 Structure of mortiamide A-D natural products that isolated form *Mortierella* sp.

1.7 Objectives

1. To design and to synthesize thiol-incorporated and re-engineered mortiamide peptides.

2. To conjugate thiol-incorporated peptides with GNPs and subsequently to characterize by UV-Visible, Fluorescence, Fourier transform infrared (FTIR), X-ray photoelectron (XPS) spectroscopy, and scanning electron microscopy (SEM).

3. To investigate the biological activity against a panel of bacteria (superbugs), including anti-malaria activity against both *Plasmodium falciparum*

sensitive strain (TM4/8) and *Plasmodium falciparum* multidrug-resistant strain (V1/S), including against *Mycobacterium tuberculosis* (MTB).

CHAPTER 2
REVIEW OF LITERATURE

2.1 Peptide synthesis

Peptide synthesis involves the strategic formation of amide bonds that connect individual amino acids, resulting in the assembly of peptide sequences. The first step involves activating the carboxyl group enable to improve coupling efficiency, following by the nucleophilic attack by the amino group of an amino acid counterpart onto an activated carboxylic group, resulting in the formation of a peptide bond, as depicted in **Scheme 2.1**.(Al-Warhi, Al-Hazimi, & El-Faham, 2012)

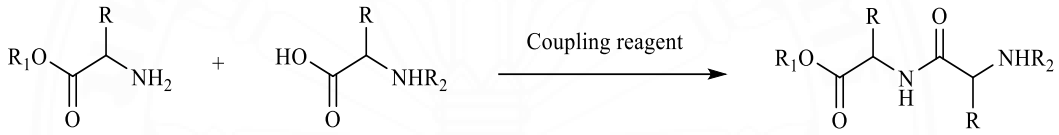

Scheme 2.1 Peptide bond formation

2.1.1 Coupling reagents

In SPPS, coupling reagents play an important role by facilitating the formation of peptide bonds between each of amino acids. The coupling reagents are widely employed in SPPS in order to enhance the reactivity of carboxyl groups, promoting the efficacy of peptide bond formation. These coupling reagents can be categorized into three groups: carbodiimides, phosphonium salt, and ammonium/uranium salts.(El-Faham & Albericio, 2011)

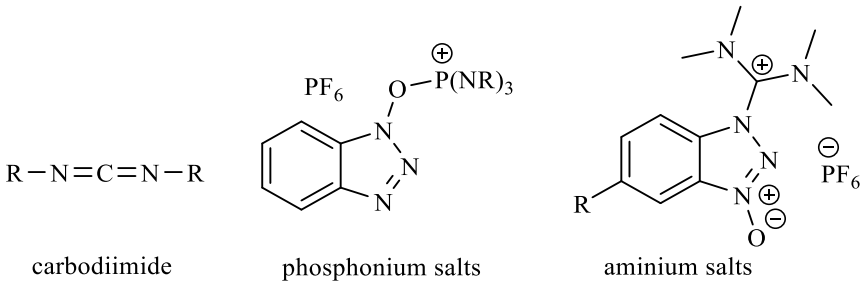

Figure 2.1 Three groups of coupling reagent

2.1.1.1 Carbodiimides

Carbodiimides are widely employed as coupling reagents in the peptide synthesis due to its effectiveness for activating carboxyl groups and promoting peptide bond formation. The commonly used carbodiimides are known, such as *N*,*N*'-diisopropylcarbodiimide (DIC), *N*,*N*'-dicyclohexylcarbodiimide (DCC), and *N*-(3-dimethylaminopropyl)-*N*'-ethylcarbodiimide (EDC). The chemical structure of these carbodiimides are shown in **Figure 2.2**.

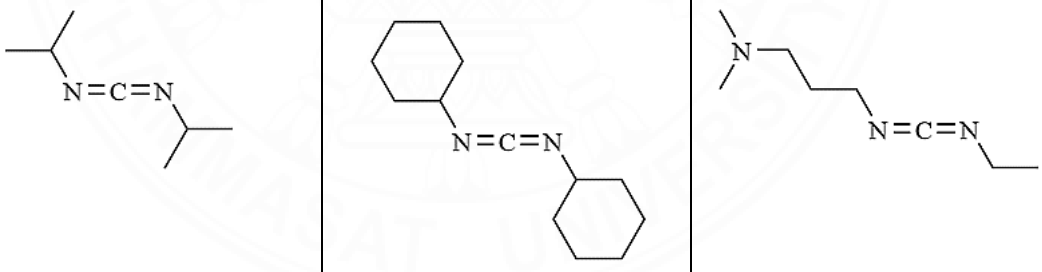

DIC	DCC	EDC

Figure 2.2 The chemical structure of DIC, DCC, and EDC

2.1.1.2 Phosphonium salts

Phosphonium salts, such as benzotriazol-l-yloxytris(dimethyl lamino)phosphonium hexafluorophosphate (BOP), benzotriazol-l-yloxytris(pyrorolidi no)phosphonium hexafluorophosphate (PyBOP), 7-(azabenzotriazol-1-yl)oxytris(dime thyllamino)phosphonium hexafluorophosphate (AOP), [(7-azabenzotriazol-1-yl)oxy]

tris(pyrrolidino)phosphonium hexafluorophosphate (PyAOP), are examples of phosphorus based coupling reagents. These compounds are commonly used in peptide synthesis and demonstrate high reactivity compared to those of carbodiimides.

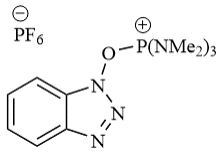	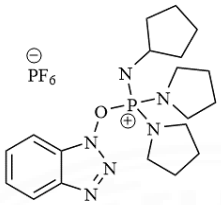	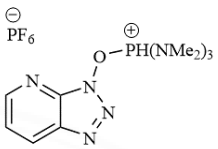	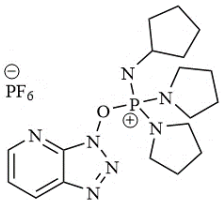
BOP	PyBOP	AOP	PyAOP

Figure 2.3 The chemical structure of BOP, PyBOP, AOP, and PyAOP

2.1.1.3 Aminium/uranium salts

Aminium/uranium salts are recognized for their efficiency, mild reaction conditions, and ability to minimize racemization during the formation of peptide bonds. The commonly used aminium/uranium salts are known; such as 1-[Bis(dimethylamino)methylene]-1H-1,2,3-triazolo[4,5-bipyrinidium-3-oxide hexafluorophosphate (HATU), (2-(1H-benzotriazol-l-yl)-1,1,3,3-tetramethyluronium hexafluorophosphate (HBTU) and 1-[Bis(dimethylamino)methylene]-5-chlorobenzotriazolium-3-oxide hexafluorophosphate (HCTU). The chemical structure of these aminium/uranium are shown in **Figure 2.4**.

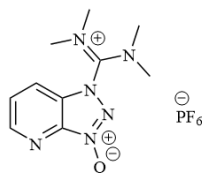	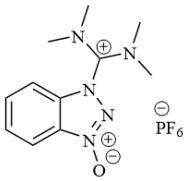	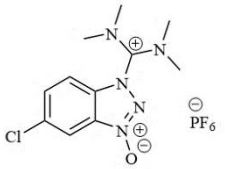
HATU	HBTU	HCTU

Figure 2.4 The chemical structure of HATU, HBTU, and HCTU

Furthermore, some additives were introduced in the peptide synthesis, serving as an activator, enhancing the coupling efficiency while also minimizing racemization. Examples of some additives include N-hydroxysuccinimide (HOSu), 1-hydroxylbenzotriazole (HOBt), 7-aza-1-hydroxybenzotriazole (HOAt) and 4-dimethylaminopyridine (DMAP) as depicted in **Figure 2.5**.

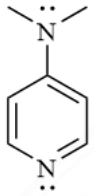	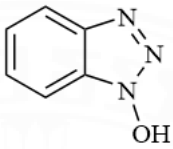	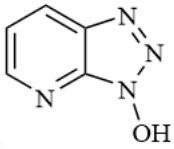
DMAP	HOBt	HOAt

Figure 2.5 The chemical structure of DMAP, HOBt, and HOAt

2.1.2 Solid phase peptide synthesis (SPPS)

In the early 1960s, Merrifield introduced the novel approach involving a polystyrene-based solid support for the peptide synthesis. This approach enabled the sequential assembly of peptides from the C to N terminus by N_{α}-protected amino acids. Subsequently, in 1970, Carpino introduced the 9-Fluorenylmethoxycarbonyl (Fmoc) group as an N_{α}-protection agent. The Fmoc group, distinct for its requirement of a basic condition for deprotection, presented a chemically gentle alternative to the acid-sensitive Boc-group.(Stawikowski & Fields, 2012) This method significantly influenced the subsequent advancements in peptide synthesis. Presently, SPPS has emerged as the standard approach for peptide and protein synthesis. SPPS provides notable advantages over solution-based synthesis, as coupling reactions can be conducted with greater speed, efficiency, and easy to remove unreacted amino acid through simple washing.

The solid phase peptide synthesis (SPPS) is a process encompassing three important steps; (1) first amino acid loading, (2) assembly of amino acids, and (3) cleavage of the peptide chain.

2.1.2.1 First amino acid loading

The initiation of the peptide synthesis process through the loading of the first amino acid is highly important in SPPS, as it directly affects the overall yield as shown in **Scheme 2.1**.

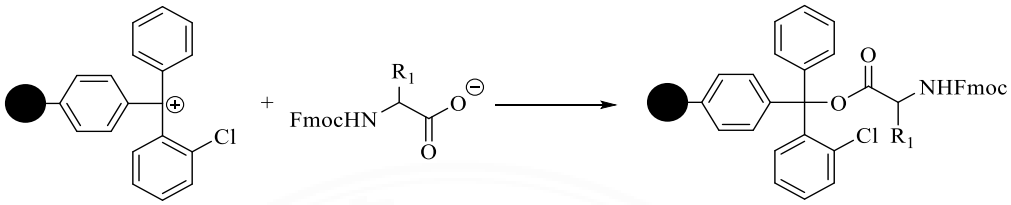

Scheme 2.2 The first amino acid attachment on 2-chlorotrityl chloride resin

2.1.2.2 An amino acid assembly

To this step, the process of amino acid assembly is of most significance. This procedure encompasses the sequential integration of individual amino acids to systematically construct the peptide chain as shown in **Scheme 2.3**. Through a step-by-step approach, protected amino acids are coupled onto the elongating peptide chain, resulting in the formation of the desired peptide sequence.

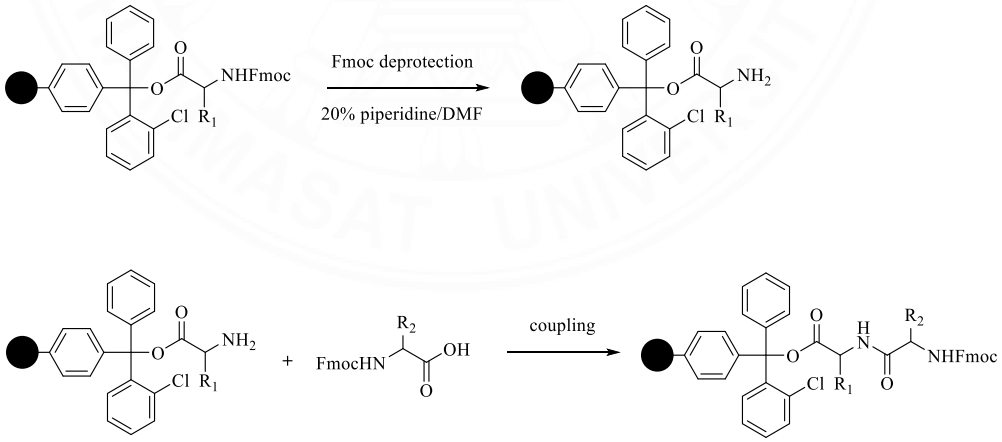

Scheme 2.3 The amino acid assembly process

2.1.2.3 Peptide chain cleavage

After completion of amino acid assembly, the peptide chain was cleaved by using a resin specific-deprotection cocktail. For example, the cleavage of the 2-chlorotrityl chloride resin was achieved using a 1% TFA in DCM, releasing the fully protected peptide chain as illustrated **Scheme 2.4**.

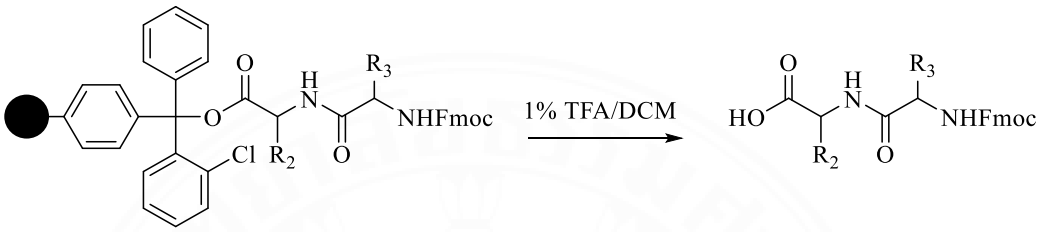

Scheme 2.4 The peptide chain cleavage from 2-chlorotrityl chloride resin

2.2 The peptide-GNPs conjugate

The conjugation of peptides with gold nanoparticles (GNPs) presents numerous attributes that provide this hybrid material promising for various applications. The advantage of peptide-GNPs conjugates is enhanced antimicrobial activity, a broad spectrum of biological activity, target delivery, and diagnostic applications.

2.2.1 Cellular imaging and colorimetric detection

Alexander G. Tkachenko and coworkers reported the peptide-modified gold nanoparticle for intracellular delivery of therapeutic agents and imaging probes. The investigation involved the synthesis of modified gold nanoparticles using nuclear localization peptides derived from three distinct peptides terminated with cysteine (SV40 large T NLS, HIV-1 Tat protein NLS, and adenoviral NLS) and evaluated their subcellular distribution in HeLa, 3T3/NIH and HepG2 cells. The nanoparticle transportation into the cytoplasm and nucleus was found on the specific peptide sequences. As seen in **Figure 2.6**, it was a phenomenon potentially observable through video-enhanced color differential interference contrast and transmission

electron microscopy methods.(A. Tkachenko, Xie, Franzen, & Feldheim, 2005; A. G. Tkachenko et al., 2004)

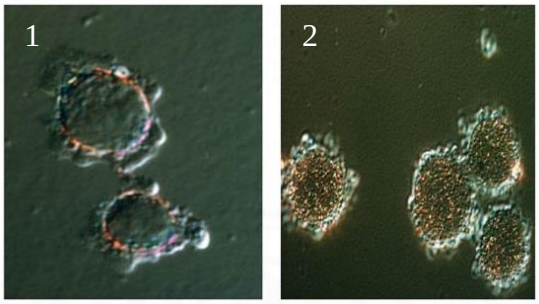

Figure 2.6 Incubation of HeLa cells with 20 nm gold nanoparticles after 3 h by video enhanced color differential interference contrast microscopy; (1) gold nanoparticle carrying Large T NLS accumulated around nuclear membrane (2) gold nanoparticle carrying adenovirus NLS accumulated inside nucleus

Hiroshi Tsutsumi and co-workers studied the development of GNPs conjugated with monosaccharide-modified peptides serving as optical probes for detection of lectins, molecules crucial for cell adhesion, signaling, and disease progression. The mannose-modified peptide, these results exhibited an absorption shift to longer wavelengths (from 534 nm to 620 nm) upon interaction with concanavalin A (ConA) neighboring particles. This interaction-induced change was visually observable as a transition in color from red to violet under the naked eye as shown in **Figure 2.7**. The aggregation of the gold nanoparticles was assessed on hydrophobic amino acid residues, effectively enhancing the binding affinity and selectivity for detecting the lectin.(Tsutsumi et al., 2012)

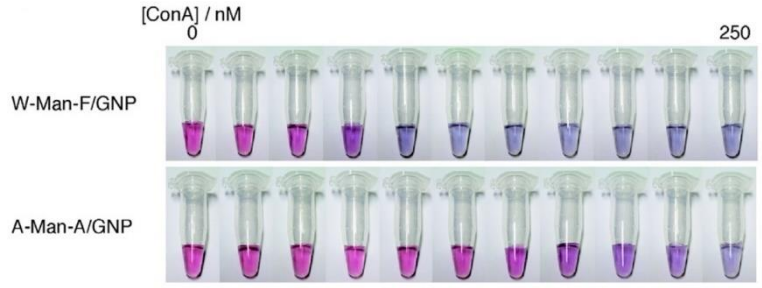

Figure 2.7 Photographs of Ac-WAE(Man)AF-$(aeea)_2$-C-NH_2/GNP (W-Man-F/GNP) and Ac-AAE(Gal)AA-$(aeea)_2$-C-NH_2 (A-Man-A/GNP) solutions in the presence of ConA with different concentration

Wei-Chen and coworkers devised and subsequently synthesized a novel of multifunctional AuNPs by incorporating a peptide sequence, Asp-Glu-Val-Asp (DEVD). This design aimed to induce apoptosis in cancer cells and enable real-time apoptosis monitoring through the incorporation of rhodamine B (RB) as a red fluorescence marker. In addition, the AuNPs were conjugated with dual-targeting pro-apoptotic peptide (DTP), which encompassed a folate moiety designed for cancer cell targeting, resulting in the formulation RB-DEVD-AuNP-DTP. The efficacy of RB-DEVD-AuNP-DTP demonstrated through its capacity to selectively target and eliminated cancer cells to induce the apoptosis of cancer cells.(W.-H. Chen et al., 2014)

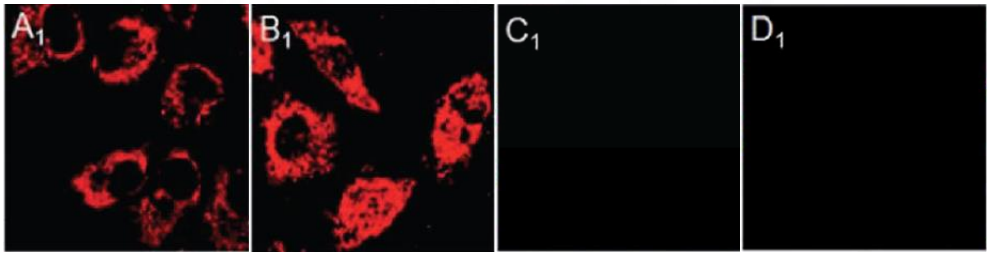

Figure 2.8 Confocal laser scanning microscopy (CLSM) images of KB cancer cells incubated with RB-DEVD-AuNP-DTP (A_1) 12 h (B_1) 24 h CLSM images of normal COS7 cells incubated with RB-DEVD-AuNP-DTP (C_1) 12 h and (D_1) 24 h

Qingyu Chen and coworkers reported a study involving the synthesis of a gold nanoconjugate referred to as Au@P937 NRs, wherein the peptide P937 was engineered using phage display biopanning technology and demonstrated a distinctive affinity for binding to bacterial targets. The resulting Au@P937 NRs exhibited a remarkable selectivity for bacterial detection, coupled with efficiency in achieving photothermal ablation of both gram-negative and gram-positive bacteria. The study revealed a detection limit of 46 cfumL^{-1} for *E. coli* and 89 cfumL^{-1} for *S. aureus*. Moreover, the spectra characteristics of Au@P937 NRs showed λ_{max} peak, slight red-shifted, and broaden bands which are evidence of a stronger interaction between Au@P937 NRs and bacteria compared to that of Au NRs. Impressively, under 808 nm laser irradiation, the Au@P937 NRs successfully abolished both *E. coli* and *S. aureus* within a 10-min. Notably, the Au@P937 NRs exhibited lower cytotoxicity in comparison to pure gold nanoparticles, demonstrating their potential as a promising for effective antimicrobial strategies.(Q. Chen et al., 2018)

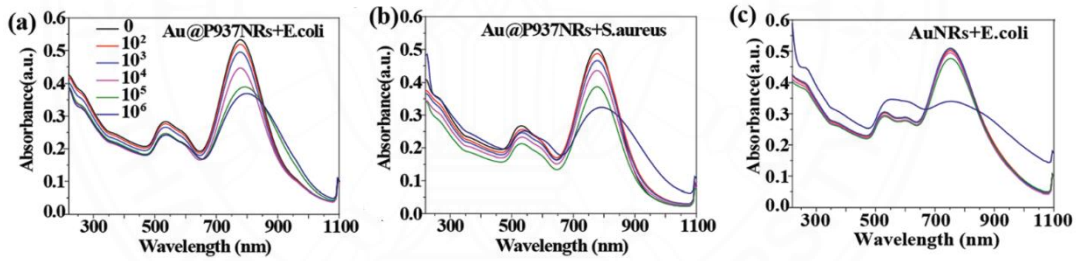

Figure 2.9 The UV-Vis spectra of the Au@P937 NRs mixed with *E. coli* (a) and *S. aureus* (b) and (c) Au NRs mixed with *E. coli* at different concentration

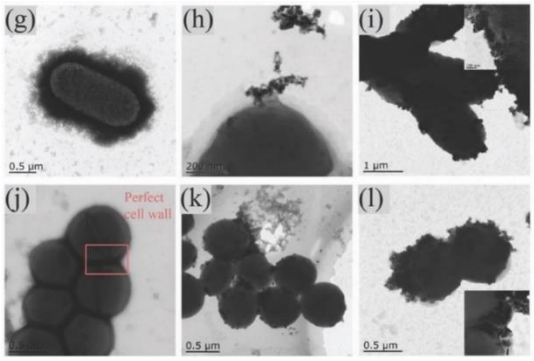

Figure 2.10 TEM images of (g) *E. coli* (h) *E. coli* incubated with Au NRs (i) Au@P937 NRs under NIR irradiation (j) *S. aureus* (k) *S. aureus* incubated with Au NRs and (l) Au@P937 NRs under NIR irradiation

2.2.2 Antimicrobial, antitumoral activities and cancer therapeutic

Ngoc Thi Thanh Tran and coworkers presented the synthesis peptides derived from the Rev peptide with varied sizes and shapes of GNPs, serving as potential applications in cancer therapy. In addition, cytotoxicity was observed towards the MOSEC cell line with 56.1% and 24.1% after 24 and 48 h of incubation, respectively. Furthermore, TEM images of MOSEC cells revealed the internalization of Rev-AuNPs. Interestingly, no Rev-AuNPs were detected within the cells after 0 h, while after 24 h, the AuNPs were localized within intracellular membrane-bound vesicles which was distinct from being freely distributed throughout the cytoplasm.(Tran et al., 2011)

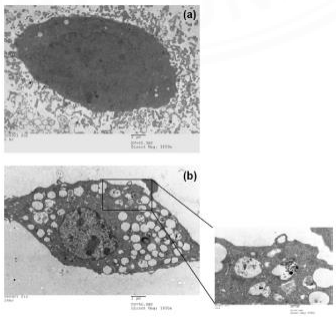

Figure 2.11 TEM images of MOSEC internalization of Rev-AuNPs after (a) 0 h and (b) 24 h

Sushma Kalmodia and co-workers reported their work involving the preparation, characterization, and functional effectiveness of GNP-HDM2 in retinoblastoma cells (RB cell). The results of GNP-HDM2 treatment on RB cells in *vitro* indicated a mechanism involving the capture of RB cells at the G2M phase of the cell cycle, subsequently initiating apoptosis. Furthermore, observing on the cellular internalization *via* TEM and hyperspectral imaging, combined with the phase of the cell cycle supported the initiating apoptosis. Furthermore, observation impact on the cell cycle and apoptosis suggested that the conjugates played a main role in enhancing the stability of the peptide. This enhancement was attributed to the prevention of peptides against protease degradation, thereby facilitating its efficient delivery into the cytosol.(Kalmodia et al., 2017)

David Limon and coworkers conducted a study by synthesizing the cyclic peptide BPC734, possessing an anti-cancer activity and coupled with water-soluble gold nanoparticles. A notable observation was that the attachment of peptide BPC732 to gold nanoparticles resulted in enhanced effectiveness against cancer cells, particularly HT29 cells. Moreover, when peptide BPC734 was in a solution, it exhibited toxicity towards BJ cells, with a cell viability rate of 84.3% at a concentration of 100 µM. In contrast, the combination of GNP.OH/BPC734 displayed cytotoxicity, resulting in cell viability rates of 59.9% in BJ cells and 42.5% in HT29 cells at 1.89 µM.(Limón et al., 2021)

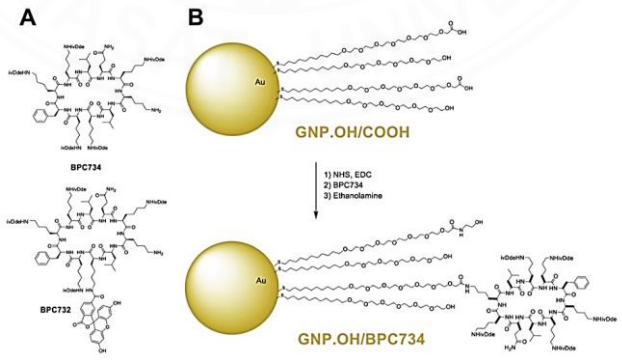

Figure 2.12 (a) The chemical structure of peptide BPC734 and BPC732 (b) The functionalized GNPs with peptide BPC734 and BPC732

Daniela M.D. Formaggio and coworkers functionalized of AuNPs with two therapeutic peptides simultaneously. These peptides, namely C7H2 and HuaL1, were selected due to their antitumor and antimicrobial properties. The AuNPs conjugated with peptides were subsequently evaluated for anti-microbial properties against *E. coli*, *P. aeruginosa*, and *C. albicans*, demonstrating an inhibition of microbial growth ranging from 23% to 57%. Moreover, their anti-tumoral potentials were evaluated in *vitro* by examining the viability of the human foreskin fibroblast (Hs68) cell lines. The results showed viability rates of 39%, 54%, and 40% for H-AuNPs, C-AuNPs, and HC-AuNPs, respectively, indicating its cytotoxicity against the Hs68 cells. In comparison, AuNPs exhibited a viability rate of 77%, thus not displaying cytotoxicity.(Formaggio et al., 2022)

2.3 The anti-*Plasmodium* peptides

Carine Baraguey reported a significant contribution through the discovery and syntheses of two cycloctapeptides and a cyclononapeptide, which were identified as chevalierins A and B, and C, as depicted in **Figure 2.13**. These cyclic peptides were successfully isolated from the latex of *Jatropha chevalieri*, a member of the *Euphorbiaceae* family, a plant well-known for their abundance of bioactive cyclic peptides. Importantly, chevalierin A demonstrated a notable potential against *Plasmodium falciparum*, displaying a moderate level of activity with an IC_{50} value of 8.9 μM.(Baraguey et al., 1998)

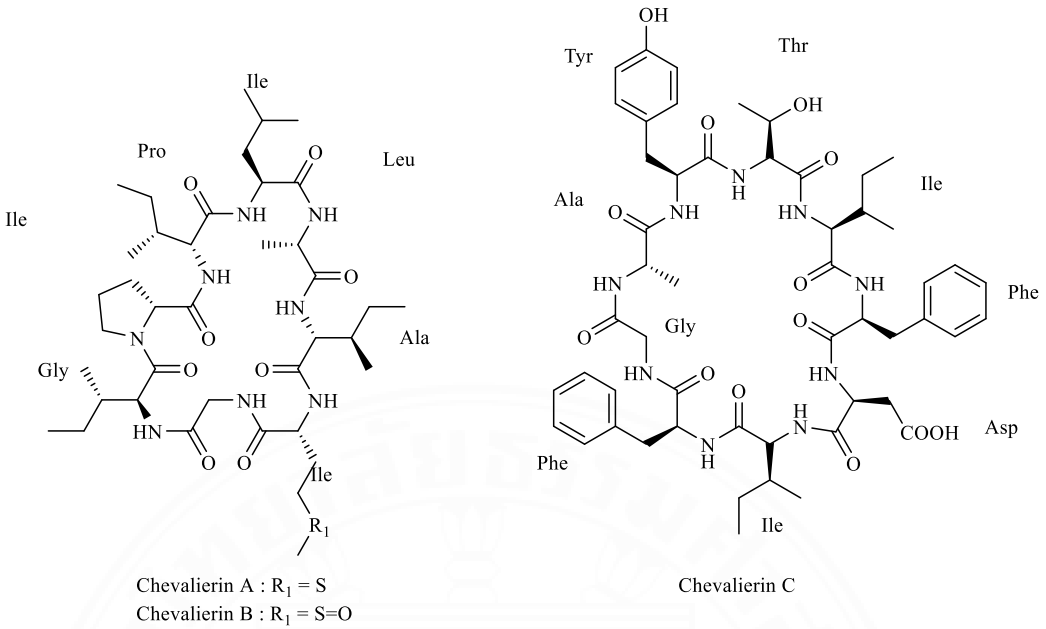

Figure 2.13 The chemical structure of chevalierins A, B, and C

Catherine Auvin-Guette reported the discovery of three novel cyclic peptides, namely pohlianins A, B, and C as shown in **Figure 2.14**. These peptides were extracted from *Jatropha pohliana*, a plant species found in the Recife area of Brazil. Impressively, these cyclic peptides exhibited moderate antimalarial activity, with respective IC_{50} values of 57, 25, and 16 μM.(Auvin-Guette et al., 1999)

Aggie Lawer achieved the first syntheses of *Jatropha*-derived cyclic peptides pohlianin C, which is the most potent member of this series. The derivative of pohlianin C as depicted in **Figure 2.15** by replacing the glycine-glycine segment with a *p*-aminobenzoic acid, demonstrated significant potentials for anti-malarial activity with an IC50 value of 4 μM, surpassing the activity of pohlianin C.(Lawer et al., 2014)

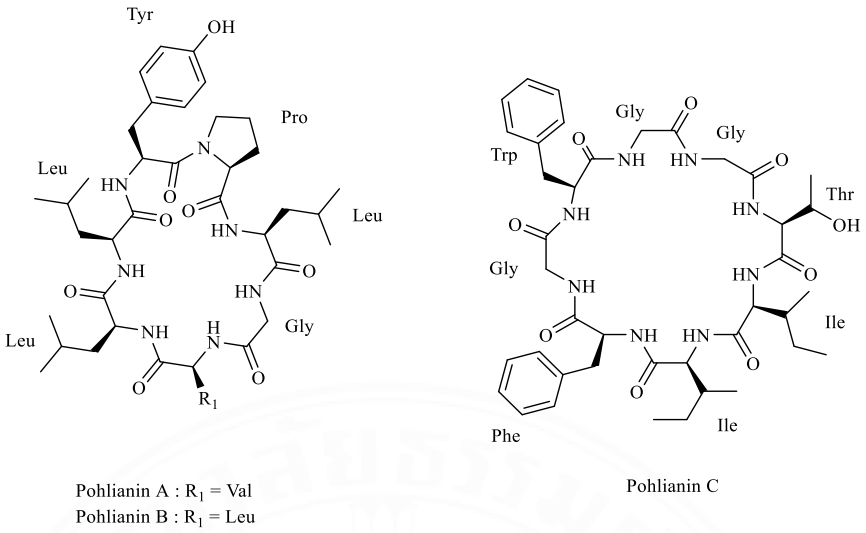

Figure 2.14 The chemical structure of pohlianin A, B, and C

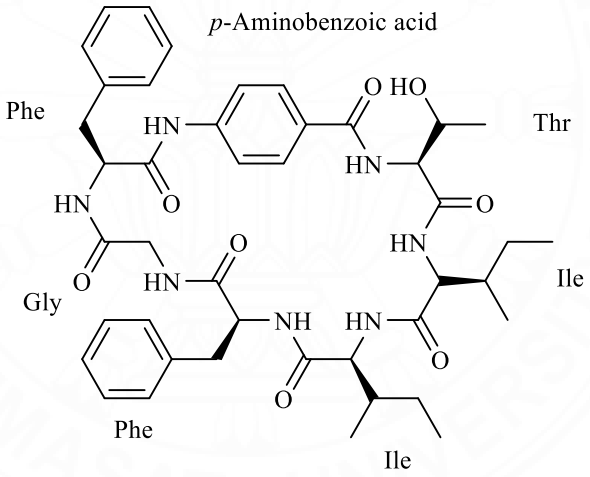

Figure 2.15 The chemical structure of pohlianin C derivative

In 1999, Matthew K. Renner discovered cycloheptapeptides, namely cyclomarins A-C. These peptides were obtained from extracts of a cultured marine *streptomycete* CNB-928, collected in the vicinity of San Diego. Cyclomarin A, the major metabolite, consists of three common proteinogenic amino acids, specifically (*S*)-Ala, (*S*)-Val, and *N*-methylated-(*S*)-Lue, along with four unusual amino acids as depicted in **Figure 2.16**. Cyclomarin A has emerged as one of the most potent anti-inflammatory agents in both in *vivo* and *vitro* assays.(Renner et al., 1999)

Additionally, in 2015, Nathalie identified cyclomarins as potent growth inhibitors of *Plasmodium falciparum*, effectively targeting the PfAp3Aase (diadenosine triphosphate hydrolase) enzymes in the protozoan parasite. The inhibitory activity against PfAp3Aase was particularly impressive with IC_{50} values measuring at 0.004, 0.007, and 2.15 for cyclomarins A, B, and C, respectively.(Bürstner et al., 2015)

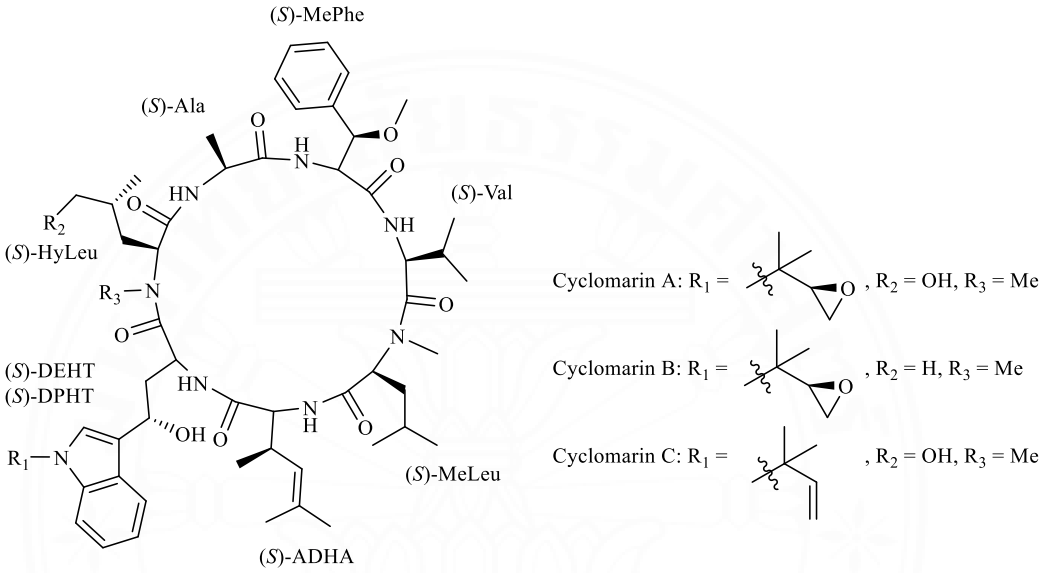

Figure 2.16 The chemical structure of cyclomarins A-C

Carine Baraguey showed the study; involving the isolation and syntheses of a cyclic heptapeptide named mahafacyclin B. This peptide consists of seven residues with a high proportion of hydrophobic amino acids. It was extracted from the latex of *Jatropha mahafalensis*, a known rich source of bioactive cyclic peptides. The specific composition of mahafacyclin B includes four phenylalanines, two glycines, and one threonine as illustrated in **Figure 2.17**. Impressively, this cyclic peptide exhibited significant antimalarial activity with an IC50 value of 2.2 μM.(Baraguey et al., 2001)

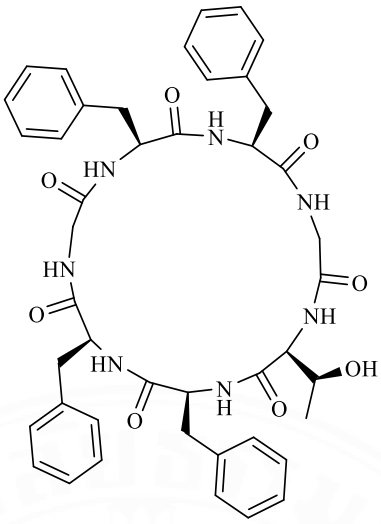

Figure 2.17 The chemical structure of mahafacyclin B

Namphung Vongvanich discovered a novel cyclohexadepsipeptide with anti-mycobacterial and anti-malarial properties, named hirsutellide A. Hirsutellide A was isolated from fungi of genus *Hirsutella kobayasii* BCC 1660. The chemical structure of hirsutellide A consists of *allo*-isoleucine (*allo*-Ile), (*R*)-2-hydroxy-3-phenylpropanoic acid (HPPA), and sarcosine (Sar) as depicted in **Figure 2.18**. Notably, hirsutellide A demonstrated potent anti-mycobacterial activity with a MIC ranging from 6-12 μg/mL. Importantly, it exhibited no cytotoxic effects against Vero cells at a concentration of 50 μg/mL. Additionally, hirsutellide A displayed promising in *vitro* anti-malarial activity with an IC50 value of 2.8 μg/mL.(Vongvanich et al., 2002)

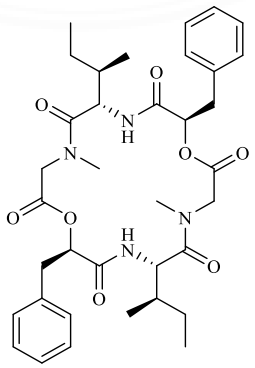

Figure 2.18 The chemical structure of hirsutellide A

Furthermore, Henok Asfaw Sahile synthesized and subsequent evaluated hirsutellide A as a potential lead for further structural optimization. The synthesized hirsutellide A demonstrated a comparable anti-plasmodial potency with an IC_{50} value of 2.3 μM consistent with the reported activity of natural hirsutellide A (IC_{50} = 2.8 μM). Moreover, they modified the exocyclic substituents of the depsipeptide ring, including the replacement of *allo*-Ile (11), Gly (12), and demethylation of the *N*-methyl sarcosine (13) as depicted in **Figure 2.19**. Interestingly, these alterations resulted in a reduction of anti-plasmodial activity. Conversely, peptide analogues of hirsutellide A (15-17) exhibited greater efficacy against *Plasmodium falciparum* strain 3D7 with IC50 values ranging from 1.8-7.7 μM. This was in contrast to those of depsipeptide analogues (11-13), displaying IC50 values of 7.5-20.1 μM.(Sahile, Martínez-Martínez, Dillenberger, Becker, & Imming, 2020)

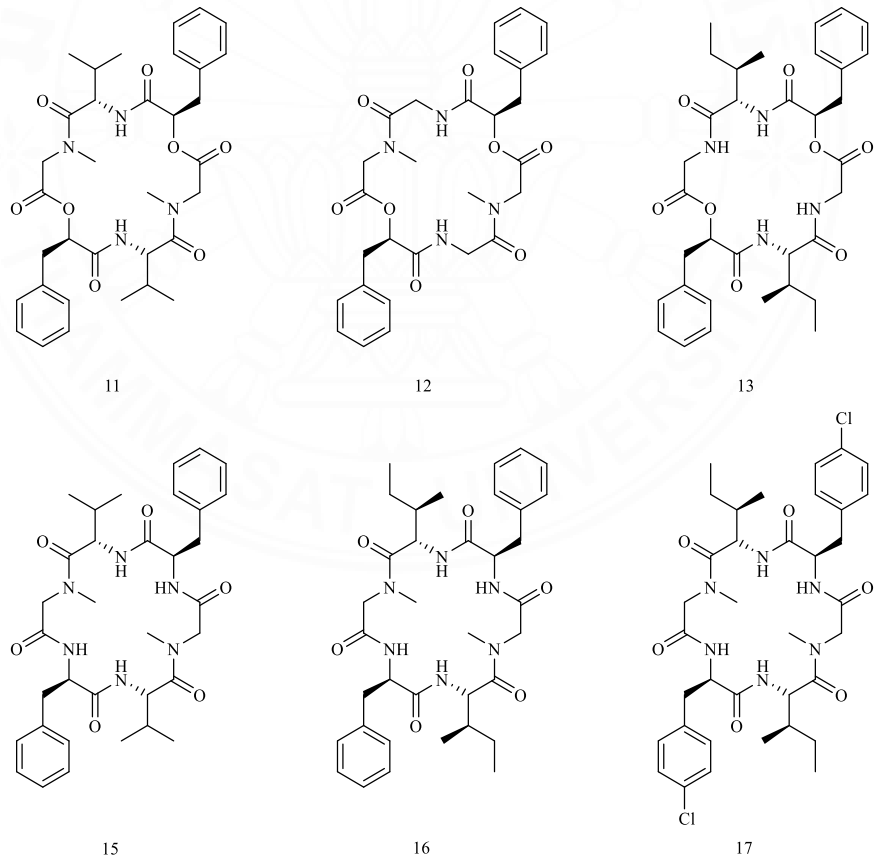

Figure 2.19 The chemical structure of depsipeptide analogues (11-13) and hirsutellide A analogues (15-17)

Vatcharin Rukachaisirikul published a significant discovery, the isolation of a novel cycloheptapeptide known as cordyheptapeptide A from the insect pathogenic fungus *Cordyceps* sp. BCC 1788. This compound was accompanied by the identification of four previously known bioxanthracenes (2-5), as mentioned previously.(Jaturapat et al., 2001) Cordyheptapeptide A consists of a sequence of amino acids, including L-*N*-Me-Tyr, L-Ile, L-Leu, D-*N*-Me-Phe, L-Pro, *N*-Me-Gly, and L-Phe, as shown in **Figure 2.20**. Notably, this compound exhibited an anti-malarial activity against *Plasmodium falciparum* K1 with an IC_{50} value of 5.35 μM. Moreover, it demonstrated low cytotoxicity towards Vero cells with a concentration >56.88 μM.(Rukachaisirikul et al., 2006)

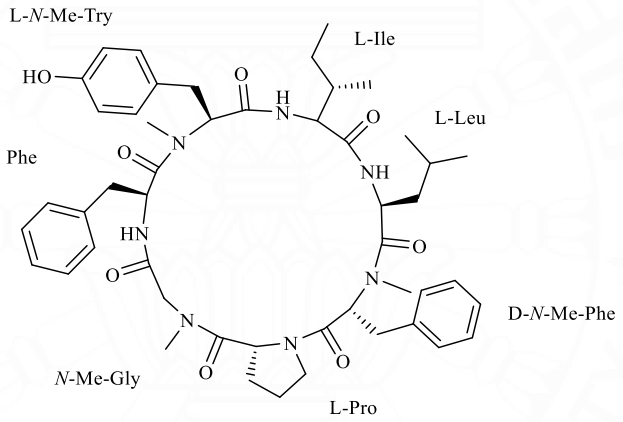

Figure 2.20 The chemical structure of cordyheptapeptide A

Jiraporn Thongtan studied the isolation, structural elucidation, and evaluation of biological activities of a novel tetrapeptide known as hirsutellic acid A. This tetrapeptide was obtained from a fermentation broth of the entomopathogenic fungus *Hirsutella* sp. BCC 1528. Hirsutellic acid A was discovered as a linear tetrapeptide characterized by the presence of an anthranilic acid residue at the C-terminus, along with L-*allo*-Ile, *N*-Me-D-Phe, and L-Leu, as illustrated in **Figure 2.21.** Notably, hirsutellic acid A displayed significant activity against the malarial parasite *Plasmodium falciparum* strain K1, with an IC_{50} value of 8.0 μM. Remarkably, this compound exhibited no cytotoxic effects on various cell lines, including Vero cells, KB

cells, BC cells, and NCI-H187, at a concentration >95 μM.(Thongtan, Saenboonrueng, Rachtawee, & Isaka, 2006)

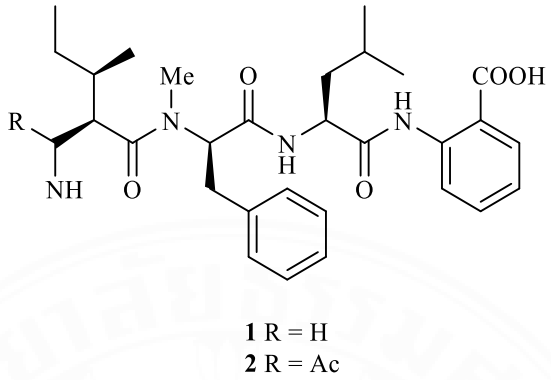

Figure 2.21 The chemical structure of hirsutellic acid A

Meri Emili F. Pinto published a significant discovery and syntheses of ribifolin isolated from *Jatropha ribifolia*, belonging to the *Euphorbiaceae* family, specifically the subfamily *Crotonideae*. The chemical structure of ribifolin as depicted in **Figure 2.22**, consists of the amino acids Ile, Leu, Gly, and Ser. Ribifolin, both cyclic form and its linear counterpart, was synthesized through the solid-phase peptide synthesis (SPPS) procedure. Ribifolin exhibited a noteworthy anti-plasmodial activity with an IC_{50} of 42 μM against *Plasmodium falciparum* strain 3D7. In contrast, the linear form of ribifolin demonstrated a considerably lower anti-plasmodial activity with an IC_{50} value of 519 μM. This comparison emphasizes the significance of cyclization in enhancing the biological activity of ribifolin. Crucially, both cyclic and linear ribifolin compounds exhibited no cytotoxicity towards human embryonic kidney cells (HEK293T) at the concentration range of 0.001-100 μM.(Pinto et al., 2015)

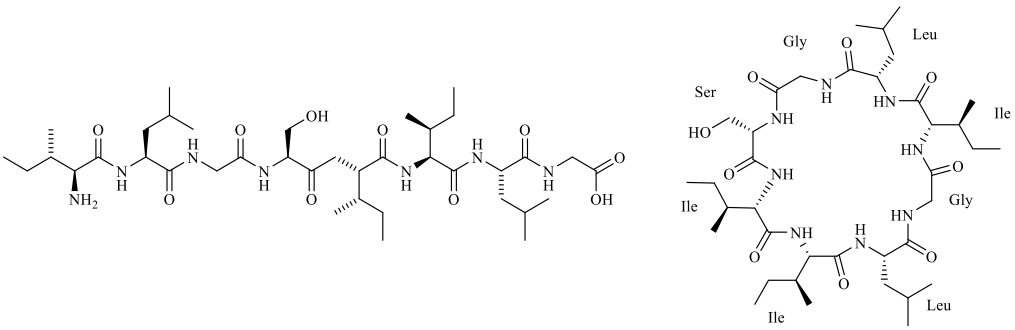

Figure 2.22 The chemical structure of linear and cyclic ribifolin

Thomas Tremblay designed, synthesized, and evaluated a series of hybrid compounds. These hybrids consisted of squaramide tethered to chloroquine, clindamycin, and mortiamide D. From their previous studies, mortiamide D emerged as a promising candidate, displaying impressive IC_{50} values of 1.31 and 0.94 μM against *Plasmodium falciparum* strain 3D7 and Dd2, respectively. Furthermore, their studies revealed that a clindamycin analogue (4) and all chloroquine intermediates (8-10) displayed low IC_{50} values against the 3D7 strain, particularly compound 8 possessing an IC_{50} of 2.8±0.0009 nM. Additionally, the chloroquine homodimer (17) exhibited IC_{50} values of 0.0313±0.0049 μM and 0.0809±0.0146 μM against 3D7 and Dd2 strain, respectively. Moreover, the hybrid compounds chloroquine-mortiamide D (19) and clindamycin-chloroquine (21) demonstrated IC_{50} values of 0.0801±0.0092 μM and 0.1292±0.1097 μM against the 3D7 strains, and 0.6476±0.1076 μM and 1.0130±0.1123 μM against the Dd2 strain, respectively. Interestingly, the tethering of a mortiamide D analogue to a chloroquine scaffold resulted in superior activity compared to that of clindamycin-mortiamide D hybrid. Furthermore, it was a clear evidence that the presence of the mortiamide D derivatives played a crucial role for biological activity against the 3D7 strain. This was substantiated by the observation that chloroquine-lysine (23) exhibited a higher IC_{50} values of 0.2231±0.0389 μM as compared to that of hybrid (19) (0.0801±0.0092 μM). Importantly, these compounds did not exhibit any cytotoxicity within the range of concentrations tested (0.39 nM to 12.8 μM) against red blood cells.(Tremblay et al., 2023)

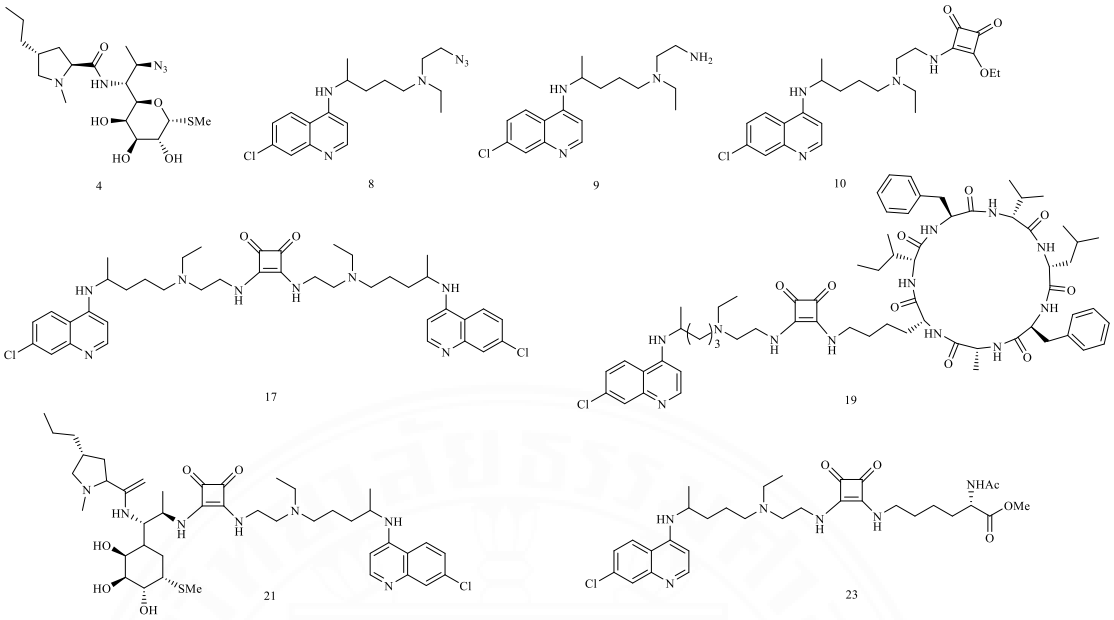

Figure 2.23 The chemical structure of clindamycin analogue (4), chloroquine intermediates (8-10), chloroquine homodimer (17), hybrid compounds chloroquine-mortiamide D (19) and clindamycin-chloroquine (21) and chloroquine-lysine (23)

CHAPTER 3
RESEARCH METHODOLOGY

3.1 Research scope

The design of thiol-incorporated peptides-GNPs involves the discovery of peptides containing sulfur that exhibits robust binding affinity to GNPs and can self-assemble into a dense layer.(Lévy et al., 2004) Lugdunin, a novel peptide containing thiazolidine, has been selected as a promising candidate for the modification of GNPs-peptides interactions. The design of thiol-incorporated peptides was carried out in two important criteria. In series I, we focused on the replacement of key amino acids at thiol-incorporated peptides. The main purpose of these modifications is greatly related to the specific binding of thiol incorporated peptides with GNPs. Thiol incorporated peptides were designed and subsequently synthesized by the replacement of thiazolidine at lugdunin sequence with a cysteine residue, while other amino acids and stereochemistry (D-L-L-D-L-D-L) were kept consistent with the native lugdunin as shown in **Figure 3.1**. The presence of a thiol group in a cysteine residue of thiol-incorporated is the most important factor for a covalent bond formation with GNPs, while amino groups also contributed to the binding affinity with GNPs. Furthermore, the presence of a positively charge ammonium group in proximity to the thiol group significantly enhances the adsorption kinetics of thiols onto GNPs that are stabilized with citrate.(Lévy et al., 2004) In series II, we concentrated on the investigation of the stereochemical integrity of the resulting thiol-incorporated peptides, comprising three D-amino acid residues, namely Val, Val, and Leu at positions I, IV, and VI, respectively. To this approach, thiol-incorporated peptides were designed by replacing all D-amino acids from the lugdunin sequence with L-amino acid (known as “mutagenesis”). The resulting thiol-incorporated peptide-GNPs, developed through systematic modifications in both amino acid constituents and stereochemistry, hold the potential to enhance their binding affinity with GNPs.

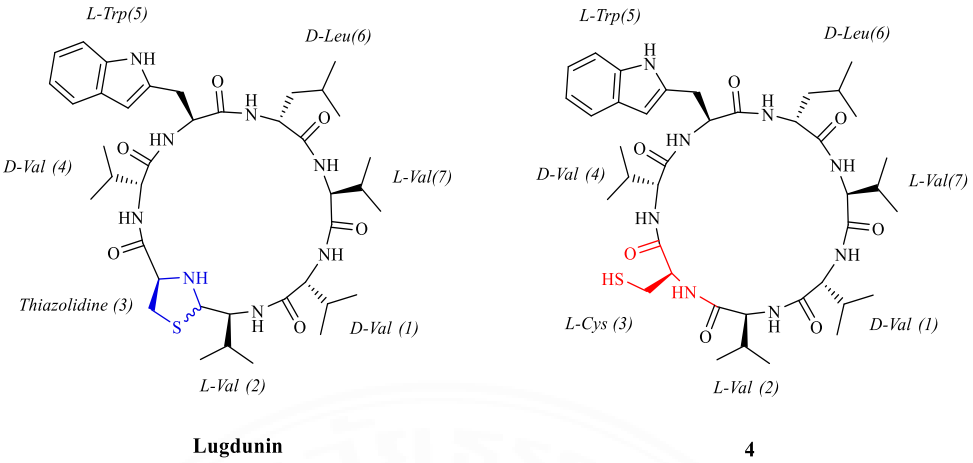

Figure 3.1 Structure of native lugdunin with amino acid substituents (left) and thiol incorporated peptides (right)

Subsequently, we introduced and combined two key epitopes derived from the mortiamide peptide, composed of (-D-Phe[1], L-Phe[2] and D-Val[3]) and lugdunin peptides, encompassing (-D-Leu[7], L-Val[6], D-Val[5] and L-Val[4]). The hybridization of epitopes could be potentially considerable promise as a strategy to directly target not only *Plasmodium* parasites but also a panel of bacterial strains. According to SAR analyses, it indicated that the presence of D-Leu within the sequence is significantly critical for its biological activity, mainly attributed to the interaction between D-Leu and the hydrophobic interior bacterial membrane, effectively interrupting the formation of cell walls.(Schilling et al., 2019),(Saur et al., 2021) On the other hand, the epitope (D-Val-D-Phe-L-Phe) in mortiamide A exhibits strong relevance to its biological efficacy against the malarial parasite (*P. falciparum*). We proposed and subsequently synthesized two distinct series of re-engineered mortiamides, according to these following criteria; (1) an amino acid replacement at position (VI) and (VII), (2) the investigation of stereochemical integrity at position (II), (III), (V) and (VII).

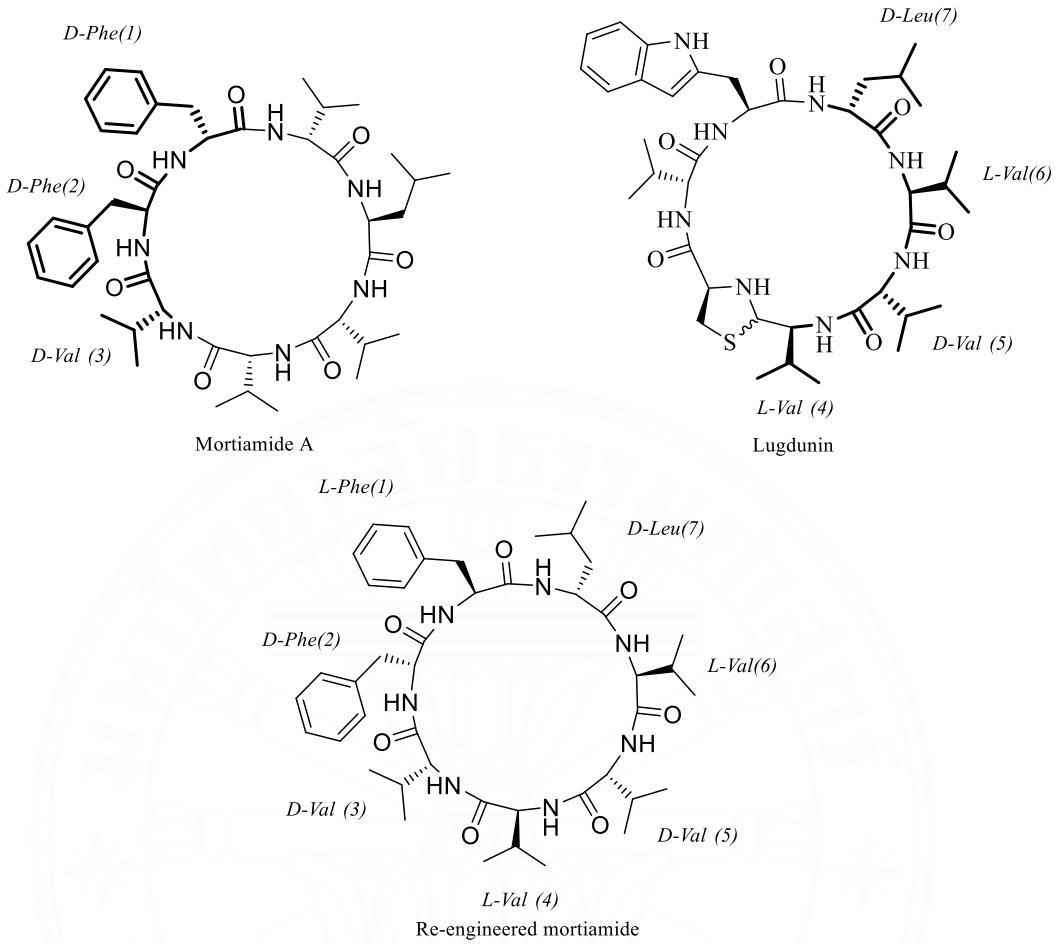

Figure 3.2 Proposed chemical structures of re-engineered mortiamide peptides derived from motiamide A (left) and lugdunin (right)

3.2 Chemicals and instruments

3.2.1 Chemicals

(1) *N*-(9-Fluorenylmethoxycarbonyl)-L-Valine, Fmoc-Val-OH

(2) *N*-(9-Fluorenylmethoxycarbonyl)-D-Valine, Fmoc-D-Val-OH

(3) *N*-(9-Fluorenylmethoxycarbonyl)-L-Leucine, Fmoc-Leu-OH

(4) *N*-(9-Fluorenylmethoxycarbonyl)-D-Leucine, Fmoc-D-Leu-OH

(5) N_{α}-(9-Fluorenylmethoxycarbonyl)-$N_{(in)}$-tert-butoxycarbonyl- L-Tryptophan, Fmoc-Trp(Boc)-OH

(6) N_{α}-(9-Fluorenylmethoxycarbonyl)-S-trityl-L-Cysteine, Fmoc-Cys(Trt)-OH

(7) *N*-(9-Fluorenylmethoxycarbonyl)-L-Phenylalanine, Fmoc-Phe-OH

(8) *N*-(9-Fluorenylmethoxycarbonyl)-D-Phenylalanine, Fmoc-D-Phe-OH

(9) *N*,*N'*-Dicyclohexylcarbodiimide, DCC

(10) 4-Dimethylaminopyridine, DMAP

(11) Hydroxy benzotriazole, HOBt

(12) 1-[Bis(dimethylamino)methylene]-1H-1,2,3- triazolo[4,5-bipyridinium 3-oxid hexafluorophosphate, N-[(Dimethylamino)-1H-1,2,3-triazolo[4,5-b]pyridine-1- ylmethylene]-N-methylmethanaminium hexafluorophosphate N-oxide, HATU

(13) *N*,*N*-Diisopropylethylamine, DIPEA

(14) Trifluoracetic acid, TFA

(15) Piperidine

(16) 1,2-Ethanedithiol, EDT

(17) Triisopropylsilane, TIS

(18) 2-Chlorotrityl chloride resin, 2-CTC resin

(19) Nitrogen gas

(20) Methanol, MeOH

(21) Dichloromethane, DCM

(22) Diethyl ether

(23) Dimethylformamide, DMF

(24) Methanol HPLC grade

(25) Acetonitrile HPLC grade

(26) Distilled water

(27) Deionized water

(28) Phosphate buffer pH 7.0

(29) Sodium citrate, $C_6H_9Na_3O_9$

(30) Chloroauric acid, $HAuCl_4$

(31) Dimethyl sulfoxide-d_6, DMSO-D_6

(32) Formic acid, HCOOH

3.2.2 Instruments

(1) Laboratory glasswares

(2) Glass filtration kit

(3) Syringes and syringe filters

(4) Cuvette

(5) Heating mentle

(6) Solid phase reaction vessel

(7) Magnetic stirrer

(8) Shaker, stuart mini orbital shaker SSM1

(9) Balance 4 digit, METTLER TOLEDO JE-1103C

(10) Rotary evaporator, BUCHI vacuum controller V-800 and rotavapor R-205

(11) Vacuum pump, EDWARDS model RV8

(12) Freeze dryer, Flexi-Dry^{TM} MP

(13) Ultraviolet-visible spectrophotometer, Jasco V-730

(14) Fluorescence spectrophotometer, Jasco FP-8200

(15) Analytical high-performance liquid chromatography, Jasco HPLC, PU-4180, Jasco UV-4070 UV/Vis Detector

(16) Preparative high performance liquid chromatography, Jasco preparative HPLC PU-4086-Binary pump, Jasco UV-4075 UV/Vis Detector

(17) Scanning electron Microscopy, Field Emission Scanning Electron Microscopy, FESEM JEOL JSM-7800F with EDS Oxford

(18) Fourier transform infrared spectroscopy, Thermo Scientific/Nicolet iS50

(19) Nuclear magnetic resonance spectrometer (NMR) Bruker ADVANCE 400 NMR spectrometer with TopSpin 4.0.7 software.

(20) Liquid chromatography mass spectrometry (LCMS), Bruker/micrOTOF-Q II/UHPLC Ultimate 3000.

(21) Centrifuge, ONILAB-D1008

(22) X-ray photoelectron spectroscopy (XPS), AXIS Ultra DLD

(23) Circular dichroism spectrometer (CD), Jasco J-815 spectropolarimeter using a 1 cm quartz cell using a 260-190 nm
(24) Finepak SIL C18T-5, 5 μm, C18, 300 °A column (4.6 mm. × 250 mm), Jasco
(25) COSMOSIL 5C4-AR-300 5 μm, C4, 300 °A column (4.6 mm. × 150 mm), COSMOSIL
(26) TopCount microplate scintillation counter (Packard, USA).

3.3 Experiments

3.3.1 The synthesis of thiol-incorporated peptides-GNPs

The thiol-incorporated peptides were designed and subsequently synthesized by substituting the thiazolidine at lugdunin sequence with a cysteine residue, while other amino acids and stereochemistry (D-L-L-D-L-D-L) were kept consistent with the native lugdunin. The presence of a thiol group in a cysteine residue of modified lugdunin is crucial for forming a covalent bond with GNPs to generate thiol-incorporated peptides-GNPs. The syntheses of thiol-incorporated peptides-GNPs are categorized into three important parts: (1) amino acid assembly of linear peptide precursor (**1** and **2**) *via* SPPS (2) macrocyclization between the C_{α}-carboxyl group of L-Val and the N_{α}-amino group of D-Val under high dilution condition that favors the intramolecular reaction without epimerization to release **3** and **4**; and (3) the peptide conjugation with the gold nanoparticle (GNPs) to provide **5-8**.

3.3.1.1 Synthesis of linear peptides chain *via* solid phase peptide synthesis (SPPS)

(1) The first amino acid loading on 2-chlorotrityl chloride resin

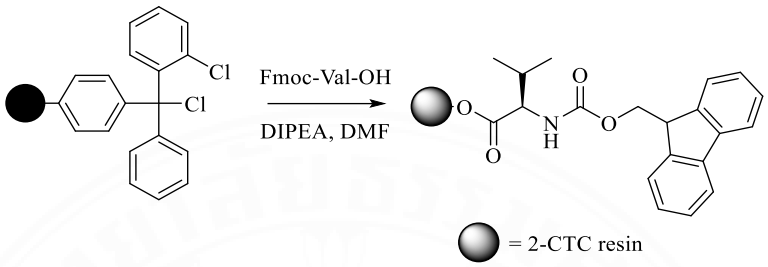

9 10

Scheme 3.1 The first amino acid Fmoc-Val-OH assembly on 2-chlorotrityl chloride resin

Under a nitrogen atmosphere, 2-chlorotrityl chloride resin (2.0 g, 0.84 mmol) was added by Fmoc-L-Val-OH (0.8553 g, 2.52 mmol), DMF (15 ml), and DIPEA (428.6 µL, 2.52 mmol). The reaction mixture was shaken at ambient temperature overnight. Subsequently, the reaction mixture was filtered and washed sequentially with DMF (3×2 mL), DCM (3×2 mL), and diethyl ether (1×2 mL). The resin was then dried in *vacuo*.

(2) Calculate first amino acid loading by Fmoc test

Fmoc-Val-O-resin (2 mg) was placed in a vial, and then 20% piperidine/DMF (3 mL) was added. The mixture was shaken for 30 min. The absorption intensity of the reaction solution was measured at 301 nm using UV spectroscopy. Subsequently, the percentage of amino acid loading was calculated using the following equation:

mmol amino acid/gram of resin = (Abs.)/(1.65×mg)

% amino acid loading = [(mmol of amino acid/gram of resin)/(mmol/gram of loading resin)]×100

The first amino acid loading was found to be approximately 65%.

(3) Amino acid assembly of linear peptides precursor *via* SPPS (L- and DL-configuration)

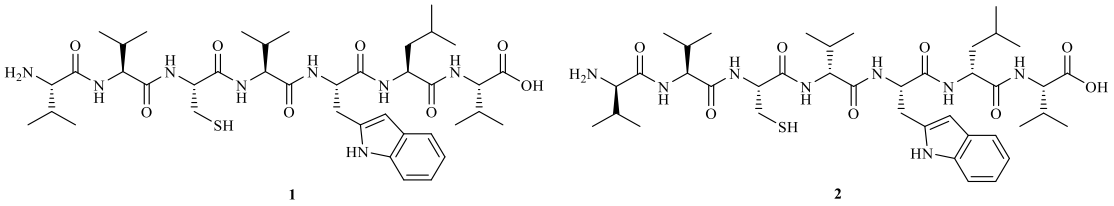

Figure 3.3 Chemical structure of linear thiol-incorporated peptides (**1** and **2**)

After preloading Fmoc-Val-O-resin (1 eq., 0.2 g, 0.13 mmol) was allowed to shake at ambient temperature by DMF (3 mL) for 30 min. The resin was capped by the reaction with MeOH/DIPEA (10:1). The purpose of this step is to quench unreacted 2-chlorotrityl chloride resin. Subsequently, the Fmoc group was removed using 20% piperidine in DMF (3 mL, 30 min), and the resin was washed with DMF (3×2 mL). The free amino acid of Fmoc-Leu-OH (2 eq., 0.0952 g, 0.2691 mmol) was coupled using a mixture of DCC (2 eq., 0.0555 g, 0.2691 mmol) in DMF (0.5 mL), DMAP (2 eq., 0.0329 g, 0.2691 mmol) in DMF (0.5 mL) and HOBt (2 eq., 0.0455 g, 0.2691 mmol) in DMF (0.5 mL) as a coupling agent. The reaction mixture was allowed to shake for 60 min at ambient temperature for coupling an amino group. The resin was drained off and washed by DMF (3×3 mL). This synthetic procedure was repeated by using other amino acids, namely; Fmoc-Trp(Boc)-OH (2 eq., 0.1417 g, 0.2691 mmol), Fmoc-Val-OH (2 eq., 0.0913 g, 0.2691 mmol), Fmoc-Cys(Trt)-OH (2 eq., 0.1567 g, 0.2691 mmol), Fmoc-Val-OH (2 eq., 0.0913 g, 0.2691 mmol), and Fmoc-Val-OH (2 eq., 0.0913 g, 0.2691 mmol) in DMF (1 mL), respectively. On the other hand, the substitution of L-configuration with D-configuration at Leu^2 (Fmoc-D-Leu-OH; 2 eq., 0.0952 g, 0.2691 mmol), Val^4 (Fmoc-D-Val-OH; 2 eq., 0.0913 g, 0.2691 mmol), and Val^7 (Fmoc-D-Val-OH; 2 eq., 0.0913 g, 0.2691 mmol) residues to provide **1** and **2** as shown in **Figure 3.3**. After the synthesis was completed, the resin was filtered and washed with DMF (3×3 mL), DCM (3×3 mL), and diethyl ether (3×3 mL), respectively. The resin was then dried in *vacuo* for 24 h. The peptide was cleaved by treatment with 1% TFA/DCM for 5 min and globally deprotected by 97%TFA: 1.25% EDT: 1.25%

H_2O: 0.5% TIS for 2 h to afford a linear thiol re-engineered lugdunin. The solvent was removed under nitrogen gas and purified with preparative RP-HPLC (gradient of 30%-100% methanol in water). Linear thiol-incorporated peptides **1** and **2** were obtained as a white fluffy powder (60% and 65%). ^{1}H NMR (400 MHz, DMSO-d_6): δ (ppm) 10.74 (d, 1H, *J* = 11.6 Hz), 8.31-8.28 (m, 1H) , 8.22-8.15 (m, 1H), 8.08 (dd, 2H, *J* = 12.0, 8.1 Hz), 7.78 (q, 2H, *J* = 8.4, 7.4 Hz), 7.57 (q, 1H, *J* = 10.9, 9.4 Hz), 7.30 (d, 1H, *J* = 8.1 Hz), 7.15-7.00 (m, 3H), 6.95 (t, 2H, *J* = 7.4 Hz), 4.59 (tt, 1H, *J* = 10.9, 5.3 Hz), 4.46-4.36 (m, 2H), 4.26 (td, 2H, *J* = 8.1, 6.9, 2.7 Hz), 4.19-4.09 (m, 2H), 3.55 (d , 1H, *J* = 5.5 Hz), 3.12-3.05 (m, 2H), 2.92 (dd, 1H, *J* = 14.7, 8.9 Hz), 2.74-2.59 (m, 1H), 2.08-1.98 (m, 3H), 1.97-1.89 (m, 2H), 1.60 (tt, 1H, *J* = 13.0, 6.1 Hz), 1.51-1.40 (m, 2H), 0.92-0.89 (m, 3H), 0.88-0.85 (m, 14H), 0.83-0.81 (m, 6H), 0.77 (dd, 7H, *J* = 9.3, 7.5 Hz). ^{13}C NMR (100 MHz, DMSO-d_6): δ (ppm) 175.56, 171.83, 171.44, 170.59,170.20, 169.48, 136.09, 127.01, 123.97, 120.78, 118.18, 111.20, 109.51, 60.25, 60.12, 57.73, 57.12, 55.87, 53.88, 50.58, 30.77, 30.09, 29.58, 28.95, 26.68, 25.82, 24.08, 22.94, 22.70, 22.02, 21.38, 19.70, 19.60, 19.32, 18.63, 18.41, 18.36, 18.02, 17.21. HR-TOF-MS (ESI) *m/z* found 817.9582 $[M+H]^+$, HPLC t_r = 20.41min.

(4) The syntheses of cyclic thiol-incorporated peptides

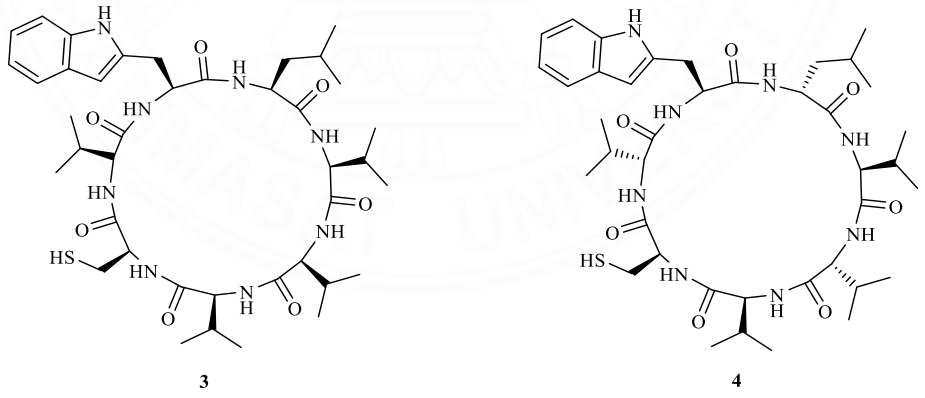

Figure 3.4 Chemical structures of cyclic thiol-incorporated peptides (**3** and **4**)

To stir the solution of linear thiol-incorporated peptides **1** and **2** (0.02 g, 0.0245 mmol) in DMF (20 mL), HOBt (2.25 eq., 0.0187 g, 0.1102 mmol), and DIPEA (3eq., 25 μL, 0.1269 mmol) were added at room temperature under high

dilution condition (1 mg:1 mL). HATU (1.5 eq., 0.0279 g, 0.0734 mmol) was dissolved in DMF (250 μL) and slowly added (1 h: 2 drops) to the solution of the linear thiol-incorporated peptide. The yellow solution was stirred for 2 days at room temperature. Subsequently, the reaction mixture was neutralized, lyophilized, and extracted with DCM. The cyclic thiol-incorporated peptides **3** and **4** were purified with preparative RP-HPLC (gradient of 30%-100% methanol in water). Cyclic thiol-incorporated peptides **3** and **4** were obtained as white fluffy powder (59% and 61%). ^{1}H NMR (400 MHz, DMSO-d_6): δ (ppm) 10.81 (s, 1H), 8.21 (d, 1H, *J* = 6.7 Hz) , 8.06 (d, 1H, *J* = 9.3 Hz), 7.87 (d, 1H, *J* = 7.2 Hz), 7.50 (dd, 2H, *J* = 10.3, 8.1 Hz), 7.36 (d, 1H, *J* = 6.5 Hz), 7.31 (d, 1H, *J* = 8.0 Hz), 7.08 (d, 4H, *J* = 22.1 Hz), 6.97 (t, 1H, *J* = 7.4 Hz), 4.34-4.39 (m, 2H), 4.22-4.17 (m, 1H), 4.07 (dd, 2H, *J* = 104, 5.7 Hz), 3.91 (t, 1H, *J* = 7.1 Hz), 3.57 (d , 2H, *J* = 8.1 Hz), 3.52-3.48 (m, 2H), 3.08-3.00 (m, 2H), 2.12-2.02 (m, 2H), 1.47 (t, 1H, *J* = 9.7 Hz), 1.37-1.29 (m, 2H), 0.97 (d, 2H, *J* = 0.63 Hz), 0.94 (s, 1H), 0.92 (d, 3H, *J* = 3.6 Hz), 0.90 (d, 3H, *J* = 3.3 Hz), 0.88-0.86 (m, 4H), 0.84 (d, 4H, *J* = 5.0 Hz), 0.82-0.79 (m, 8H), 0.73 (d, 3H, *J* = 6.7 Hz), 0.64 (d, 2H, *J* = 6.7 Hz). ^{13}C NMR (100 MHz, DMSO-d_6): δ (ppm) 170.97, 167.43, 165.24, 153.05, 141.17, 132.19, 131.98, 130.05, 129.56, 129.13, 128.61, 127.62, 127.33, 127.08, 126.73, 125.98, 123.54, 118.76, 114.72, 70.26, 65.49, 63.57, 44.02, 43.93, 42.16, 34.00, 33.81, 32.74, 31.87, 31.75, 31.15, 30.48, 29.47, 29.15, 29.04, 24.92, 24.23, 22.72, 22.55, 19.60, 19.12, 14.40, 14.00. HR-TOF-MS *m/z* found at 821.4336 $[M+Na]^+$. The HPLC retention time was observed at 22.15 min.

3.3.1.2 The synthesis of gold nanoparticles by citrate reduction

Gold nanoparticles (15 nm) were synthesized using a citrate reduction method with $HAuCl_4$. Initially, an aqueous solution of $HAuCl_4$ (20 mL, 0.5 mM) was heated with stirring to 80°C over a heating mantle. Subsequently, 2 mL 38.8 mM trisodium citrate dihydrate was rapidly added to the heated solution. The resulting mixture was further stirred for 30 min until a ruby color solution was observed. Finally, the solution was allowed to be stored at room temperature in a dark place.

3.3.1.3 The synthesis of thiol-incorporated peptides conjugated with GNPs

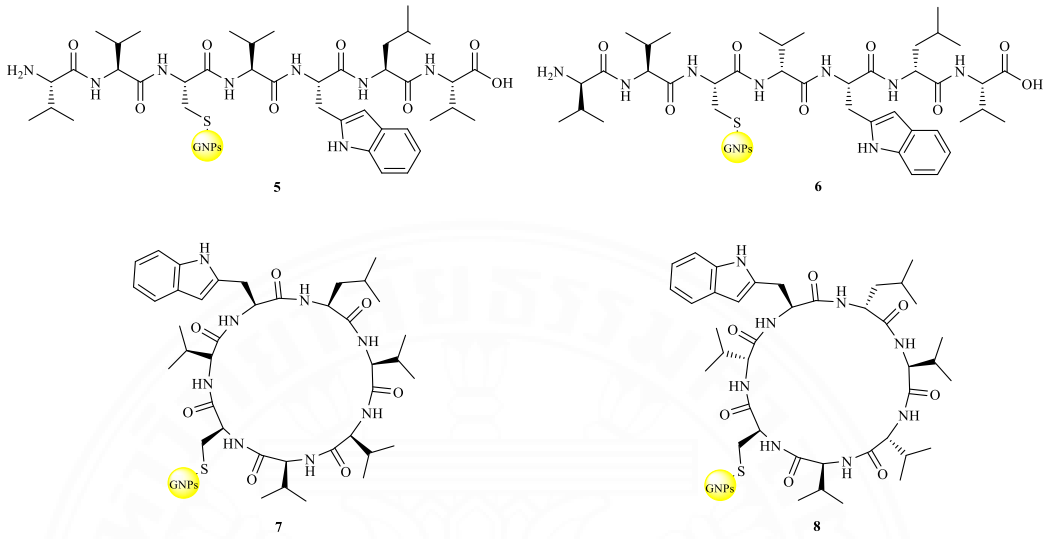

Figure 3.5 Chemical structures of thiol-incorporated linear and cyclic peptides-GNPs (**5-8**)

The synthetic linear and cyclic thiol-incorporated peptides (1 mg, 1.22 µmol) were dissolved in 1 mL of phosphate buffer pH 7.0 to prepare stock solution with approximate of 1.2248 mM. Next, pipette 10 µL of the peptide stock solution into a round bottom flask, and the volume was adjusted to 1 mL with phosphate buffer pH 7.0. Then, 1 mL of 2.4872 nM of synthetic GNPs solution was added. A peptide-modified GNPs was prepared by mixing thiol-incorporated peptides with at the molar ratio of peptide: GNPs = 5000:1. After 3 h the solution was centrifuged using ONILAB-D1008 (7,000 rpm, 15 min) to remove the unbound peptide, resulting in a pellet that was subsequently resuspended in phosphate buffer to provide thiol-incorporated peptides-GNPs both in linear and cyclic forms (**5-8**) as shown in **Figure 3.5**.

3.3.2 The synthesis of re-engineered mortiamide peptides

The synthetic approach of re-engineered mortiamide peptides based on the combination of mortiamide A and lugdunin scaffold. These cyclic peptides, composed of seven amino acid residues, were initially isolated from *Mortierella sp.* and

S. lugdunensis. The syntheses of re-engineered mortiamide peptides involved three key stages: (1) the first amino acid loading, (2) an assembly of linear re-engineered mortiamide precursor and (3) re-engineered mortiamide peptide cyclization.

3.3.2.1 Synthesis of linear peptides chain *via* solid phase peptide synthesis (SPPS)

(1) Amino acid assembly of linear peptide precursors *via* SPPS (L- and DL- configuration)

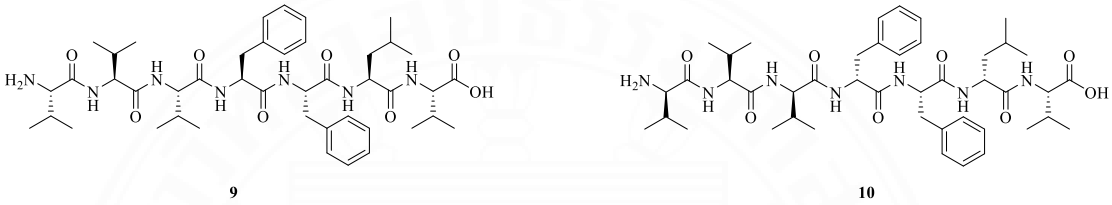

9 **10**

Figure 3.6 Chemical structures of linear re-engineered mortiamide peptides (**9** and **10**)

After preloading Fmoc-Val-O-resin (1 eq., 0.2 g, 0.13 mmol) was allowed to shake at ambient temperature by DMF (3 mL) for 30 min. To prevent any unreacted 2-chlorotrityl chloride resin, the resin was capped by reacting with MeOH/DIPEA (10:1). Following this, the Fmoc protective group was removed using 20% piperidine in DMF (3 mL, 30 min), and the resin was washed with DMF (3×2 mL). Next, Fmoc-Leu-OH (2 eq., 0.0918 g, 0.2598 mmol) was coupled using a mixture of DCC (2 eq., 0.0526 g, 0.2598 mmol) in DMF (0.5 mL), DMAP (2 eq., 0.0317 g, 0.2598 mmol) in DMF (0.5 mL) and HOBt (2 eq., 0.0440 g, 0.2598 mmol) in DMF (0.5 mL) as a coupling agent. This reaction was allowed to shake for 60 min at ambient temperature for coupling an amino group. Afterward, the resin was drained off and washed with DMF (3×3 mL). This synthetic procedure was repeated using other amino acids, namely; Fmoc-Phe-OH (2 eq., 0.1006 g, 0.2598 mmol), Fmoc-Phe-OH (2 eq., 0.1006 g, 0.2598 mmol), Fmoc-Val-OH (2 eq., 0.0882 g, 0.2598 mmol), Fmoc-Val-OH (2 eq., 0.0882 g, 0.2598 mmol), and Fmoc-Val-OH (2 eq., 0.0882 g, 0.2598 mmol) in DMF (1 mL), respectively. On the other hand, the substitution of L-configuration with D-configuration at Leu^2 (Fmoc-D-Leu-OH; 2 eq., 0.0918 g, 0.2598 mmol), Phe^4 (Fmoc-D-Phe-OH; 2 eq., 0.1006 g, 0.2598 mmol), Val^5 (Fmoc-D-Val-OH; 2 eq., 0.0882 g,

0.2598 mmol), and Val[7] (Fmoc-D-Val-OH; 2 eq., 0.0882 g, 0.2598 mmol) residues to provide (**9** and **10**) as depicted in **Figure 3.6**. The reaction mixture was allowed to shake for 60 min at ambient temperature for coupling an amino group. Once the synthesis was completed, the resin was filtered and washed with DMF (3×3 mL), DCM (3×3 mL) and diethyl ether (3×3 mL), respectively. Then the resin was dried *in vacuo* for 24 h. The peptide was cleaved by treatment with 1% TFA/DCM for 5 min. The solvent was removed under reduced pressure and purified with preparative RP-HPLC (gradient of 30%-100% methanol in water). Linear re-engineered mortiamide (**9** and **10**) were obtained as a white fluffy powder (70% and 75%). ^{1}H NMR (400 MHz, DMSO-d_6): δ (ppm) 8.58 (s, 1H), 8.39 (d, 1H, *J* = 6.4 Hz), 8.24-8.14 (m, 3H), 7.97 (d, 1H, *J* = 9.7 Hz), 7.83 (d, 1H, *J* = 9.1 Hz), 7.52 (d, 1H, *J* = 5.7 Hz), 7.30-7.24 (m, 4H), 7.25-7.16 (m, 2H), 7.19-7.13 (m, 4H), 4.61 (q, 1H, *J* = 8.5 Hz), 4.27-4.21 (m, 1H), 4.18 (d, 1H, *J* = 9.8 Hz), 4.10 (dd, 1H, *J* = 8.9, 4.2 Hz), 3.98-3.86 (m , 2H), 3.56-3.48 (m, 1H), 3.22 (d, 2H, *J* = 4.2 Hz), 2.78 (d, 2H, *J* = 8.1 Hz), 2.43-2.30 (m, 2H), 1.88 (dp, 1H, *J* = 9.2, 6.5 Hz), 1.66 (h, 1H, *J* = 6.7 Hz), 1.37-1.20 (m, 1H), 0.99 (s, 2H), 0.96 (s, 3H), 0.93 (d, 3H, *J* = 6.2 Hz), 0.92 (s, 3H), 0.89-0.83 (m, 9H), 0.80 (d, 3H, *J* = 6.1 Hz), 0.74 (d, 3H, *J* = 6.7 Hz), 0.70 (d, 3H, *J* = 6.0 Hz), 0.54 (d, 3H, *J* = 6.8 Hz). ^{13}C NMR (100 MHz, DMSO-d_6): δ (ppm) 172.90, 172.81, 172.72, 171.41,171.08, 170.60, 168.83, 139.46, 137.66, 129.34, 129.31, 128.71, 128.57, 126.90, 126.56, 60.89, 60.63, 59.12, 58.55, 57.13, 56.61, 52.10, 37.96, 34.76, 29.19, 28.83, 28.55, 28.15, 24.06, 24.03, 23.25, 21.89, 19.67, 19.39, 19.38, 19.34, 19.25, 18.85, 18.77, 18.34. HR-TOF-MS (ESI) *m/z* found 907.9995 $[M+2MeOH+Na]^{+}$HPLC t_r = 20.137min.

(2) The syntheses of cyclic re-engineered mortiamide peptides

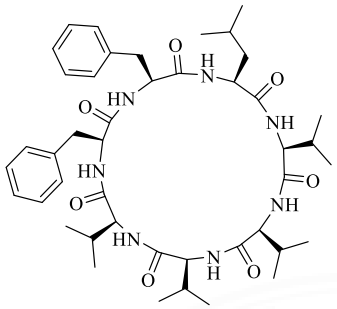

11

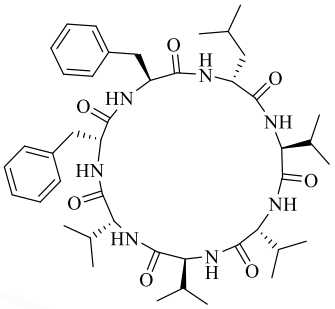

12

Figure 3.7 Chemical structures of cyclic re-engineered mortiamide peptide (**11** and **12**)

To stir the solution of linear re-engineered mortiamide peptides **9** and **10** (0.02 g, 0.0243 mmol) in DMF (20 mL), HOBt (2.25 eq., 0.0093 g, 0.0548 mmol), and DIPEA (3 eq., 12.4 μL, 0.073 mmol) were added at room temperature under high dilution condition (1mg:1 mL). HATU (1.5 eq., 0.0185 g, 0.0487 mmol) was dissolved in DMF (250 μL) and slowly added (1 h:2 drops) to the solution of the linear thiol-incorporated peptide. The yellow solution was stirred for 2 days at room temperature. Subsequently, the reaction mixture was neutralized, lyophilized, and extracted with DCM. The cyclic re-engineered mortiamide **11** and **12** were purified with preparative RP-HPLC (gradient of 30%-100% methanol in water). Cyclic thiol-incorporated peptides (**11** and **12**) were obtained as white fluffy powder (49% and 53%). ^{1}H NMR (400 MHz, DMSO-d_6): δ (ppm) 8.42 (s, 1H), 8.39 (s, 1H), 8.33 (d, 1H, *J* = 4.5 Hz), 8.26 (d, 1H, *J* = 8.3 Hz), 7.86 (d, 1H, *J* = 9.2 Hz), 7.78 (d, 1H, *J* = 10.4 Hz), 7.60 (d, 1H, *J* = 4.5 Hz), 7.34-7.27 (m, 4H), 7.28-7.17 (m, 2H), 7.17-7.06 (m, 4H), 4.28 (dt, 1H, *J* = 9.3, 4.4 Hz), 4.12-4.03 (m, 3H), 3.96 (ddd, 1H, *J* = 12.4, 8.8, 4.2 Hz), 3.92 (d, 2H, *J* = 3.2), 3.83 (dd, 1H *J* = 9.3, 3.9),2.73-2.46 (m, 2H), 2.39 (qd, 1H, *J* = 7.0, 4.2 Hz), 2.27-2.21 (m, 2H), 2.19-2.11 (m, 1H), 1.82 (dt, 1H, *J* = 9.1, 6.5 Hz), 1.67 (dq, 1H, *J* = 13.0, 6.5), 1.50-1.42 (m, 1H), 1.31-1.20 (m, 2H), 0.94 (d, 3H, *J* = 6.5 Hz), 0.91 (d, 12H, *J* = 6.5 Hz), 0.87-0.77 (m, 12H), 0.75 (d, 3H, *J* = 6.4 Hz). ^{13}C NMR (100 MHz, DMSO-d_6): δ (ppm) 172.38, 172.10, 171.36, 170.42, 170.42, 170.36, 169.58, 136.61, 136.09, 129.27, 128.85, 128.08, 127.97, 126.44, 126.35, 60.74, 60.43, 58.23,

57.64, 56.06, 54.86, 50.73, 36.59, 35.77, 31.42, 28.79, 28.58, 27.72, 24.46, 23.19, 21.97, 20.35, 19.84, 19.38, 19.01, 18.93, 18.69, 18.63, 16.30, 13.84. HRMS (LCMS-IT-TOF) *m/z* found 804.5582 $[M+H]^+$. HPLC t_r = 19.620min.

3.3.3 Antimicrobial assay

The efficacy of the 96-well plate assay in determining the minimum inhibitory concentration (MIC) for assessing the drug susceptibility of each peptide was demonstrated. The anti-microbial properties of the peptides against both gram-positive and gram-negative bacteria, including *Bacillus cereus* (ATCC 11778), *Listeria monocytogenes* (10403s), *Staphylococcus aureus* (ATCC 25923), *Staphylococcus epidermidis* (ATCC 12228), *Acinetobacter baumannii* (ATCC 19606), *Escherichia coli* (ATCC 25922), *Pseudomonas aeruginosa* (ATCC 27853), *Salmonella typhimurium* (ATCC 13311), and *Shigella sonnei* (ATCC 11060), was assessed.

To evaluate the MIC of each peptide, a broth microdilution assay was performed based on a modified protocol described by the National Committee for Clinical Laboratory Standards (NCCLS).(Hsueh et al., 2010) In this assay, 50 µl of bacterial solution was incubated with 50 µl of peptides serially diluted (ranging from 0.49 to 125 µg/ml in 0.1% DMSO), and then incubated at 37°C for 24 h under continuous shaking at 220 rpm. The MIC values were defined as the lowest concentration of anti-microbial agents that either inhibited bacterial growth or showed no turbidity upon visible inspection.(Andrews, 2001)

3.3.4 In *vitro* anti-*Plasmodium falciparum* assay

The parasites were cultivated in RPMI-1640 medium supplemented with 25 mM HEPES (N-2-hydroxyethylpiperazine-N'-2-ethanesulfonic acid), 25 mM $NaHCO_3$, 10% heat-activated human serum, and 3% erythrocytes. The culture was incubated at 37°C in a humidified incubator with 3% CO_2, and daily passages were performed using fresh medium containing erythrocytes to sustain parasite growth. Prior to the assay, parasites in the early ring-stage growth were collected and prepared to create a parasite mixture with 1% parasitemia in 1.5% erythrocytes.(Trager & Jensen, 1976)

The antimalarial assay was conducted in duplicate using 96-well plates. The test samples were subjected to serial dilution, generating at least six concentrations. Then, 25 µl of each diluted sample was added to wells containing 200

µl of a parasite mixture composed of 1% parasitemia and 1.5% erythrocytes. The plate was then incubated for 24 h. Subsequently, 25 µl of medium containing 0.5 µCi of [3H]hypoxanthine was added to each well and further incubated for 18-20 h. The levels of incorporated radioactive labeled hypoxanthine, which indicate parasite growth, were quantified using the TopCount microplate scintillation counter (Packard, USA).(Desjardins, Canfield, Haynes, & Chulay, 1979)

CHAPTER 4
RESULTS AND DISCUSSION

4.1 The synthetic strategy of thiol-incorporated peptides-GNPs

4.1.1 The synthesis of linear peptide precursors *via* solid phase peptide synthesis (SPPS)

For the assembly of the linear peptide precursor (**1**), a sequence consisting of valine (Val), leucine (Leu), tryptophan (Trp), valine (Val), cysteine (Cys), valine (Val), and valine (Val) was constructed using the Fmoc based solid phase peptide synthesis (SPPS) approach. On contrary, the linear peptide precursor (**2**) was composed of valine (Val), D-leucine (D-Leu), tryptophan (Trp), D-valine (Val), cysteine (Cys), valine (Val), and D-valine (D-Val). The Fmoc-based approach provided a gentle deprotection procedure by employing 20% piperidine in DMF to remove the Fmoc group at the N-terminus. Moreover, the resin could be selectively cleaved under mild acidic condition (1% TFA in DCM) to release the linear peptide precursor with a free carboxyl group, while retaining the protective groups on the side chains. Finally, global deprotection of the side chain protecting groups in the thiol-incorporated peptides was accomplished using a mixture of 97% TFA, 1.25% EDT, 1.25% H2O, and 0.5% TIS.

According to the **Scheme 4.1**, the initial amino acid, Fmoc-Val-OH was loaded on 2-chlorotrityl chloride resin, leading to the formation of Fmoc-Val-O-chlorotrityl chloride resin (**14**) with an efficiency of approximately 65%, calculated based on the initial loading of 2-chlorotrityl chloride resin. Subsequently, the preloaded amino acid residue was capped by using 1:10 (DIPEA:MeOH) for 1 h. The purpose of this step was to quench an unreacted trityl group with a small nucleophile, such as methanol. Next, Fmoc-Val-O-chlorotrityl chloride resin (**14**) was treated with 20% piperidine in DMF to provide NH_2-valine-O-chlorotrityl chloride resin (**15**), which was subsequently coupled with Fmoc-D-Leu-OH by using DCC, DMAP, and HOBt as a standard coupling agent to prevent the racemization providing (**16**). The reaction was repeatedly synthesized as previous step by assembling with Fmoc-Trp(Boc)-OH, Fmoc-D-Val-OH, Fmoc-Cys(Trt)-OH, Fmoc-Val-OH, and Fmoc-D-Val-OH, respectively to give **21**. In contrast, a substitution of D-

configuration with L-configuration was replaced at Leu^2, Val^4, and Val^7. The resulting protected peptide attached to 2-chlrotrityl chloride resin was subsequently cleaved from the solid support by using 1% TFA in DCM. Finally, NH_2-Val-Val-Cys(Trt)-Val-Trp-Leu-Val-COOH and NH_2-D-Val-Val-Cys(Trt)-D-Val-Trp-D-Leu-Val-COOH were globally deprotected via a combination of 97% TFA, 1.25% EDT, 1.25% H_2O, and 0.5% TIS. Subsequently, the crude peptides were subjected to purification *via* preparative HPLC to afford **1** and **2** with yield of 60% and 65%, respectively.

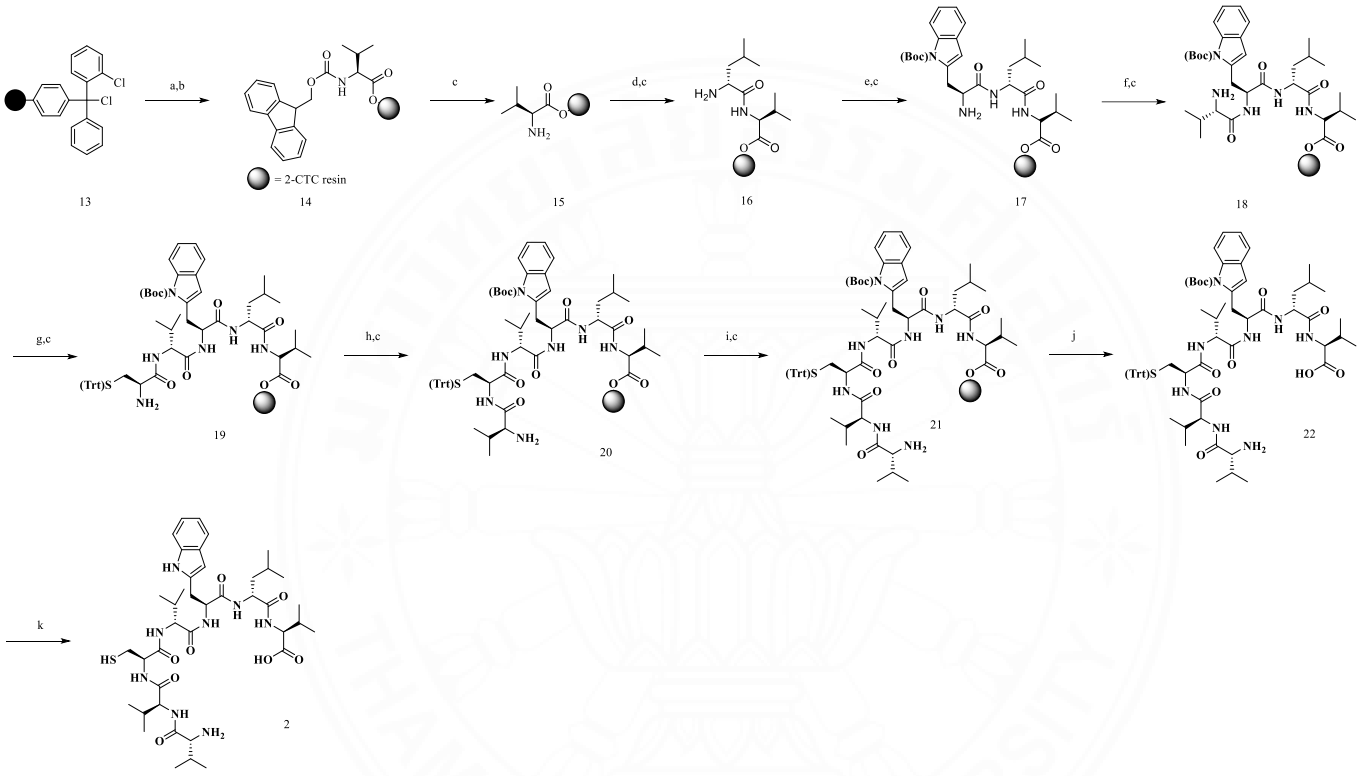

Scheme 4.1 Reagents and conditions for the synthesis of linear thiol-incorporated peptides: (a) Fmoc-Val-OH, DIPEA, DMF, overnight; (b) MeOH/DIPEA (10:1), 1h; (c) 20% piperidine/DMF 30min; (d) Fmoc-D-Leu-OH, DCC, DMAP and HOBt/ DMF 1h; (e) Fmoc-Trp(Boc)-OH, DCC, DMAP and HOBt/ DMF 1h; (f) Fmoc-D-Val-OH, DCC, DMAP and HOBt/ DMF 1h; (g) Fmoc-Cys(Trt)-OH, DCC, DMAP and HOBt/ DMF 1h; (h) Fmoc-Val-OH, DCC, DMAP and HOBt/ DMF 1h; (i) Fmoc-D-Val-OH, DCC, DMAP and HOBt/ DMF 1h; (j) 1% TFA/DCM 5min; (k) 97%TFA/1.25%EDT/1.25%H_2O/0.5%TIS 2h.

4.1.1.1 Characterization of linear thiol-incorporated peptides

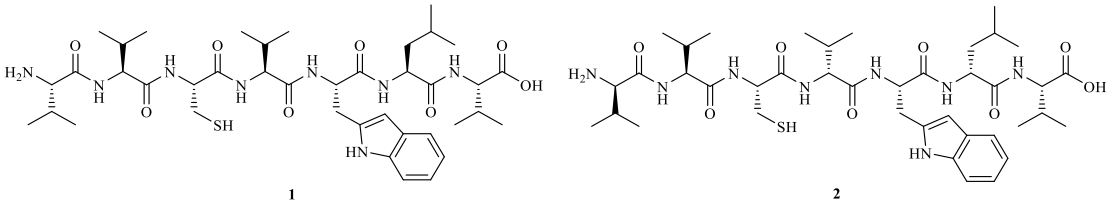

Figure 4.1 Chemical structures of linear thiol-incorporated peptides (**1** and **2**)

Name: linear thiol-incorporated peptides (**1** and **2**)

Chemical formula: $C_{40}H_{64}N_8O_8S$

(1) Mass spectrum and HPLC chromatogram

TOF-MS: Found; 428.2087 $[M+K+H]^{2+}$ and 817.9582 $[M+H]^{+}$; Calculated 816.46 $[M]^{+}$

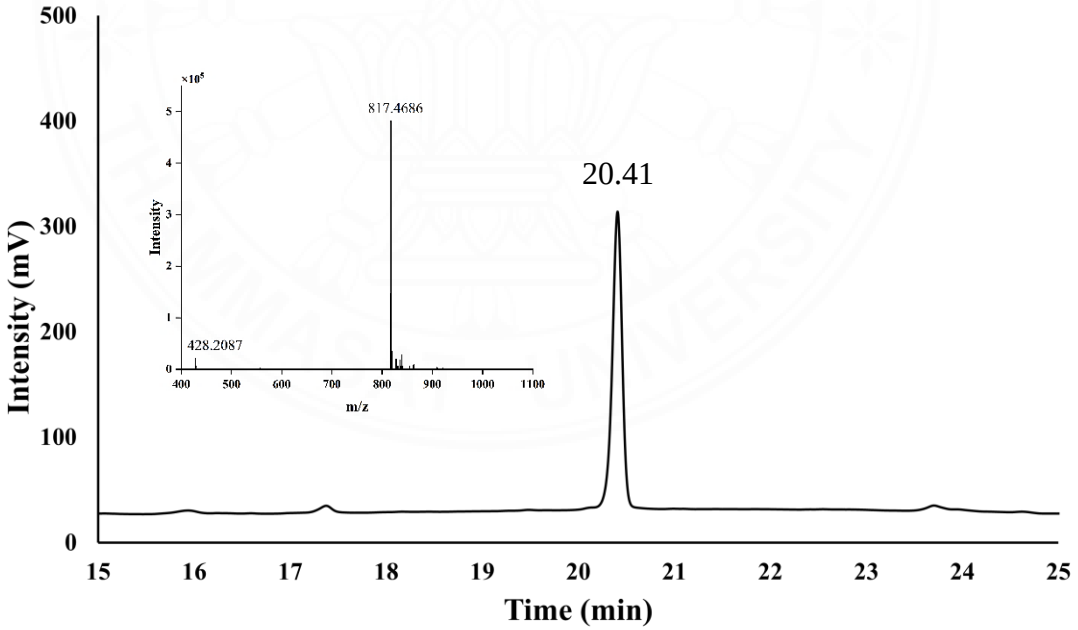

Figure 4.2 HPLC chromatogram and ESI-MS spectrum of linear thiol-incorporated peptides (**1** and **2**)

The purity of linear thiol-incorporated peptides was checked through analytical HPLC analysis. The retention time of a linear peptide was determined to be 20.41 min. Moreover, the TOF-MS spectrum revealed molecular mass of *m/z* = 428.2087 and 817.9582 corresponding to the molecular mass adduct $[M+K+H]^{2+}$ and $[M+H]^{+}$, respectively. The calculated molecular mass was found to be 816.46. This provided a conclusive evidence that syntheses of the linear thiol-incorporated peptides was successfully achieved.

(2) ^{1}H and ^{13}C NMR

^{1}H NMR (400 MHz, DMSO-d_6): δ (ppm) 10.74 (d, 1H, *J* = 11.6 Hz), 8.31-8.28 (m, 1H) , 8.22-8.15 (m, 1H), 8.08 (dd, 2H, *J* = 12.0, 8.1 Hz), 7.78 (q, 2H, *J* = 8.4, 7.4 Hz), 7.57 (q, 1H, *J* = 10.9, 9.4 Hz), 7.30 (d, 1H, *J* = 8.1 Hz), 7.15-7.00 (m, 3H), 6.95 (t, 2H, *J* = 7.4 Hz), 4.59 (tt, 1H, *J* = 10.9, 5.3 Hz), 4.46-4.36 (m, 2H), 4.26 (td, 2H, *J* = 8.1, 6.9, 2.7 Hz), 4.19-4.09 (m, 2H), 3.55 (d , 1H, *J* = 5.5 Hz), 3.12-3.05 (m, 2H), 2.92 (dd, 1H, *J* = 14.7, 8.9 Hz), 2.74-2.59 (m, 1H), 2.08-1.98 (m, 3H), 1.97-1.89 (m, 2H), 1.60 (tt, 1H, *J* = 13.0, 6.1 Hz), 1.51-1.40 (m, 2H), 0.92-0.89 (m, 3H), 0.88-0.85 (m, 14H), 0.83-0.81 (m, 6H), 0.77 (dd, 7H, *J* = 9.3, 7.5 Hz).

^{13}C NMR (100 MHz, DMSO-d_6): δ (ppm) 175.56, 171.83, 171.44, 170.59,170.20, 169.48, 136.09, 127.01, 123.97, 120.78, 118.18, 111.20, 109.51, 60.25, 60.12, 57.73, 57.12, 55.87, 53.88, 50.58, 30.77, 30.09, 29.58, 28.95, 26.68, 25.82, 24.08, 22.94, 22.70, 22.02, 21.38, 19.70, 19.60, 19.32, 18.63, 18.41, 18.36, 18.02, 17.21.

4.1.2 The synthesis of cyclic thiol-incorporated peptides

The synthetic strategy of cyclic thiol-incorporated peptides, two cyclization of linear precursors **1** (NH_2-Val-Val-Cys-Val-Trp-Leu-Val-COOH) and **2** (NH_2-D-Val-Val-Cys-D-Val-Trp-D-Leu-Val-COOH) were performed and further investigated the cyclization efficacy.(Luo, Yin, Tang, Wang, & Liang, 2018) To the cyclization strategy, HATU was utilized as an effective coupling agent in the presence of DIPEA and HOBt. This approach prevented the formation of side reactions, including the racemization.

The macrocyclization of linear thiol-incorporated precursors (**1** and **2**) were performed smoothly under very high dilution condition (approximately 0.1 mg/mL) enable to prevent the formation of undesired cyclodimerization products that is greatly associated with the significant entropy loss during the

macrocyclization.(Marti-Centelles, Pandey, Burguete, & Luis, 2015) To this reaction, the excess HATU (1.5 eq.) was dissolved in DMF, and slowly added to the reaction solution of **1**, **2**, DIPEA (3 eq.), and HOBt (2.25 eq.). The reaction mixture was allowed to react for two days to complete the cyclization process. As a result, the linear peptide (**1** and **2**) without the side chain protecting group were successfully cyclized with high yields to afford all cyclic thiol-incorporated peptides (**3** and **4**) without any oligomerization and dimerization observed. Subsequently, the crude peptides were subjected to purification *via* preparative HPLC to afford **3** and **4** with yields of 59% and 61%, respectively.

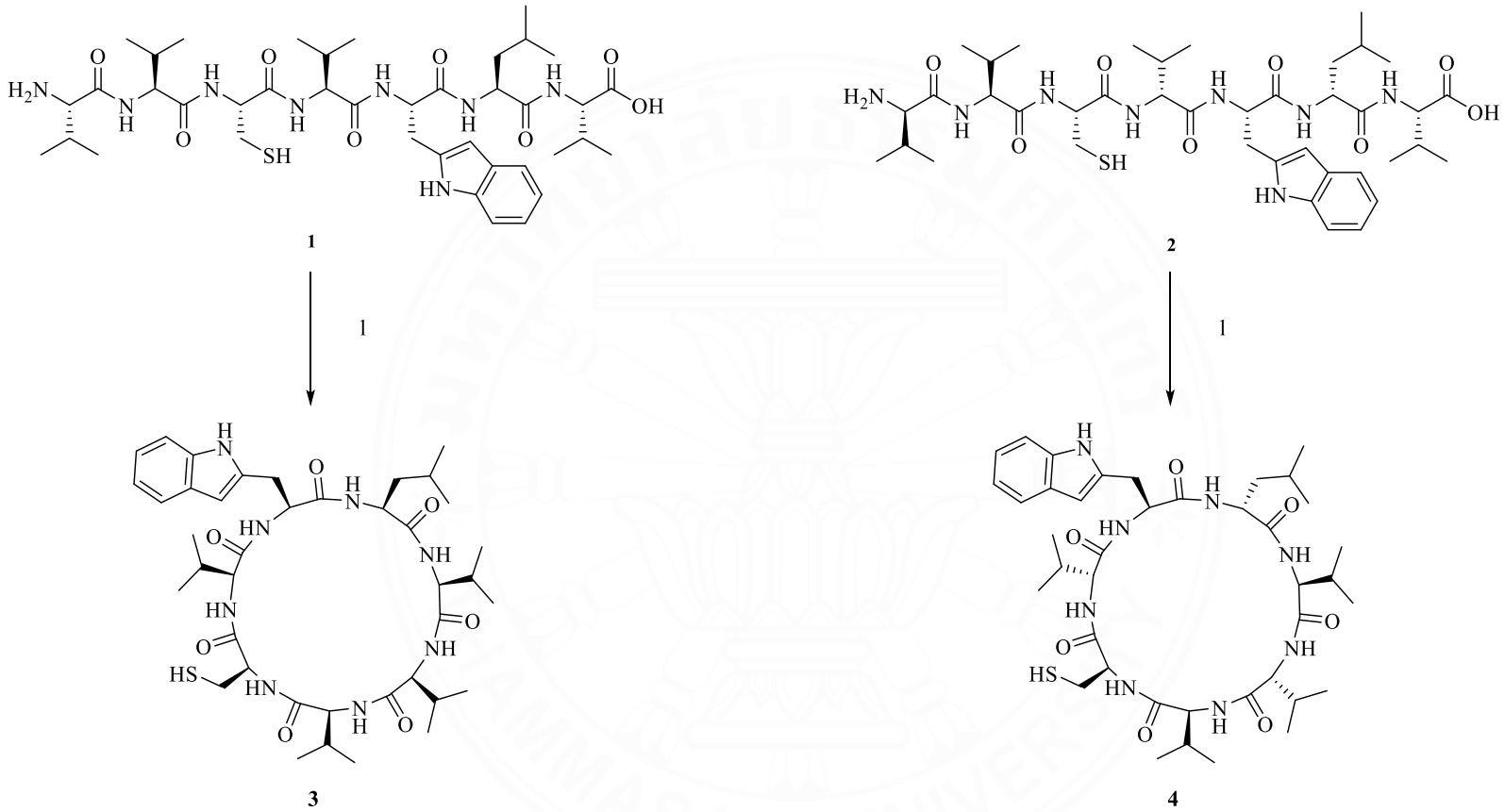

Scheme 4.2 Reagents and conditions for the synthesis of cyclic thiol-incorporated peptides: (l) HATU, HOBt, DIPEA/ DMF (1mg:1ml) 2 days.

4.1.2.1 Characterization of cyclic thiol-incorporated peptides

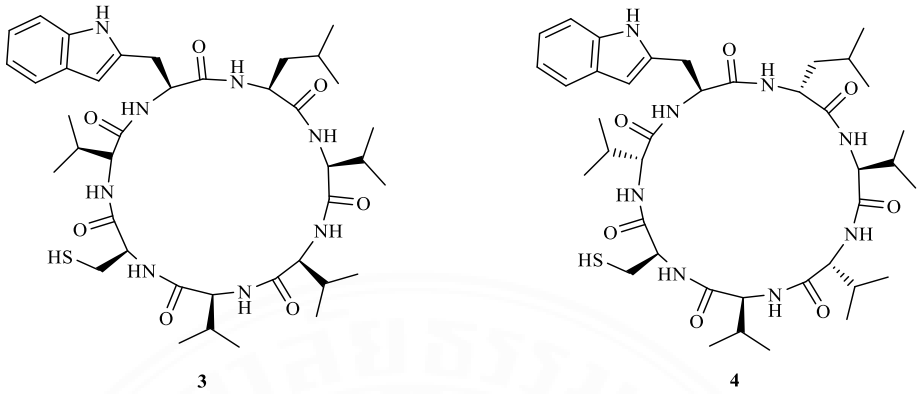

Figure 4.3 Chemical structures of cyclic thiol-incorporated peptides (**3** and **4**)

Name: cyclic thiol-incorporated peptides (**3** and **4**)

Chemical formula: $C_{40}H_{62}N_8O_7S$

(1) Mass spectrum and HPLC chromatogram

TOF-MS: Found; 821.4336 $[M+Na]^+$; Calculated 798.45 $[M]^+$

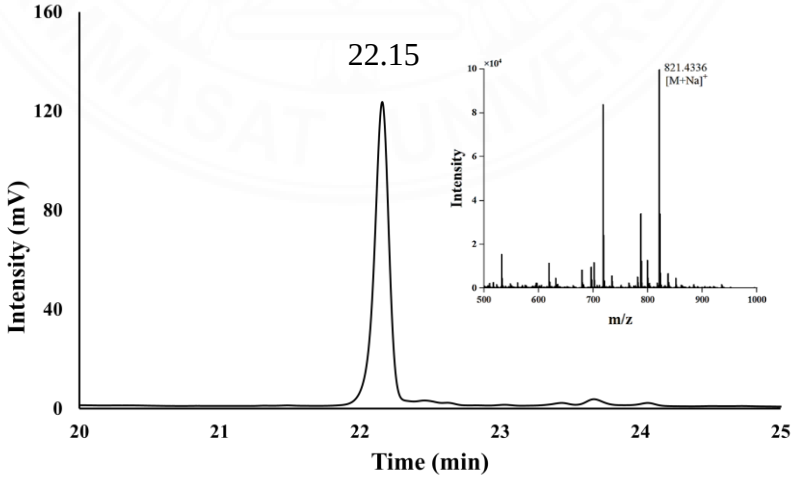

Figure 4.4 HPLC chromatogram and ESI-MS spectrum of cyclic thiol-incorporated peptides (**3** and **4**)

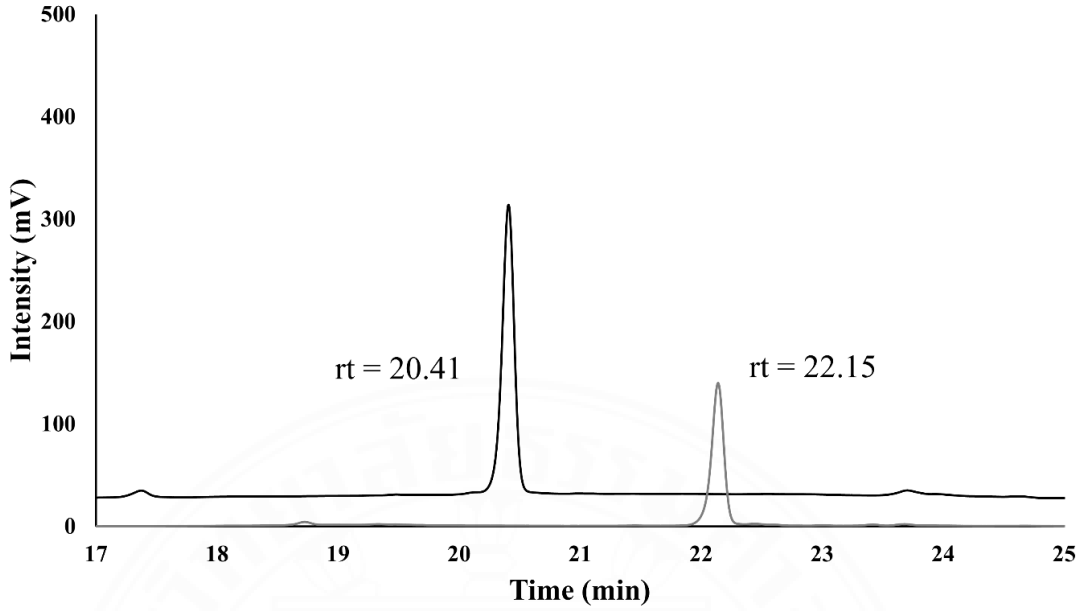

Figure 4.5 Comparison of HPLC chromatogram between linear (black line) and cyclic (grey line) thiol-incorporated peptides

(2) ^{1}H and ^{13}C NMR

^{1}H NMR (400 MHz, DMSO-d_6): δ (ppm) 10.81 (s, 1H), 8.21 (d, 1H, *J* = 6.7 Hz) , 8.06 (d, 1H, *J* = 9.3 Hz), 7.87 (d, 1H, *J* = 7.2 Hz), 7.50 (dd, 2H, *J* = 10.3, 8.1 Hz), 7.36 (d, 1H, *J* = 6.5 Hz), 7.31 (d, 1H, *J* = 8.0 Hz), 7.08 (d, 4H, *J* = 22.1 Hz), 6.97 (t, 1H, *J* = 7.4 Hz), 4.34-4.39 (m, 2H), 4.22-4.17 (m, 1H), 4.07 (dd, 2H, *J* = 104, 5.7 Hz), 3.91 (t, 1H, *J* = 7.1 Hz), 3.57 (d , 2H, *J* = 8.1 Hz), 3.52-3.48 (m, 2H), 3.08-3.00 (m, 2H), 2.12-2.02 (m, 2H), 1.47 (t, 1H, *J* = 9.7 Hz), 1.37-1.29 (m, 2H), 0.97 (d, 2H, *J* = 0.63 Hz), 0.94 (s, 1H), 0.92 (d, 3H, *J* = 3.6 Hz), 0.90 (d, 3H, *J* = 3.3 Hz), 0.88-0.86 (m, 4H), 0.84 (d, 4H, *J* = 5.0 Hz), 0.82-0.79 (m, 8H), 0.73 (d, 3H, *J* = 6.7 Hz), 0.64 (d, 2H, *J* = 6.7 Hz). ^{13}C NMR (100 MHz, DMSO-d_6): δ (ppm) 170.97, 167.43, 165.24, 153.05, 141.17, 132.19, 131.98, 130.05, 129.56, 129.13, 128.61, 127.62, 127.33, 127.08, 126.73, 125.98, 123.54, 118.76, 114.72, 70.26, 65.49, 63.57, 44.02, 43.93, 42.16, 34.00, 33.81, 32.74, 31.87, 31.75, 31.15, 30.48, 29.47, 29.15, 29.04, 24.92, 24.23, 22.72, 22.55, 19.60, 19.12, 14.40, 14.00.

Based on the HPLC chromatogram, cyclic thiol-incorporated peptides showed a single peak observed at a retention time of 22.15 min, indicating a

longer retention time (increased hydrophobicity) compared to that of linear thiol-incorporated peptides at 20.41 min. The time difference between the two peaks was approximately 2 min, as depicted in **Figure 4.5**. Moreover, the TOF-MS analysis of cyclic thiol-incorporated peptides revealed the molecular mass adduct at *m/z* 821.4336, corresponding to the $[M + Na]^+$. The calculated molecular mass was found to be 798.45. As a consequence, this clearly demonstrated the successful synthesis of the cyclic thiol-incorporated peptides, as shown in **Figure 4.4**.

4.1.3 The synthesis of thiol-incorporated peptides conjugated with GNPs

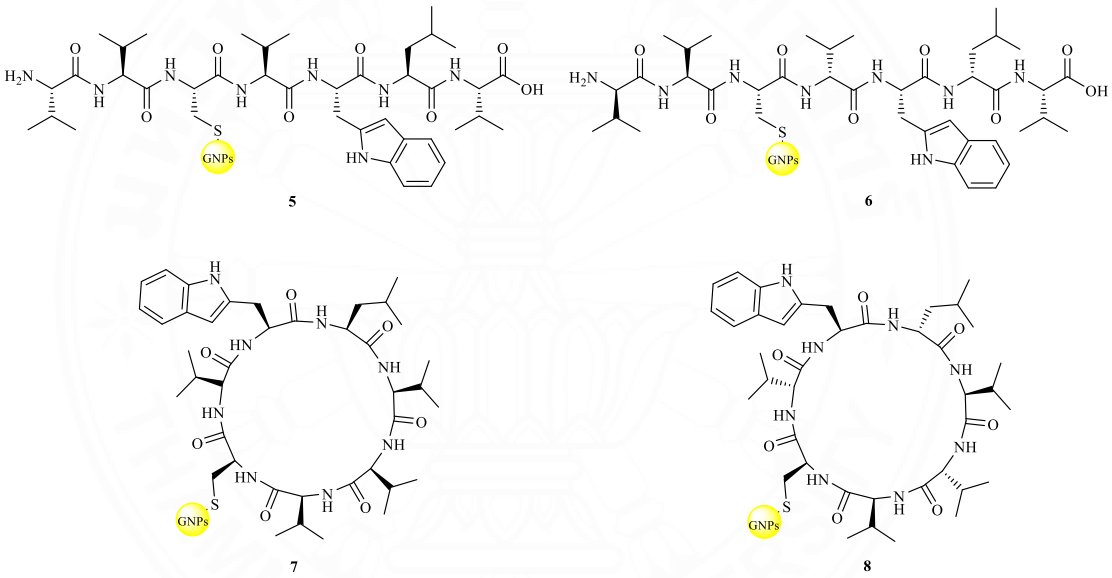

Figure 4.6 Chemical structures of thiol-incorporated linear and cyclic peptides-GNPs (**5-8**)

The conjugation between linear and cyclic thiol-incorporated peptides with GNPs through S-Au bonding is depicted in **Figure 4.6**. GNPs with diameters of 15 nm was synthesized by using sodium citrate as reducing agent.(Turkevich et al., 1951)

4.2 The characterization of thiol-incorporated peptides-GNPs

4.2.1 The characterization of thiol-incorporated peptides-GNPs by light scattering

Gold nanoparticles (GNPs) exhibited unique physical and electronic properties; such as surface plasmon resonance (SPR). Notably, once GNPs conjugated with thiol-incorporated peptides *via* Au-S bonding, the color change of the GNP solution clearly turned from ruby to purple under the naked eye which can be attributed to the characteristic of SPR of GNP as depicted in **Figure 4.7a**. This definitely indicated the complete conjugation between linear and cyclic thiol-incorporated peptides with GNPs. Furthermore, under the dark, when gold nanoparticles (GNPs) are exposed to the laser beam, only Tyndall effect (TE) is observed due to their small particle size at the nanoscale. However, when the laser beam is directed towards both linear and cyclic thiol-incorporated lugdunin-GNPs, light scattering is clearly seen as shown in **Figure 4.7b**. Thiol-incorporated lugdunin-GNPs demonstrates greater light scattering compared to GNPs alone, because the particle size of thiol-incorporated lugdunin is larger than that of GNPs as demonstrated in **Figure 4.7b**. This is a clear evidence of successful conjugation between GNPs and thiol-incorporated peptides.

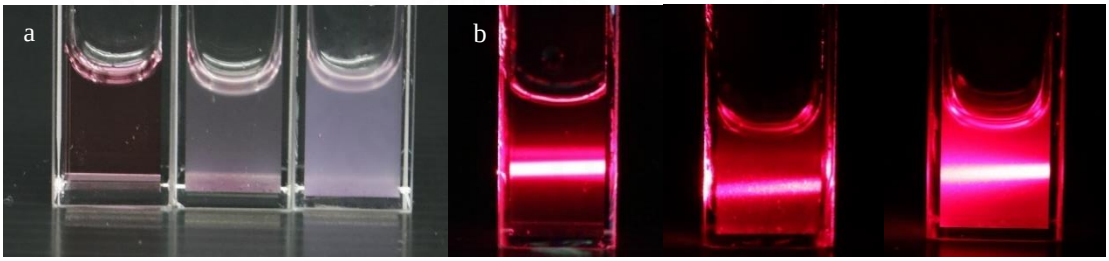

Figure 4.7 Photographs of GNPs, linear thiol-incorporated linear and cyclic thiol-incorporated-GNPs conjugate solutions in (a) under the light and (b) under the dark

4.2.2 The characterization of thiol-incorporated peptides-GNPs by SEM

Thiol-incorporated peptide-GNPs were further characterized by SEM and EDS analyses to investigate the conjugation of thiol-incorporated peptides with GNPs and to determine the morphological shape of the surface layer of GNPs. According to microscopic analyses (**Figure 4.8**), it clearly indicated that GNPs are predominantly spherical shapes with an average diameter approximately 15 nm (**Figure 4.8a**). After the conjugation with peptides, the morphological shape of GNP conjugates is slightly changed, and deviated from the right morphological shape, but retained its sphericity. The size of GNP conjugates is approximately 70-80% higher compared to GNPs alone (**Figure 4.8b** and **4.8c**). Furthermore, analyses with EDS experiments showed that the element composition of the GNP conjugates is exclusively comprised of 70% of Au. The element ration (O:C:Au) of linear and cyclic GNPs conjugates measured by EDS analyses demonstrated 36%, 17%, and 26% elements and 28%, 11%, and, 42%.These results clearly proved that thiol-incorporated peptides were perfectly conjugated onto the surface of GNPs. These findings clearly proved the successful attachment of thiol-modified peptides onto the surface of the GNPs.

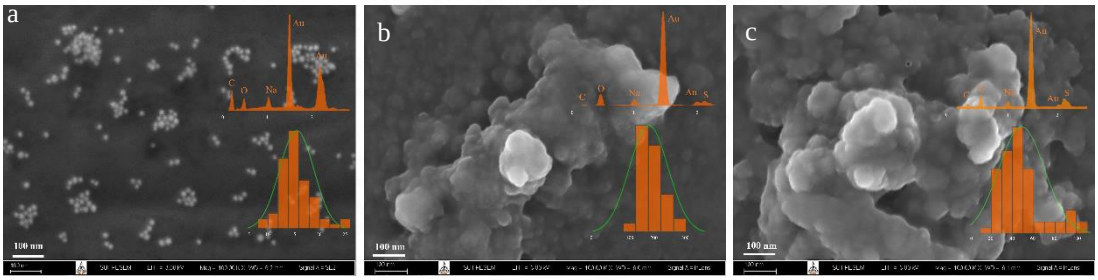

Figure 4.8 SEM pictures with particle size distribution diagrams, and EDS spectrums of (a) GNPs (b) linear thiol-incorporated peptide-GNPs (**6**) and (d) cyclic thiol-incorporated peptide-GNPs (**8**)

4.2.3 The characterization of thiol-incorporated peptides-GNPs by UV and fluorescence spectroscopy

The optical characteristics of thiol-incorporated peptides and thiol-incorporated peptides-GNPs (**1**-**8**) were further investigated *via* UV-vis and fluorescent spectroscopy. According to the results as shown in **Figure 4.9a**, GNPs demonstrated a distinct absorption peak centered at 522 nm, corresponding to horizontal and vertical plasmon resonance (LSPR) of GNPs, and it is an important characteristic of GNPs. Interestingly, thiol-incorporated linear peptides-GNPs (**6**) showed a distinct spectrum centered at 543 nm, which is slightly shifted approximately 21 nm with lightly decreased intensity. Similarly, the thiol-incorporated cyclic peptides-GNPs (**8**) exhibited an absorption peak at 535 nm, accompanied by decreased in intensity. These spectral changes can be attributed to the effective conjugation of thiol-modified peptides onto the GNPs' surface, which consequently led to modifications in the electron oscillation of the GNPs.

Additionally, the presence of tryptophan in thiol incorporated peptides has generated a promising applicability for the investigation of thiol incorporated peptides-GNPs conjugates. Typically, tryptophan demonstrated an excited wavelength at 280 nm, and emission wavelength at 350 nm. The results as shown in **Figure 4.9b** illustrated the fluorescent intensity of tryptophan within the thiol incorporated peptides, displaying an emission peak at 358 and 305 nm for linear and cyclic thiol incorporated, respectively. Additionally, the loading capacity was determined by conjugating thiol-incorporated peptides to GNPs, resulting in loading capacities of approximately 77% and 79% for linear and cyclic thiol-incorporated peptides-GNPs, respectively. Therefore, it clearly indicated the conjugation of thiol incorporated peptides with GNPs.

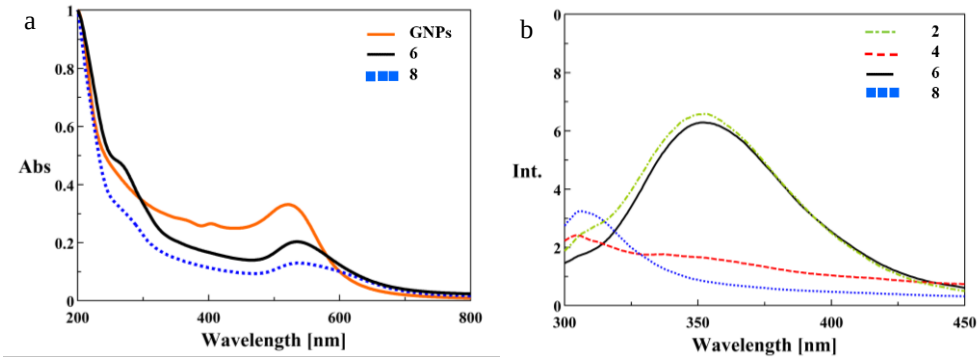

Figure 4.9 Characterization of (a) UV-visible, (b) Fluorescence spectra of GNPs, **6**, **8**, **2** and **4**

4.2.4 The characterization of thiol-incorporated peptides-GNPs by IR spectroscopy

The chemical interaction under investigation is depicted in **Figure 4.10**, where the FT-IR spectra of both GNPs and their conjugates are presented. As compared to that of thiol incorporated peptides, GNPs conjugates demonstrated a comparable characteristic to those of thiol incorporated peptides, having two important characteristic peaks at 3280 and 1600 cm^{-1}, corresponding to the overtone of NH stretching vibration and the C=O stretching vibration, respectively. This obviously establishes the successful conjugation of thiol-modified peptides onto the surfaces of the GNPs.

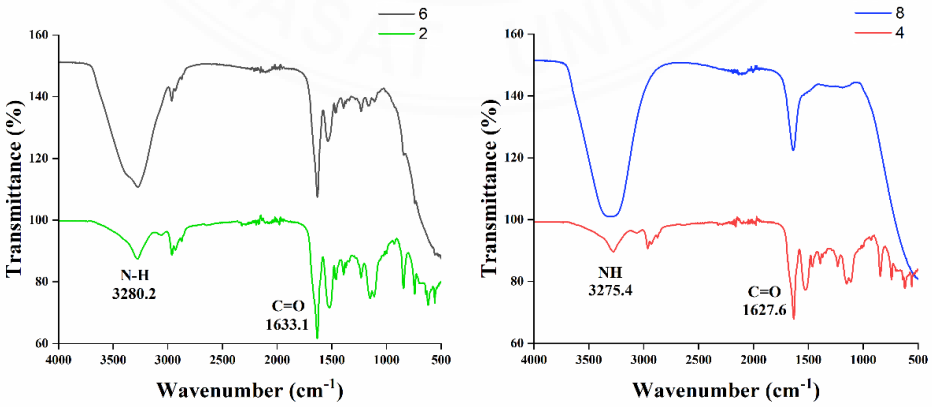

Figure 4.10 Infrared spectra comparison between linear and thiol-incorporated peptides (**2** and **4**) and linear and cyclic thiol-incorporated peptides-GNPs (**6** and **8**)

4.2.5 The characterization of thiol-incorporated peptides-GNPs by XPS spectroscopy

The chemical composition of resulting GNPs conjugates was further investigated by X-ray photoelectron spectroscopy (XPS). According to the XPS full scan, GNPs conjugates represented these major peaks of Au 4f at 88 eV, S 2p at 164 eV, C 1s at 285 eV, N 1s at 400 eV and O 1s at 532 eV as shown in **Figure 4.11**. Regarding to high resolution spectra of each element, Au 4f signal of GNPs conjugates revealed two distinct peaks of Au $4f_{7/2}$ at 84.1 eV and Au $4f_{5/2}$ at 87.3 eV which are slightly shifted from the typical signal of Au $4f_{7/2}$ at 83.7 eV and Au $4f_{5/2}$ at 87.4 eV. This minor shift in the Au 4f signal toward increased binding energy is attributed to Au atoms bound to sulfur.(Camci, Ulgut, Kocabas, & Suzer, 2017),(Tao, Ziemer, & Gill, 2014) The low intensity of peptides-GNPs signal at the Au 4f energy level resulted from the attenuation caused by an abundance of peptide units agglomerated onto the GNPs surface. Likewise, high-resolution spectra of thiol incorporated peptides displayed the signal of $S2p_{3/2}$ and $S2p_{1/2}$ peaks at 163.8 eV and 165.0 eV. While, thiol incorporated peptides-GNPs conjugates showed the observed S2p and S2s peaks of at 163.9 eV and 165.1 eV which are slightly shifted relative to that of peptides alone, which could be attributed to the sulfidation of the surface of GNPs via a strong covalently bond of Au-S bonding as shown in **Figure 4.12b**.(Castner, Hinds, & Grainger, 1996) These results undoubtedly implied the success of the conjugation of thiol incorporated peptides on the surface of the GNPs. Besides, the presence of C 1s, O 1s, and N 1s XPS signals definitely supported the presence of thiol incorporated peptides attached to the surfaces of the GNPs. The C 1s spectra of thiol-incorporated peptide-GNP conjugates are deconvoluted into four distinct peaks at 284.9, 286.3, 288.2, and 289.1 eV, corresponding to C-H, C-N or C-S, H_2N-C-COOH, and O-C=O groups, respectively, as depicted in **Figure 4.12d**. The N 1s spectra of thiol incorporated peptides reveal two peaks at 400.0 and 401.5 eV, represented to the C-NH-C of tryptophan and $–NH_2$, respectively. For thiol-incorporated linear and cyclic peptides-GNPs, the N 1s spectra are deconvoluted into three and one peaks, respectively. The linear form appears at 400.0 (C-NH-C of Tryptophan), 401.0 (NH_2), and 402.2 eV (NH_3^+), while the cyclic form is assigned at 400.1 eV (C-NH-C of Tryptophan).(Artemenko et al., 2021) The O 1s energy level signal remains consistent

in both thiol-incorporated peptide and thiol-incorporated peptide-GNP spectra. The XPS signals in both spectra exhibit three distinct peaks at 531.3, 532.4, and 533.9 eV, corresponding to O=C-N, O=C-OH, and O=C-OH, respectively as depicted in **Figure 4.12e**. These thorough XPS analyses conclusively confirm the successful conjugation of thiol-incorporated peptides with the GNPs.

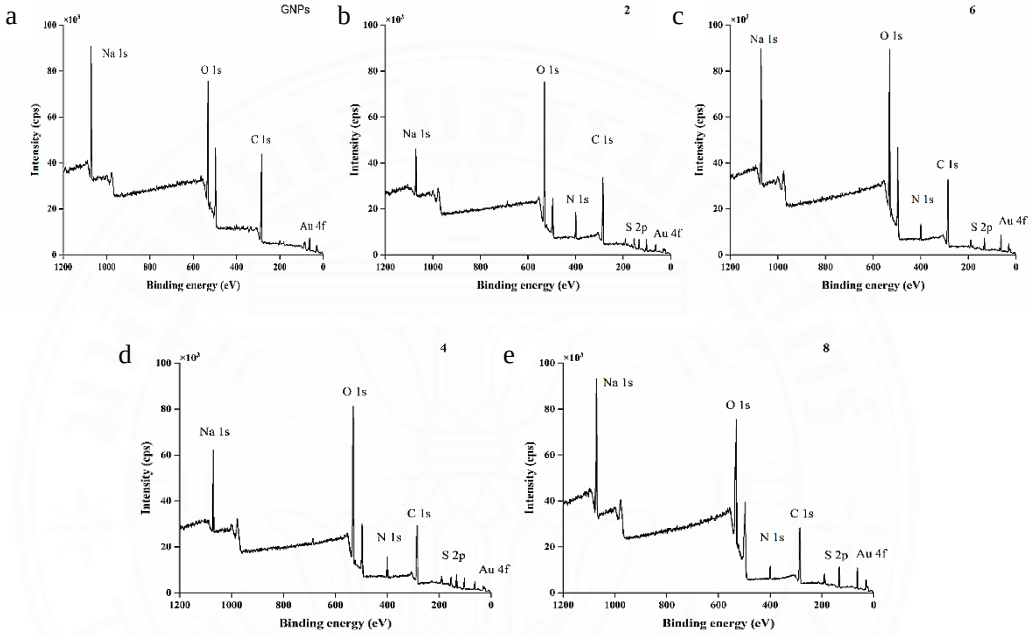

Figure 4.11 XPS full scan of GNPs (a) GNPs, (b) linear thiol-incorporated peptide (**2**), (c) linear thiol-incorporated peptide-GNPs (**6**), (d) cyclic thiol-incorporated peptide (**4**), and (e) cyclic thiol-incorporated peptide-GNPs (**8**)

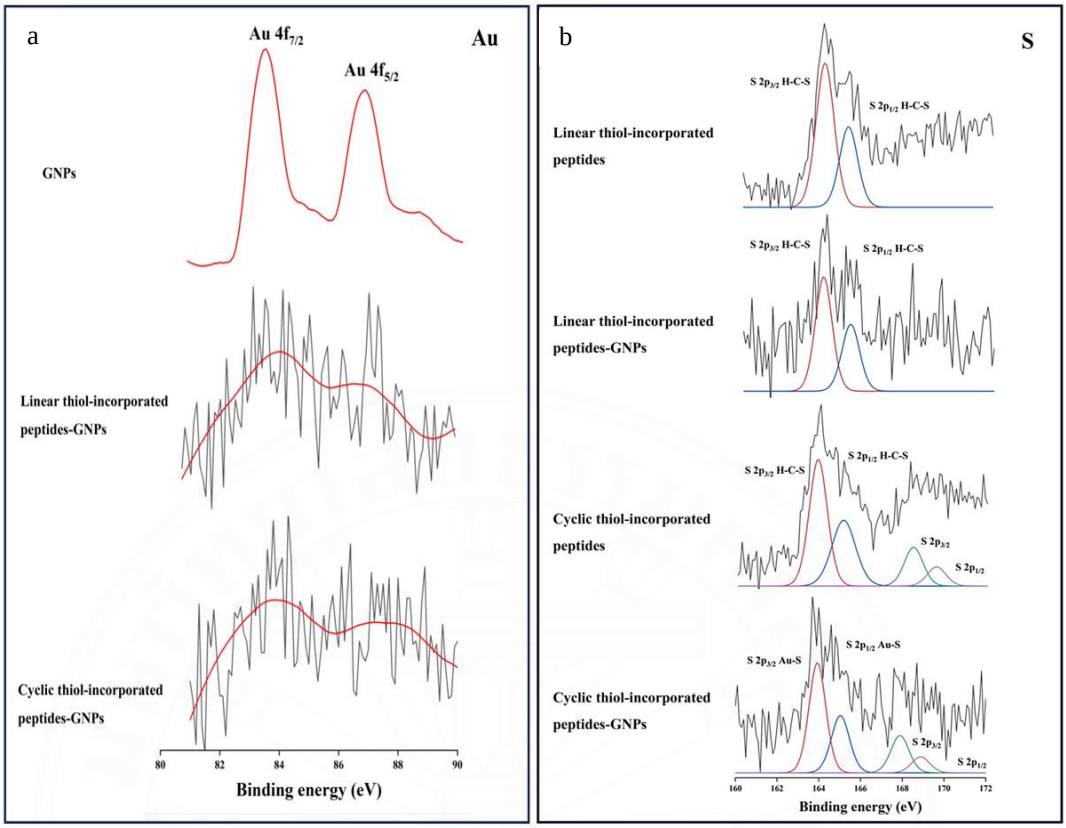

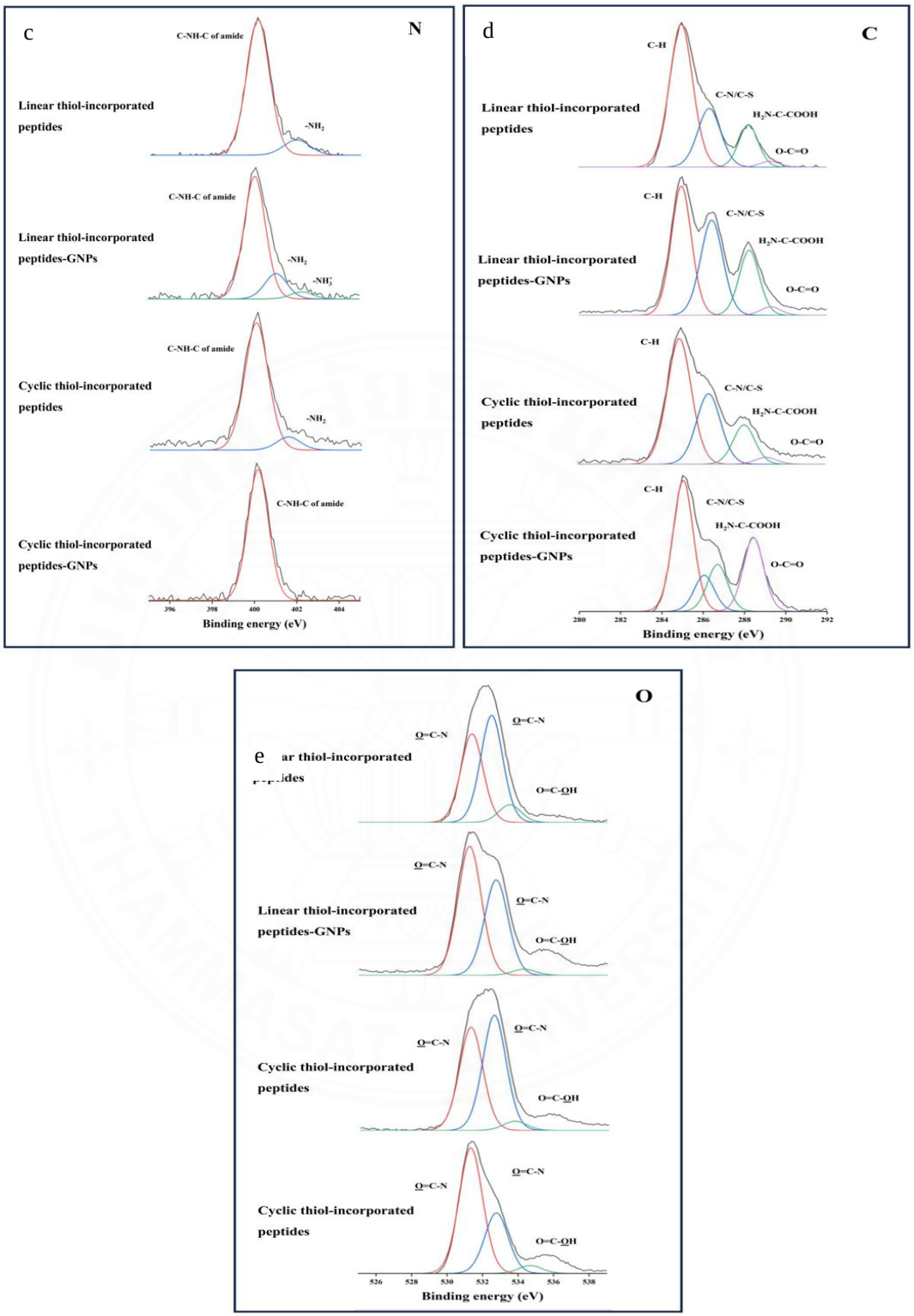

Figure 4.12 High resolution XPS spectra of (a) Au 4f, (b) S 2p (c) N 1s (d) C 1s, and (e) O 1s

4.3 The synthetic strategy of re-engineered mortiamide peptides

4.3.1 The synthesis of linear peptide precursor *via* solid phase peptide synthesis (SPPS)

A linear re-engineered precursor of mortiamide was successfully synthesized *via* solid phase peptide synthesis (SPPS) by using the Fmoc-based SPPS strategy. The process is carried out using the similar approach with thiol-incorporated peptides as previously shown in **Section 4.1.1**. This linear precursor comprises two sequences: H_2N-Val-Val-Val-Phe-Phe-Leu-Val-COOH (**1**) and H_2N-D-Val-Val-D-Val-D-Phe-Phe-D-Leu-Val-COOH (**2**). These sequences were successfully assembled by using 2-chorotrityl chloride (2-CTC) resin as a solid support, following to Fmoc-SPPS strategy without any protecting group. The assembly process for the linear re-engineered mortiamide precursors (**9** and **10**) are described in detail as follows; The initial amino acid loading, Fmoc-Val-OH, was loaded onto the 2-chlorotrityl resin using DIPEA/DMF. Then, the resin was capped with MeOH/DIPEA (10:1) for one h to prevent undesired product formation. Fmoc deprotection was carried out with 20% piperidine in DMF and DCC, DMAP and HOBt were used at the coupling stage. Importantly, a double coupling was highly required at particular residues (D-Phe and L-Phe), effectively increasing the coupling efficacy. Once the backbone assembly has reached the completion, subsequent peptide cleavage (using 1% TFA/DCM) to afford the linear re-engineered mortiamide A precursors (**Scheme 4.3**). The crude peptides were subjected to purification *via* preparative HPLC to afford **1** and **2** with yields of 70% and 75%.

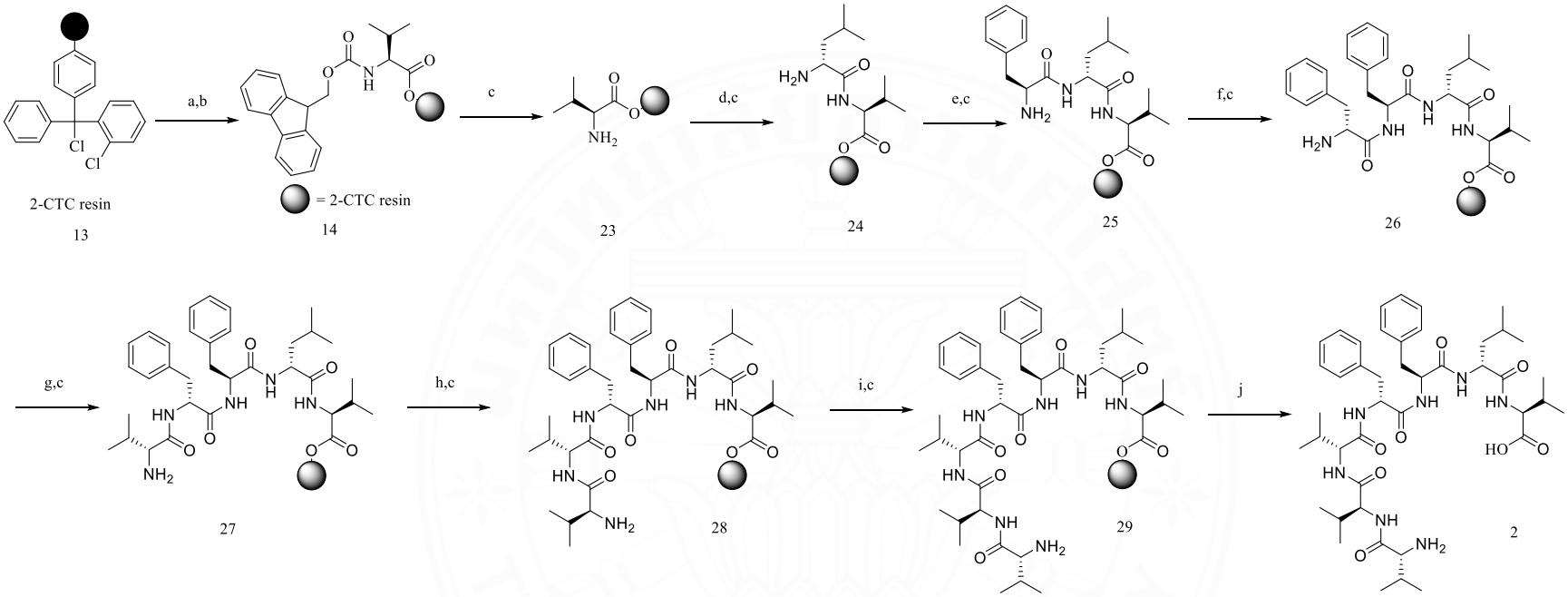

Scheme 4.3 Reagents and conditions Reagents and conditions for the synthesis of linear re-engineered mortiamide peptides: (a) Fmoc-Val-OH, DIPEA, DMF, overnight; (b) MeOH/DIPEA (10:1), 1h; (c) 20% piperidine/DMF 30 min; (d) Fmoc-D-Leu-OH, DCC, DMAP and HOBt/DMF 1h; (e) Fmoc-Phe-OH, DCC, DMAP and HOBt/DMF 1h; (f) Fmoc-D-Phe-OH, DCC, DMAP and HOBt/DMF 1h; (g) Fmoc-D-Val-OH, DCC, DMAP and HOBt/DMF 1h; (h) Fmoc-Val-OH, DCC, DMAP and HOBt/DMF 1h; (i) Fmoc-D-Val-OH, DCC, DMAP and HOBt/DMF 1h; (j) 1% TFA/DCM 5 min; (k) HATU, HOBt, DIPEA/ DMF (1:1) 2 days.

4.3.1.1 Characterization of linear re-engineered mortiamide peptides

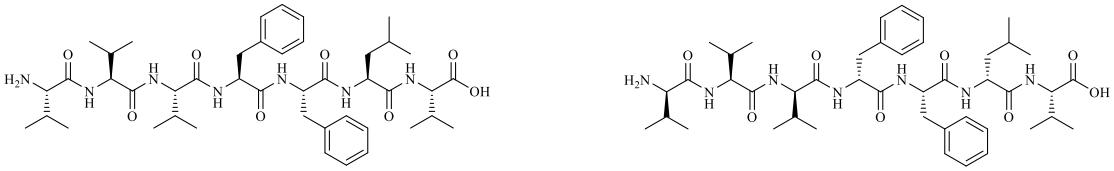

9 10

Figure 4.13 Chemical structures of linear re-engineered mortiamide peptides (**9** and **10**)

Name: linear re-engineered mortiamide peptides (**9** and **10**)

Chemical formula: $C_{44}H_{67}N_7O_8$

(1) Mass spectrum and HPLC chromatogram

TOF-MS: Found; 859.613 $[M+K]^+$ and 908.5758 $[M+2MeOH+Na]^+$; Calculated 821.51 $[M]^+$

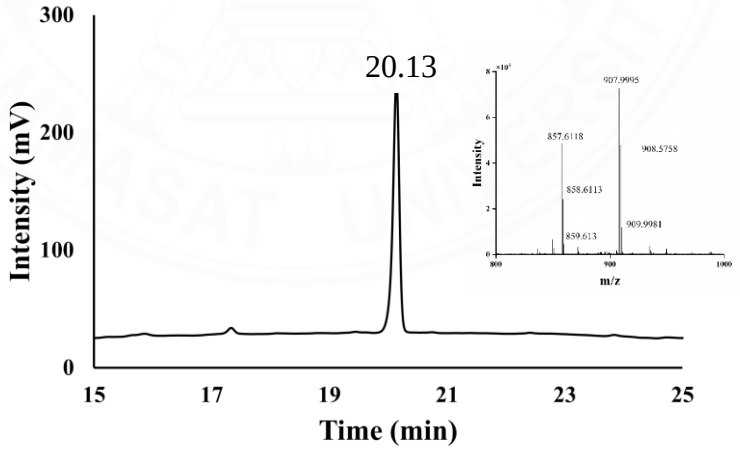

Figure 4.14 HPLC chromatogram and ESI-MS spectrum of linear re-engineered mortiamide peptides (**9** and **10**)

The purity of the linear thiol-incorporated peptides was verified by using an analytical HPLC analysis. The retention time of these peptides was determined to be 20.13 min. Moreover, the TOF-MS spectrum revealed a molecular mass of *m/z* = 859.613 and 908.5758 corresponding to the molecular mass adduct $[M+K]^+$ and $[M+2MeOH+Na]^+$, respectively. The calculated molecular mass was found to be 821.51.

(2) ^{1}H and ^{13}C NMR

^{1}H NMR (400 MHz, DMSO-d_6): δ (ppm) 8.58 (s, 1H), 8.39 (d, 1H, *J* = 6.4 Hz), 8.24-8.14 (m, 3H), 7.97 (d, 1H, *J* = 9.7 Hz), 7.83 (d, 1H, *J* = 9.1 Hz), 7.52 (d, 1H, *J* = 5.7 Hz), 7.30-7.24 (m, 4H), 7.25-7.16 (m, 2H), 7.19-7.13 (m, 4H), 4.61 (q, 1H, *J* = 8.5 Hz), 4.27-4.21 (m, 1H), 4.18 (d, 1H, *J* = 9.8 Hz), 4.10 (dd, 1H, *J* = 8.9, 4.2 Hz), 3.98-3.86 (m , 2H), 3.56-3.48 (m, 1H), 3.22 (d, 2H, *J* = 4.2 Hz), 2.78 (d, 2H, *J* = 8.1 Hz), 2.43-2.30 (m, 2H), 1.88 (dp, 1H, *J* = 9.2, 6.5 Hz), 1.66 (h, 1H, *J* = 6.7 Hz), 1.37-1.20 (m, 1H), 0.99 (s, 2H), 0.96 (s, 3H), 0.93 (d, 3H, *J* = 6.2 Hz), 0.92 (s, 3H), 0.89-0.83 (m, 9H), 0.80 (d, 3H, *J* = 6.1 Hz), 0.74 (d, 3H, *J* = 6.7 Hz), 0.70 (d, 3H, *J* = 6.0 Hz), 0.54 (d, 3H, *J* = 6.8 Hz).

^{13}C NMR (100 MHz, DMSO-d_6): δ (ppm) 172.90, 172.81, 172.72, 171.41,171.08, 170.60, 168.83, 139.46, 137.66, 129.34, 129.31, 128.71, 128.57, 126.90, 126.56, 60.89, 60.63, 59.12, 58.55, 57.13, 56.61, 52.10, 37.96, 34.76, 29.19, 28.83, 28.55, 28.15, 24.06, 24.03, 23.25, 21.89, 19.67, 19.39, 19.38, 19.34, 19.25, 18.85, 18.77, 18.34.

According to the chemical structure of linear re-engineered mortiamide peptides was further elucidated by using ^{1}H-NMR and ^{13}C-NMR spectroscopy. The linear re-engineered mortiamide peptides, comprising four valine residues, two phenylalanine residues, and one leucine residue, displayed well-dispersed NH resonance peaks at 7.52, 7.83, 7.97, 8.17, 8.21, 8.39, and 8.58 ppm. Moreover, the ^{1}H-NMR analysis revealed the chemical shift (δ) of the two phenylalanines in the linear scaffold, with aromatic carbon signals appearing at 7.16-7.27 ppm as shown in **Figure 4.15**. The structural characteristics of the linear re-engineered mortiamide peptides were also supported by the ^{13}C-NMR technique. The resonance peak of the carbonyl resonance peak of amide functionality was observed at chemical shift values (δ_C) ranging from 168.83-172.90 ppm for the linear mortiamide peptides. In particular, two

phenylalanine in a linear scaffold showed the resonance peaks at δ_{CH} = 126.56-129.34 ppm, including resonances at δ_C = 137.66 and 139.46 ppm as shown in **Figure 4.16**.

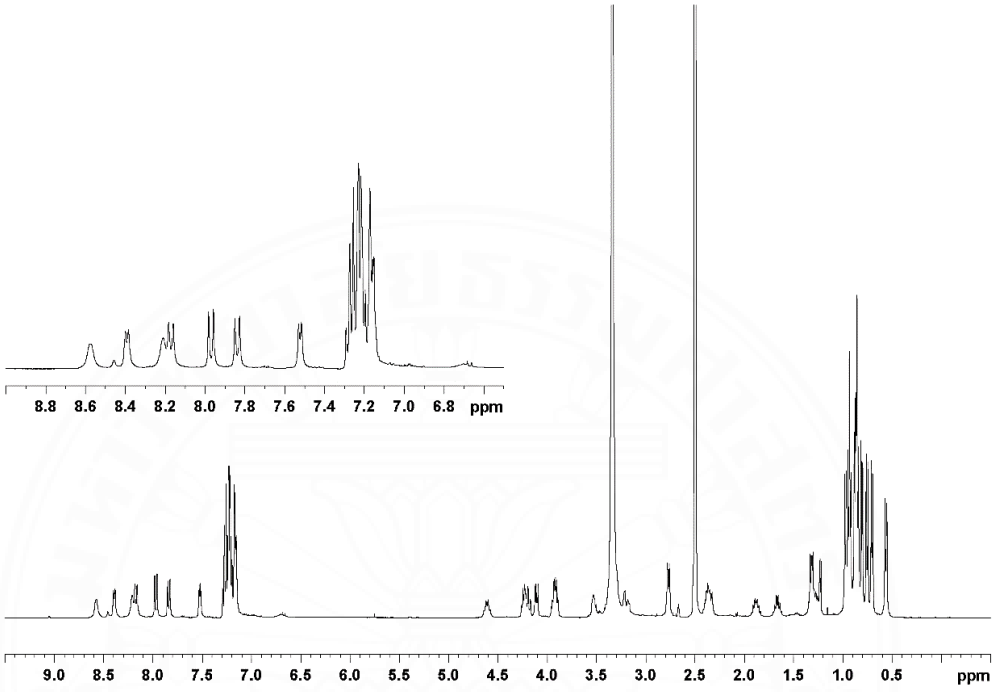

Figure 4.15 ^{1}H- NMR spectrum of linear re-engineered mortiamide (**10**) in DMSO-d_6

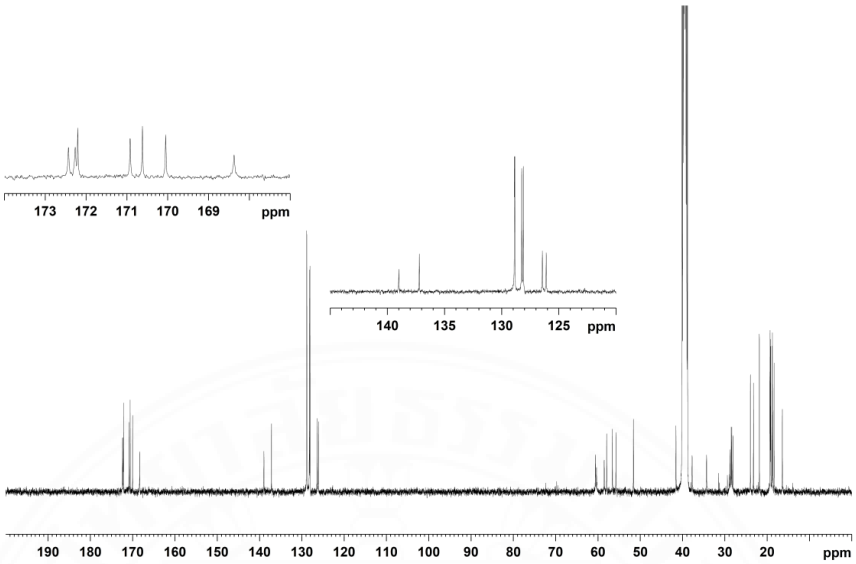

Figure 4.16 ^{13}C- NMR spectrum of linear re-engineered mortiamide (**10**) in DMSO-d_6

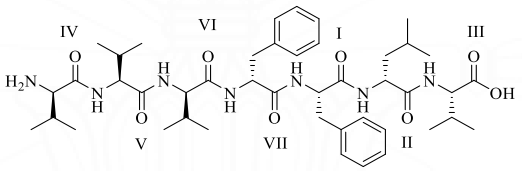

10

Table 4.1

^{1}H (400 MHz) and ^{13}C (100 MHz) NMR Data of linear re-engineer mortiamide **9** and **10** in DMSO-d_6

sequence	position	δ_C (ppm)	δ_H (ppm)
Phe^{I}	CO	168.83	
	NH		7.97 d (9.7 Hz)
	α (CH)	56.61	4.61 q (8.5 Hz)
	β (CH_2)	37.96	2.78 d (2.81 Hz)
	1'(C)	139.46	
	2' (CH)	128.71	7.27 m
	3' (CH)	129.31	7.16 m
	4' (CH)	126.90	7.22 m
Phe^{II}	CO	170.60	
	NH		8.39 d (6.4 Hz)
	α (CH)	57.13	3.94 m
	β (CH_2)	34.75	3.22 d (4.2 Hz)
	1'(C)	137.66	
	2' (CH)	128.57	7.27 m
	3' (CH)	129.34	7.16 m
	4' (CH)	126.56	7.22 m
Val^{III}	CO	171.41	
	NH		8.21 m
	α (CH)	60.89	3.54 m
	β (CH_2)	28.83	1.66 h (6.7 Hz)
	γ_1 (CH_3)	18.85	0.54 d (6.8 Hz)
	γ_2 (CH_3)	19.67	0.74 d (6.7 Hz)
Val^{IV}	CO	172.72	
	NH		8.58 s
	α (CH)	60.63	3.90 m
	β (CH_2)	28.55	1.88 dq (9.2, 6.5 Hz)

sequence	position	δ_C (ppm)	δ_H (ppm)
	γ_1 (CH_3)	23.25	0.93 d (6.2 Hz)
	γ_2 (CH_3)	19.25	0.83 m
Val^V	CO	172.90	
	NH		8.17 m
	α (CH)	58.55	4.10 dd (8.9, 4.2 Hz)
	β (CH)	29.19	2.36 m
	γ_1 (CH_3)	19.34	0.96 s
	γ_2 (CH_3)	18.39	0.84 m
Val^{VI}	CO	172.81	
	NH		7.52 d (5.7 Hz)
	α (CH)	52.10	4.22 m
	β (CH_2)	24.06	1.30 m
	γ_1 (CH_3)	21.89	0.80 d (6.1 Hz)
	γ_2 (CH_3)	24.03	0.70 d (6.0 Hz)
Leu^{VII}	CO	171.08	
	NH		7.83 d (9.1 Hz)
	α (CH)	59.12	4.18 d (9.8 Hz)
	β (CH_2)	28.15	2.35 m
	γ (CH)	19.38	0.99 s
	δ_1 (CH_3)	18.77	0.92 s
	δ_2 (CH_3)	18.39	0.86 m

4.3.2 The synthesis of cyclic re-engineered mortiamide peptides

To perform the macrocyclization of linear re-engineered mortiamide precursors, the highly diluted condition (approximately 1 mg/mL) was employed, effectively preventing the formation of open-chain oligomerization and dimerization side products. It is greatly related to the significant entropy loss during the macrocyclization.(Marti-Centelles et al., 2015) The synthetic methodology is describe in **Scheme 4.4**, illustrating the assembly and cyclization of all re-engineered mortiamide peptides. The process followed the similar approach as previously described in **Section 4.1.2**. Importantly, no epimerization is observed under high

dilution condition. The presence of alternating D- and L-configurations at N- and C-terminus in linear re-engineered mortiamide peptides induced a favorable turn-inducing effect which significantly to increase the macrocyclization efficacy.(Hill, Birch, Jeffs, & North, 2003) Interestingly, it was observed that linear re-engineered mortiamide precursor comprising of all L-configuration resulted in the formation of cyclic re-engineered mortiamide (**11**) with a yield of 49%. On the other hand, a linear precursor (**12**) incorporating alternated D- and L-configurations yielded cyclic mortiamide with a yield of 53%. This clearly indicated that the presence of alternating D- and L-configuration in a linear re-engineered mortiamide precursor is of significantly importance for the cyclization efficacy.

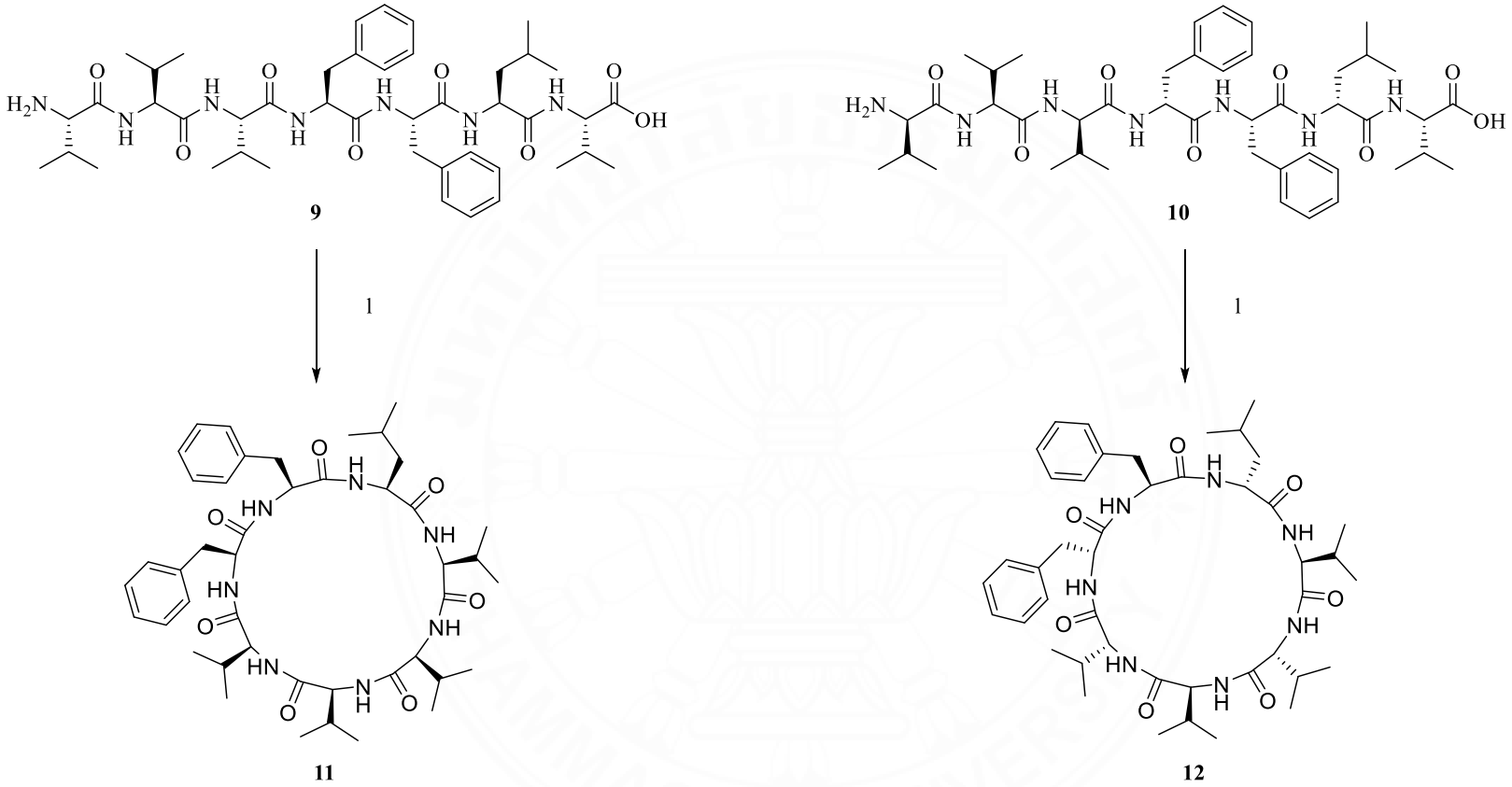

Scheme 4.4 Reagents and conditions for the synthesis of cyclic re-engineered mortiamide peptides: (l) HATU, HOBt, DIPEA/ DMF (1mg:1ml) 2 days.

4.3.2.1 Characterization of cyclic re-engineered mortiamide peptides

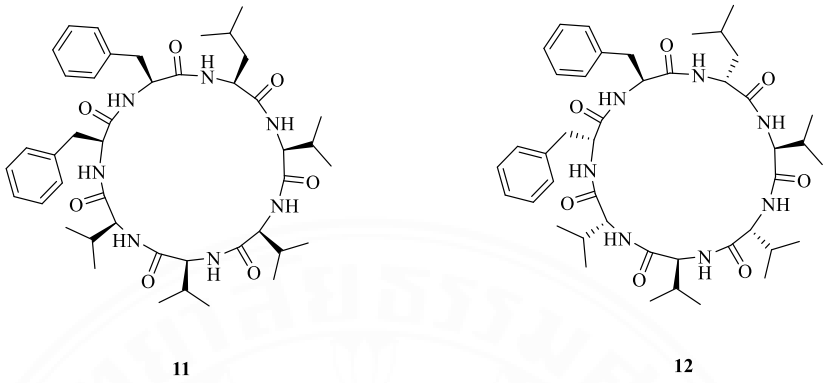

11 **12**

Figure 4.17 Chemical structures of cyclic re-engineered mortiamide peptides (**11** and **12**)

Name: cyclic re-engineered mortiamide peptides (**11** and **12**)

Chemical formula: $C_{44}H_{65}N_7O_7$

(1) Mass spectrum and HPLC chromatogram

TOF-MS: Found; 804.5582 $[M+H]^+$; Calculated 803.49 $[M]^+$

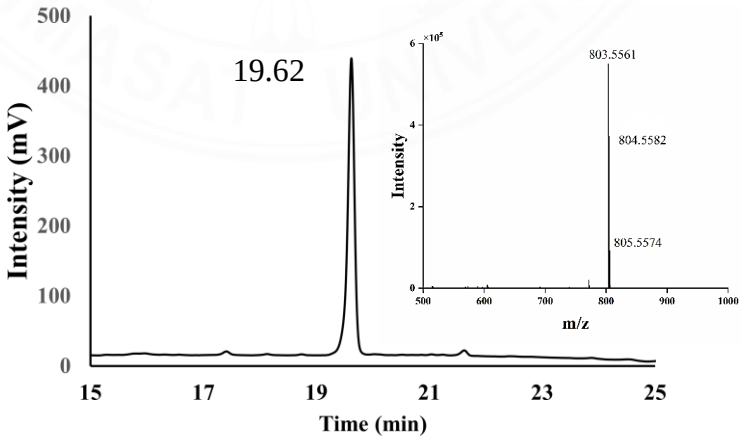

Figure 4.18 HPLC chromatogram and ESI-MS spectrum of cyclic re-engineered mortiamide peptides (**11** and **12**)

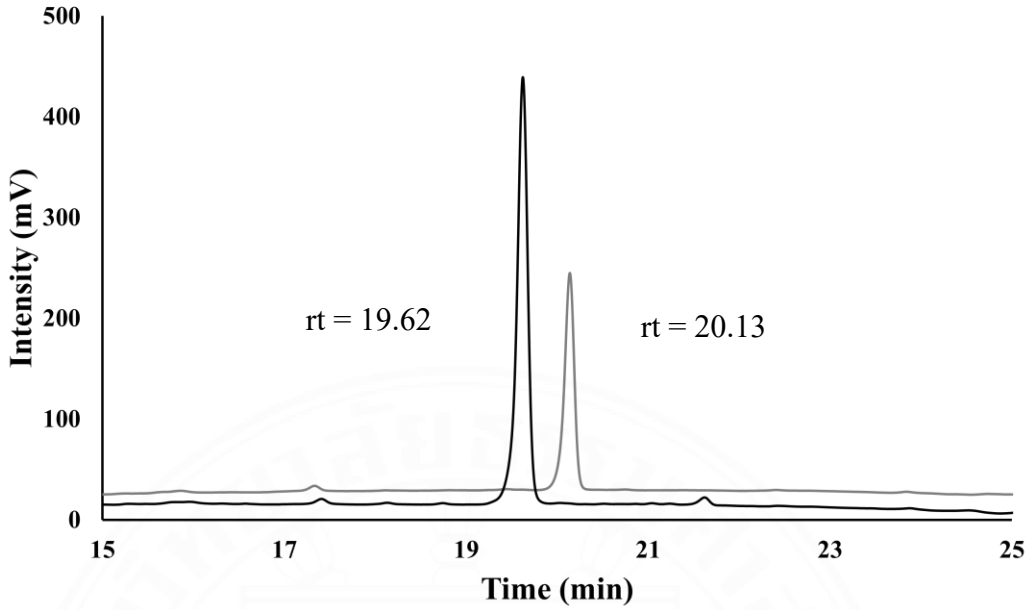

Figure 4.19 Comparison of HPLC chromatogram between linear (grey line) and cyclic (black line) re-engineered mortiamide peptides

According to HPLC chromatogram results (**Figure 4.14**), the purity of linear re-engineered mortiamide A precursors (alternated DL-configuration) was further verified by using analytical RP-HPLC, showing a single peak with the retention time at 20.31 min. While, the cyclic re-engineered mortiamide A displayed a single peak at 19.6 min that is slightly shorter (more hydrophilic) relative to that of a linear mortiamide A precursor as shown in **Figure 4.19**, clearly indicating that macrocyclization was successful. Furthermore, the re-engineered cyclic mortiamide A peptide, possessing the DL-configuration, exhibited a molecular ion at m/z 803.5561, corresponding to $[M+H]^+$. Consequently, this result demonstrates the successful synthesis of the cyclic re-engineered peptides.

(2) ^{1}H and ^{13}C NMR

^{1}H NMR (400 MHz, DMSO-d_6): δ (ppm) 8.42 (s, 1H), 8.39 (s, 1H), 8.33 (d, 1H, J = 4.5 Hz), 8.26 (d, 1H, J = 8.3 Hz), 7.86 (d, 1H, J = 9.2 Hz), 7.78 (d, 1H, J = 10.4 Hz), 7.60 (d, 1H, J = 4.5 Hz), 7.34-7.27 (m, 4H), 7.28-7.17 (m, 2H), 7.17-7.06 (m, 4H), 4.28 (dt, 1H, J = 9.3, 4.4 Hz), 4.12-4.03 (m, 3H), 3.96 (ddd, 1H, J = 12.4, 8.8, 4.2 Hz), 3.92 (d, 2H, J = 3.2), 3.83 (dd, 1H J = 9.3, 3.9),2.73-2.46 (m, 2H), 2.39 (qd, 1H, J = 7.0, 4.2

Hz), 2.27-2.21 (m, 2H), 2.19-2.11 (m, 1H), 1.82 (dt, 1H, *J* = 9.1, 6.5 Hz), 1.67 (dq, 1H, *J* = 13.0, 6.5), 1.50-1.42 (m, 1H), 1.31-1.20 (m, 2H), 0.94 (d, 3H, *J* = 6.5 Hz), 0.91 (d, 12H, *J* = 6.5 Hz), 0.87-0.77 (m, 12H), 0.75 (d, 3H, *J* = 6.4 Hz).

^{13}C NMR (100 MHz, DMSO-*d*$_6$): δ (ppm) 172.38, 172.10, 171.36, 170.42, 170.42, 170.36, 169.58, 136.61, 136.09, 129.27, 128.85, 128.08, 127.97, 126.44, 126.35, 60.74, 60.43, 58.23, 57.64, 56.06, 54.86, 50.73, 36.59, 35.77, 31.42, 28.79, 28.58, 27.72, 24.46, 23.19, 21.97, 20.35, 19.84, 19.38, 19.01, 18.93, 18.69, 18.63, 16.30, 13.84.

The chemical structure of cyclic re-engineered mortiamide peptides was further verified by using ^{1}H-NMR and ^{13}C-NMR spectroscopy. The ^{1}H-NMR analyses for the cyclic re-engineered mortiamide peptide revealed all NH resonance peaks at 7.60, 7.78, 7.86, 8.26, 8.33, 8.39, and 8.42 ppm. According to ^{1}H-NMR results, two phenylalanine residues in the cyclic scaffold exhibited distinct and well-dispersed resonance peaks within the range of δ = 7.10-7.30 ppm as shown in **Figure 4.20**. Furthermore, the difference between the two re-engineered mortiamide peptides was confirmed by using the ^{13}C-NMR technique. The resonance peak of the amide carbonyl functionality was observed at chemical shift values of δ_C ranging from 169.58-172.38 ppm. In particular, two phenylalanine in the cyclic scaffold showed the resonance peaks at δ_{CH} = 126.35-129.27 ppm, including the resonances at δ_C = 136.09 and 136.61 ppm as shown in **Figure 4.21**. This strongly indicated the achievement of mortiamide peptide cyclization. The great difference of ^{1}H-NMR pattern between two phenylalanines in both linear and cyclic mortiamide peptides could be ascribed as the results of □-□ interaction, hydrogen bonding and the anisotropic effect, resulting in the variation of folding in all re-engineered mortiamide peptides.

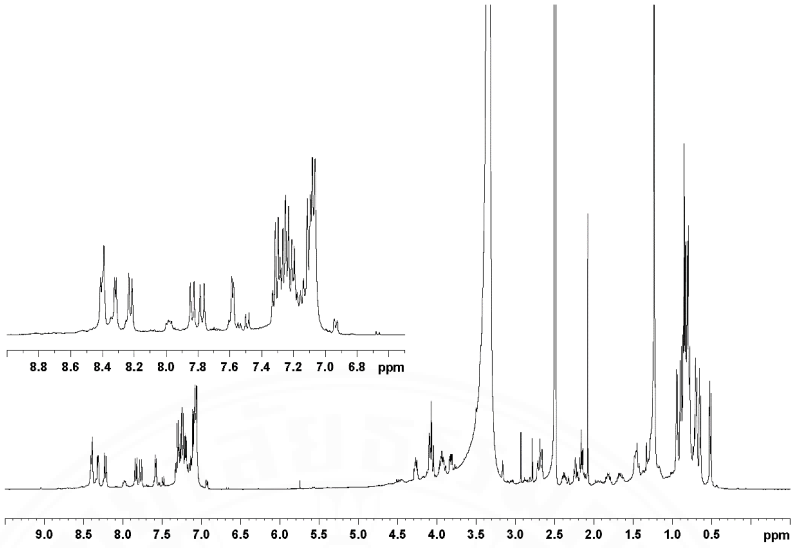

Figure 4.20 ^{1}H- NMR spectrum of re-engineered mortiamide (**12**) in DMSO-d_6

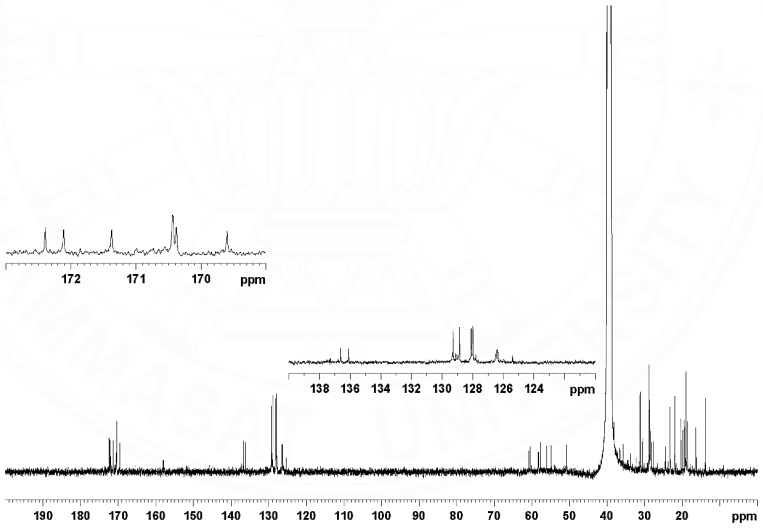

Figure 4.21 ^{13}C- NMR spectrum of re-engineered mortiamide (**12**) in DMSO-d_6

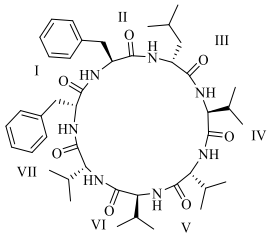

12

Table 4.2

^{1}H (400 MHz) and ^{13}C (100 MHz) NMR Data of cyclic re-engineer mortiamide **11** and **12** in DMSO-d_6

sequence	position	δ_C (ppm)	δ_H (ppm)
Phe^{I}	CO	171.36	
	NH		7.60 d (4.5 Hz)
	α (CH)	56.06	4.28 dt (9.3, 4.4 Hz)
	β_A (CH)	36.59	2.68 m
	β_B (CH)		2.24 m
	1'(C)	136.61	
	2' (CH)	129.27	7.10 m
	3' (CH)	128.08	7.30 m
	4' (CH)	126.44	7.19 m
Phe^{II}	CO	169.58	
	NH		8.39 s
	α (CH)	54.86	3.92 d (3.2 Hz)
	β_A (CH)	35.77	2.71 m
	β_B (CH)		2.25 m
	1'(C)	136.09	
	2' (CH)	128.85	7.24 m
	3' (CH)	127.97	7.30 m
	4' (CH)	126.35	7.19 m
Val^{III}	CO	170.42	
	NH		8.33 d (4.5 Hz)
	α (CH)	50.73	3.96 ddd (12.4, 8.8, 4.2
	β (CH_2)	21.97	Hz)
	γ_1 (CH_3)	23.19	1.28 m
	γ_2 (CH_3)	19.84	0.83 m
			0.91 d (6.5 Hz)
Val^{IV}	CO	170.36	

sequence	position	δ_C (ppm)	δ_H (ppm)
	NH		8.26 d (8.3 Hz)
	α (CH)	58.23	4.10 m
	β (CH_2)	27.72	2.39 m
	γ_1 (CH_3)	16.30	0.80 m
	γ_2 (CH_3)	13.84	0.88 m
Val^V	CO	172.10	
	NH		7.78 d (10.4 Hz)
	α (CH)	57.64	4.09 m
	β (CH_2)	31.42	1.67 dq (13.0, 6.5 Hz)
	γ_1 (CH_3)	19.01	0.89 d (6.5 Hz)
	γ_2 (CH_3)	18.93	0.75 d (6.4 Hz)
Val^{VI}	CO	170.42	
	NH		8.42 s
	α (CH)	60.43	3.83 dd (9.3, 3.9 Hz)
	β (CH_2)	28.79	1.82 dt (9.1, 6.5 Hz)
	γ_1 (CH_3)	20.35	0.94 d (6.5 Hz)
	γ_2 (CH_3)	18.63	0.83 m
Leu^{VII}	CO	172.38	
	NH		7.86 d (9.2 Hz)
	α (CH)	60.74	4.07 m
	β_A (CH)	24.46	1.46 m
	β_B (CH)		1.23 m
	γ (CH)	28.58	2.15 m
	δ_1 (CH_3)	18.69	0.81 m
	δ_2 (CH_3)	19.38	0.91 d (6.5 Hz)

4.4 The CD analysis and biological activity

4.4.1 CD analysis

To gain more insight about the secondary structure of re-engineered mortiamide peptides, qualitative analyses of chemical shift differences of the amide

functionality (ΔNH) and ΔH_α provided the important information about its secondary structure. The downfield shift in the H_α resonances indicates the formation of a β-sheet structure at a hydrogen-bonded site with a significant chemical shift difference (>0.1 ppm) relative to the random coil state.(Mishra, Deshmukh, & Venkatnarayan, 2014),(Pandey, Thomas, Forbes, & Zondlo, 2014) According to **Figure 4.24**, residues Phe^{I}, Val^{VI} and Leu^{VII} showed a very strong upfield shift that is typical for residues in a turn conformation as shown in **Figure 4.24b**. On contrary, Val^{III}, and Val^{IV} residues exhibited a downfield shift, which is consistent with the pattern expected for an antiparallel β-sheet. NH chemical shift dispersion as depicted in **Figure 4.24b** demonstrated the conformational characteristic pattern between unordered structure of linear mortiamide A peptides and □-hairpin structure of cyclic mortiamide A peptides, indicating that mortiamide A peptides gained a strong chemical shift dispersion of the backbone amide protons similar to those of folded peptides. These findings have significant implications for the structural characteristic of mortiamide A peptides, greatly adopting a conformational β-hairpin structure.

To further investigate the conformational characteristic for mortiamide A peptides by using circular dichroism (CD) spectroscopy. Mortiamide A peptides (0.2 μM) were dissolved in acetonitrile, and the CD spectrum of each mortiamide A solution was recorded by measuring the mean residue molar ellipticity (degree cm^2/dmol) at room temperature. For each measurement, five scans were accumulated by using resolution of 1 nm, a bandwidth of 0.5 nm, and a response time of 1s. CD spectra are mainly based on far-UV absorption region of left *versus* right circularly polarized light which exhibited excitation of electronic transition in amide groups.(Micsonai et al., 2015) According to CD results (**Figure 4.24a**), linear re-engineered mortiamide peptide (**10**) produced one positive molar ellipticity maxima between λ = 195-200 nm, and one negative molar ellipticity minima between λ = 210-220 nm, corresponding to a typical characteristic of β-sheet conformation. Interestingly, linear mortiamide A peptide with all L-configuration (**9**) demonstrated an inverse CD pattern to that of linear mortiamide A peptide (**10**), which showed negative maximum between λ = 195-200 nm, and one positive molar ellipticity minimum between λ = 210-220 nm. The deconvolution of spectrum using BeStSel program afforded 79% of β-sheet in linear mortiamide A peptide (**9**), 72% of β-sheet in linear re-engineered

mortiamide peptide (**10**), 56.5% of β-sheet in cyclic re-engineered mortiamide peptide (**11**), and 77.8% of β-sheet in cyclic re-engineered mortiamide peptide (**12**). The comparison of CD spectra between linear and cyclic mortiamide scaffold provided the great insights in their conformational structures. Notably, the largest difference of secondary structure between linear and cyclic mortiamide peptides is observed in **Figure 4.24** whereby the lack of secondary structure in cyclic mortiamide peptides could possibly be ascribed as the result of the significant rigidity of a cyclic moiety.

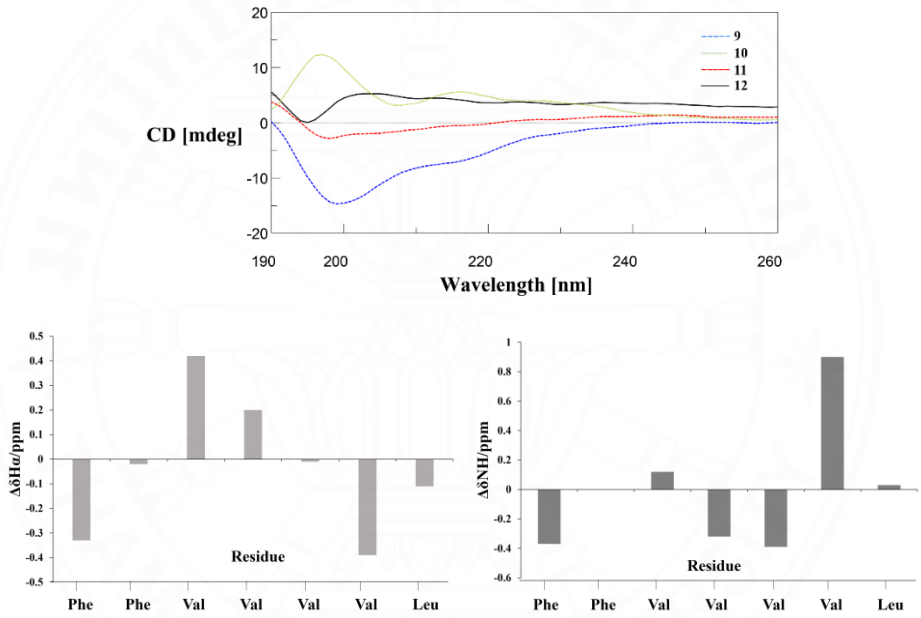

Figure 4.24 (a) CD spectra of 0.2 μM of **9** (blue), 0.25 μM of **10** (green), 0.24 μM of **11** (red) and 0.26 μM of **12** (black) dissolved in acetonitrile (ACN). (b) Bar plot of the H_α and NH chemical shift differences ($\Delta\delta_{cyclic\text{-}linear}$) between re-engineered linear and cyclic mortiamide peptides

4.4.2 The antimicrobial activity

The re-engineered heptapeptides **9**-**12** were assayed for biological activity against both gram-positive and -negative bacteria including *Bacillus cereus* (ATCC 11778), *Listeria monocytogenes* (10403s), *Staphylococcus aureus* (ATCC 25923), *Staphylococcus epidermidis* (ATCC 12228), *Acinetobacter baumannii* (ATCC

19606), *Escherichia coli* (ATCC 25922), *Pseudomonas aeruginosa* (ATCC 27853), *Salmonella typhimurium* (ATCC 13311) and *Shigella sonnei* (ATCC 11060). However, the results indicated that no compound exhibited significant activity at a concentration of 125 μg/mL.

Table 4.3

The MIC values of antibiotics test

MIC (MBC) (μg/mL)				
	9	**10**	**11**	**12**
Gram-positive bacteria				
Bacillus cereus ATCC 11778	>125	>125	>125	>125
Listeria monocytogenes 10403s	>125	>125	>125	>125
Staphylococcus aureus ATCC 25923	>125	>125	>125	>125
Staphylococcus epidermidis ATCC 12228	>125	>125	>125	>125
Gram-negative bacteria				
Acinetobacter baumannii ATCC 19606	>125	>125	>125	>125
Escherichia coli ATCC 25922	>125	>125	>125	>125
Pseudomonas aeruginosa ATCC 27853	>125	>125	>125	>125
Salmonella Typhimurium ATCC 13311	>125	>125	>125	>125
Shigella sonnei ATCC 11060	>125	>125	>125	>125

4.4.3 In *vitro* anti-*Plasmodium falciparum* activity

Interestingly, an inhibitory activity of the *Plasmodium falciparum* proliferation was further investigated *via* in *vitro* susceptibility assays for the determination of the IC_{50}. To this assay, we performed an antiplasmodium activity against two strains of *plasmodium falciparum* parasites; *Plasmodium falciparum* sensitive strain TM4/8.2 and multidrug resistance strain V1/S by using cycloguanil and

pyrimethamine as the positive control. As seen from **Table 4.4**, a linear re-engineered mortiamide peptide **(9)**, and its cyclic counterpart with all L-configuration **(11)**, not only showed the antiplasmodium inhibition against *Plasmodium falciparum* sensitive strain TM4/8.2 with the IC_{50} values of 23.6 ± 1.80 μM and 6.25 ± 0.52 μM, respectively. But, they also demonstrated an impressive inhibitory activity against *Plasmodium falciparum* multidrug resistance strain V1/S with the IC_{50} values of 15.4 ± 2.96 μM and 5.04 ± 2.60 μM, respectively. Likewise, a cyclic re-engineered mortiamides with DL-configuration **(12)** demonstrated IC_{50} values of 4.83 ± 0.10 μM and 3.75 ± 0.70 μM against *Plasmodium falciparum* sensitive strain TM4/8.2 and multidrug resistance strain V1/S, respectively. While, a linear re-engineered mortiamides **(10)** showed the greater potency relative to its cyclic counterpart **(12)** with the IC_{50} values of 3.57 ± 0.52 μM and 2.81 ± 0.70, respectively. All re-engineered mortiamide A peptides (**9-12**) were also examined for the cytotoxicity against the Vero cell line, only cyclic re-engineered mortiamide A peptides (**11** and **12**) showed a slight activity against the Vero cell line with IC_{50} values of 23.1 ± 0.91 and 20.3 ± 0.44 μM, respectively. Interestingly, a linear re-engineered mortiamide A with D/L-configuration **(10)** showed the greatest the antiplasmodial activity against both *Plasmodium falciparum* sensitive strain TM4/8.2 and multidrug resistance strain V1/S without any cytotoxicity. While, its cyclic counterpart (**12**) displayed approximately 2-fold inferior antiplasmodial inhibition with a negligible cytotoxicity. Notably, it should be summarized that the antiplasmodial inhibition of all hybrid mortiamide A peptides are greatly associated with the stereoconfiguration of amino acid component rather than the scaffold. As clearly seen from **Table 4.4**, a linear re-engineered mortiamide A peptide with D/L-configuration (**2**) showed the greater antiplasmodial inhibitory activity relative to cyclic mortiamide A peptides with D/L and all L-configuration (**12** and **11**) without any cytotoxicity.

Table 4.4

The antiplasmodial activity (IC_{50} values) and *in vitro* cytotoxic IC_{50} values against VERO cell line

Compounds	**IC_{50} (μM) ± SD**		
	P. falciparum **(TM4/8.2)**	***P. falciparum*** **(V1/S)**	**VERO**
9	23.6 ± 1.80	15.4 ± 2.96	>50
10	3.57 ± 0.52	2.81 ± 0.70	>50
11	6.25 ± 0.52	5.04 ± 2.60	23.1 ± 0.91
12	4.83 ± 0.10	3.75 ± 0.70	20.3 ± 0.44
Cycloguanil	0.11 ± 0.03	>100	>100
Pyrimethamine	0.43 ± 0.07	>100	81.6 ± 9.64

CHAPTER 5
CONCLUSIONS AND RECOMMENDATIONS

Conclusions

To this work, syntheses and conjugation of thiol-incorporated peptides with GNPs were successfully performed. The design of these thiol-incorporated peptides greatly involved the modification of lugdunin in which a cysteine residue was replaced at a thiazolidine moiety in the lugdunin sequence while retaining all other amino acids and stereochemistry. The synthetic pathway of thiol-incorporated peptides was divided into three important parts. Firstly, an assembly of linear thiol-incorporated peptides with alternated D/L and all-L stereoconfiguration amino acids NH_2-Val-Val-Cys(Trt)-Val-Trp(Boc)-Leu-Val-Fmoc and NH_2-D-Val-Val-Cys(Trt)-D-Val-Trp(Boc)-D-Leu-Val-Fmoc *via* Fmoc based SPPS strategy. Both fully protected linear precursors were subsequently globally deprotected to afford NH_2-Val-Val-Cys-Val-Trp-Leu-Val-COOH (**1**) and NH_2-D-Val-Val-Cys-D-Val-Trp-D-Leu-Val-COOH (**2**) with the yield of 60% and 65%, respectively. Next, the macrocyclization of cyclic thiol-incorporated peptides were performed, two linear precursors (**1** and **2**) were investigated the cyclization efficacy. As a result, the linear peptides (**1** and **2**) without any side chain as protecting group were cyclized perfectly with high yield to afford all cyclic thiol-incorporated peptides (**3** and **4**) with the yield of 59% and 61% without any oligomerization and dimerization byproducts observed. Finally, both linear and cyclic thiol-incorporated peptides were further conjugated with GNPs with a loading capacity of approximately 77% and 79% for linear and cyclic thiol-incorporated cyclic peptide-GNPs, respectively. Then, all thiol-incorporated-GNPs were characterized to examine the conjugation between peptide and GNPs under spectroscopic approaches (with UV-Vis, Fluorescence, IR, XPS spectroscopy, including scanning electron microscopy). Furthermore, all synthetic thiol-incorporated peptide-GNPs will be investigated the biological activity against a panel of bacteria, including against anti-TB in the future.

Secondly, a novel synthetic strategy of re-engineered mortiamide peptides was reported, including the assessment of an anti-plasmodial inhibitory activity against *Plasmodium falciparum* sensitive strain TM4/8.2 and multidrug resistance strain V1/S. These re-engineered mortiamide peptides were designed based mainly on the combination of mortiamide and lugdunin scaffold, resulting in two series with alternated D/L and all-L stereoconfiguration amino acids according to Fmoc based SPPS strategy. All of re-engineered mortiamide peptides demonstrated anti-plasmodial inhibitory activities against both sensitive strain TM4/8.2 and multidrug resistance strain V1/S. Among all re-engineered mortiamide A peptides (**9-12**), a linear mortiamide A peptide with alternated D/L configuration (**10**) effectively showed an impressive anti-plasmodial activity against *Plasmodium falciparum* sensitive strain TM4/8.2 with an IC_{50} value of 3.57 ± 0.52, and also displayed an inhibition against multidrug resistance strain V1/S with an IC_{50} value of 2.81 ± 0.70, which is the highest potency against *Plasmodium falciparum* in the series without any cytotoxicity. All cyclic re-engineered mortiamide A peptides with alternated D/L and all-L configuration (**12** and **11**) not only showed the antiplasmodial activity against *Plasmodium falciparum* sensitive strain TM4/8.2 with an IC_{50} value of 4.83 ± 0.10 μM and 6.25 ± 0.52 μM, respectively, but they also exhibited an anti-plasmodial activity against multidrug resistance strain V1/S with an IC_{50} value of 3.75 ± 0.70 μM and 5.04 ± 2.60 μM with slight cytotoxicity. The discovery of re-engineered mortiamide A peptides with alternated D/L and all-L configuration could potentially be the great platform for further development of antimalarial drug candidates.

REFERENCES

Al-Warhi, T. I., Al-Hazimi, H. M., & El-Faham, A. (2012). Recent development in peptide coupling reagents. *Journal of Saudi Chemical Society, 16*(2), 97-116.

Andrews, J. M. (2001). Determination of minimum inhibitory concentrations. *Journal of antimicrobial Chemotherapy, 48*(suppl_1), 5-16.

Artemenko, A., Shchukarev, A., Štenclová, P., Wågberg, T., Segervald, J., Jia, X., & Kromka, A. (2021). *Reference XPS spectra of amino acids.* Paper presented at the IOP Conference Series: Materials Science and Engineering.

Auvin-Guette, C., Baraguey, C., Blond, A., Xavier, H. S., Pousset, J.-L., & Bodo, B. (1999). Pohlianins A, B and C, cyclic peptides from the laxes of Jatropha pohliana ssp. molissima. *Tetrahedron, 55*(38), 11495-11510.

Bai, X., Wang, Y., Song, Z., Feng, Y., Chen, Y., Zhang, D., & Feng, L. (2020). The basic properties of gold nanoparticles and their applications in tumor diagnosis and treatment. *International journal of molecular sciences, 21*(7), 2480.

Baraguey, C., Auvin-Guette, C., Blond, A., Cavelier, F., Lezenven, F., Pousset, J.-L., & Bodo, B. (1998). Isolation, structure and synthesis of chevalierins A, B and C, cyclic peptides from the latex of Jatropha chevalieri. *Journal of the Chemical Society, Perkin Transactions 1*(18), 3033-3040.

Baraguey, C., Blond, A., Cavelier, F., Pousset, J.-L., Bodo, B., & Auvin-Guette, C. (2001). Isolation, structure and synthesis of mahafacyclin B, a cyclic heptapeptide from the latex of Jatropha mahafalensis. *Journal of the Chemical Society, Perkin Transactions 1*(17), 2098-2103.

Bérubé, C., Gagnon, D., Borgia, A., Richard, D., & Voyer, N. (2019). Total synthesis and antimalarial activity of mortiamides A–D. *Chemical Communications, 55*(52), 7434-7437.

Bisht, R., Katiyar, A., Singh, R., & Mittal, P. (2009). Antibiotic resistance-A global issue of concern. *Asian journal of pharmaceutical and clinical research, 2*(2), 34-39.

Bürstner, N., Roggo, S., Ostermann, N., Blank, J., Delmas, C., Freuler, F., . . . Liechty, B. (2015). Gift from nature: Cyclomarin A kills mycobacteria and

malaria parasites by distinct modes of action. *ChemBioChem, 16*(17), 2433-2436.

Camci, M. T., Ulgut, B., Kocabas, C., & Suzer, S. (2017). In-situ XPS monitoring and characterization of electrochemically prepared Au nanoparticles in an ionic liquid. *ACS omega, 2*(2), 478-486.

Castner, D. G., Hinds, K., & Grainger, D. W. (1996). X-ray photoelectron spectroscopy sulfur 2p study of organic thiol and disulfide binding interactions with gold surfaces. *Langmuir, 12*(21), 5083-5086.

Chen, Q., Zhang, L., Feng, Y., Shi, F., Wang, Y., Wang, P., & Liu, L. (2018). Dual-functional peptide conjugated gold nanorods for the detection and photothermal ablation of pathogenic bacteria. *Journal of Materials Chemistry B, 6*(46), 7643-7651.

Chen, W.-H., Luo, G.-F., Xu, X.-D., Jia, H.-Z., Lei, Q., Han, K., & Zhang, X.-Z. (2014). Cancer-targeted functional gold nanoparticles for apoptosis induction and real-time imaging based on FRET. *Nanoscale, 6*(16), 9531-9535.

Chung, P. Y., & Khanum, R. (2017). Antimicrobial peptides as potential anti-biofilm agents against multidrug-resistant bacteria. *Journal of microbiology, immunology and infection, 50*(4), 405-410.

Desjardins, R. E., Canfield, C., Haynes, J., & Chulay, J. (1979). Quantitative assessment of antimalarial activity in vitro by a semiautomated microdilution technique. *Antimicrobial agents and chemotherapy, 16*(6), 710-718.

Desselberger, U. (2000). Emerging and re-emerging infectious diseases. *Journal of Infection, 40*(1), 3-15.

Egorova, E. A., van Rijt, M. M., Sommerdijk, N., Gooris, G. S., Bouwstra, J. A., Boyle, A. L., & Kros, A. (2020). One peptide for them all: gold nanoparticles of different sizes are stabilized by a common peptide amphiphile. *ACS nano, 14*(5), 5874-5886.

El-Faham, A., & Albericio, F. (2011). Peptide coupling reagents, more than a letter soup. *Chemical reviews, 111*(11), 6557-6602.

Formaggio, D. M., Magalhães, J. A., Andrade, V. M., Conceição, K., Anastácio, J. M., Santiago, G. S., . . . Tada, D. B. (2022). Co-Functionalization of gold

nanoparticles with C7H2 and HuAL1 peptides: enhanced antimicrobial and antitumoral activities. *Pharmaceutics, 14*(7), 1324.

Grunwald, A. L., Berrue, F., Robertson, A. W., Overy, D. P., & Kerr, R. G. (2017). Mortiamides A–D, cyclic heptapeptides from a novel Mortierella sp. obtained from Frobisher Bay. *Journal of natural products, 80*(10), 2677-2683.

Hill, R. R., Birch, D., Jeffs, G. E., & North, M. (2003). Enantioselection in peptide bond formation. *Organic & biomolecular chemistry, 1*(6), 965-972.

Holmberg, S. D., Solomon, S. L., & Blake, P. A. (1987). Health and economic impacts of antimicrobial resistance. *Reviews of infectious diseases, 9*(6), 1065-1078.

Hsueh, P.-R., Ko, W.-C., Wu, J.-J., Lu, J.-J., Wang, F.-D., Wu, H.-Y., . . . Teng, L.-J. (2010). Consensus statement on the adherence to Clinical and Laboratory Standards Institute (CLSI) Antimicrobial Susceptibility Testing Guidelines (CLSI-2010 and CLSI-2010-update) for Enterobacteriaceae in clinical microbiology laboratories in Taiwan. *Journal of Microbiology, Immunology and Infection, 43*(5), 452-455.

Huan, Y., Kong, Q., Mou, H., & Yi, H. (2020). Antimicrobial peptides: classification, design, application and research progress in multiple fields. Front Microbiol 11: 582779. In: Epub 2020/11/13.

Jaturapat, A., Isaka, M., Hywel-Jones, N. L., Lertwerawat, Y., Kamchonwongpaisan, S., Kirtikara, K., . . . Thebtaranonth, Y. (2001). Bioxanthracenes from the insect pathogenic fungus Cordyceps pseudomilitaris BCC 1620 I. Taxonomy, fermentation, isolation and antimalarial activity. *The Journal of Antibiotics, 54*(1), 29-35.

Jeong, H. (2017). *Programmable chiral nanocolloids*. Retrieved from

Jia, W., Weng, J., Zhu, D., Ji, L., Lu, J., Zhou, Z., . . . Chen, L. (2019). Standards of medical care for type 2 diabetes in China 2019. *Diabetes/metabolism research and reviews, 35*(6), e3158.

Kalmodia, S., Parameswaran, S., Ganapathy, K., Yang, W., Barrow, C. J., Kanwar, J. R., . . . Elchuri, S. V. (2017). Characterization and molecular mechanism of peptide-conjugated gold nanoparticle inhibiting p53-HDM2 interaction in retinoblastoma. *Molecular Therapy-Nucleic Acids, 9*, 349-364.

Lawer, A., Tai, J., Jolliffe, K. A., Fletcher, S., Avery, V. M., & Hunter, L. (2014). Total synthesis and antiplasmodial activity of pohlianin C and analogues. *Bioorganic & Medicinal Chemistry Letters*, *24*(12), 2645-2647.

Lévy, R., Thanh, N. T., Doty, R. C., Hussain, I., Nichols, R. J., Schiffrin, D. J., . . . Fernig, D. G. (2004). Rational and combinatorial design of peptide capping ligands for gold nanoparticles. *Journal of the American Chemical Society, 126*(32), 10076-10084.

Limón, D., Vilà, S., Herrera-Olivas, A., Vera, R., Badia, J., Baldomà, L., . . . Pérez-García, L. (2021). Enhanced cytotoxicity of highly water-soluble gold nanoparticle-cyclopeptide conjugates in cancer cells. *Colloids and Surfaces B: Biointerfaces, 197*, 111384.

Luo, H., Yin, H., Tang, C., Wang, P., & Liang, F. (2018). Synthesis of cyclic peptide reniochalistatin E and conformational isomers. *Chinese Chemical Letters, 29*(7), 1143-1146.

Marti-Centelles, V., Pandey, M. D., Burguete, M. I., & Luis, S. V. (2015). Macrocyclization reactions: The importance of conformational, configurational, and template-induced preorganization. *Chemical reviews, 115*(16), 8736-8834.

Micsonai, A., Wien, F., Kernya, L., Lee, Y.-H., Goto, Y., Réfrégiers, M., & Kardos, J. (2015). Accurate secondary structure prediction and fold recognition for circular dichroism spectroscopy. *Proceedings of the National Academy of Sciences, 112*(24), E3095-E3103.

Mishra, B. K., Deshmukh, M. M., & Venkatnarayan, R. (2014). C–H$\cdots$ π interactions and the nature of the donor carbon atom. *The Journal of Organic Chemistry, 79*(18), 8599-8606.

Mookherjee, N., Anderson, M. A., Haagsman, H. P., & Davidson, D. J. (2020). Antimicrobial host defence peptides: functions and clinical potential. *Nature reviews Drug discovery, 19*(5), 311-332.

Mwangi, J., Hao, X., Lai, R., & Zhang, Z.-Y. (2019). Antimicrobial peptides: new hope in the war against multidrug resistance. *Zoological research, 40*(6), 488.

Pal, I., Brahmkhatri, V. P., Bera, S., Bhattacharyya, D., Quirishi, Y., Bhunia, A., & Atreya, H. S. (2016). Enhanced stability and activity of an antimicrobial

peptide in conjugation with silver nanoparticle. *Journal of colloid and interface science*, *483*, 385-393.

Pandey, A. K., Thomas, K. M., Forbes, C. R., & Zondlo, N. J. (2014). Tunable control of polyproline helix (PPII) structure via aromatic electronic effects: an electronic switch of polyproline helix. *Biochemistry*, *53*(32), 5307-5314.

Pfalzgraff, A., Brandenburg, K., & Weindl, G. (2018). Antimicrobial peptides and their therapeutic potential for bacterial skin infections and wounds. *Frontiers in pharmacology*, *9*, 281.

Pinto, M. E. F., Batista Jr, J. M., Koehbach, J., Gaur, P., Sharma, A., Nakabashi, M., . . . Gruber, C. W. (2015). Ribifolin, an orbitide from Jatropha ribifolia, and its potential antimalarial activity. *Journal of natural products*, *78*(3), 374-380.

Renner, M. K., Shen, Y.-C., Cheng, X.-C., Jensen, P. R., Frankmoelle, W., Kauffman, C. A., . . . Clardy, J. (1999). Cyclomarins A− C, new antiinflammatory cyclic peptides produced by a marine bacterium (Streptomyces sp.). *Journal of the American Chemical Society*, *121*(49), 11273-11276.

Roudi, R., Syn, N. L., & Roudbary, M. (2017). Antimicrobial peptides as biologic and immunotherapeutic agents against cancer: a comprehensive overview. *Frontiers in immunology*, *8*, 1320.

Rukachaisirikul, V., Chantaruk, S., Tansakul, C., Saithong, S., Chaicharernwimonkoon, L., Pakawatchai, C., . . . Intereya, K. (2006). A cyclopeptide from the insect pathogenic fungus Cordyceps sp. BCC 1788. *Journal of natural products*, *69*(2), 305-307.

Sahile, H. A., Martínez-Martínez, M. S., Dillenberger, M., Becker, K., & Imming, P. (2020). Synthesis and evaluation of antimycobacterial and antiplasmodial activities of hirsutellide A and its analogues. *ACS omega*, *5*(24), 14451-14460.

Saur, J. S., Wirtz, S. N., Schilling, N. A., Krismer, B., Peschel, A., & Grond, S. (2021). Distinct Lugdunins from a New Efficient Synthesis and Broad Exploitation of Its MRSA-Antimicrobial Structure. *Journal of Medicinal Chemistry*, *64*(7), 4034-4058.

Schilling, N. A., Berscheid, A., Schumacher, J., Saur, J. S., Konnerth, M. C., Wirtz, S. N., . . . Peschel, A. (2019). Synthetic lugdunin analogues reveal essential

structural motifs for antimicrobial action and proton translocation capability. *Angewandte Chemie International Edition, 58*(27), 9234-9238.

Stawikowski, M., & Fields, G. B. (2012). Introduction to peptide synthesis. *Current protocols in protein science, 69*(1), 18.11. 11-18.11. 13.

Su, K.-H., Wei, Q.-H., Zhang, X., Mock, J., Smith, D. R., & Schultz, S. (2003). Interparticle coupling effects on plasmon resonances of nanogold particles. *Nano letters, 3*(8), 1087-1090.

Tang, M., Zhang, J., Yang, C., Zheng, Y., & Jiang, H. (2020). Gold nanoclusters for bacterial detection and infection therapy. *Frontiers in Chemistry, 8*, 181.

Tao, W., Ziemer, K. S., & Gill, H. S. (2014). Gold nanoparticle–M2e conjugate coformulated with CpG induces protective immunity against influenza A virus. *Nanomedicine, 9*(2), 237-251.

Thongtan, J., Saenboonrueng, J., Rachtawee, P., & Isaka, M. (2006). An antimalarial tetrapeptide from the entomopathogenic fungus Hirsutella sp. BCC 1528. *Journal of natural products, 69*(4), 713-714.

Tkachenko, A., Xie, H., Franzen, S., & Feldheim, D. L. (2005). Assembly and characterization of biomolecule-gold nanoparticle conjugates and their use in intracellular imaging. *Nanobiotechnology protocols*, 85-99.

Tkachenko, A. G., Xie, H., Liu, Y., Coleman, D., Ryan, J., Glomm, W. R., . . . Feldheim, D. L. (2004). Cellular trajectories of peptide-modified gold particle complexes: comparison of nuclear localization signals and peptide transduction domains. *Bioconjugate chemistry, 15*(3), 482-490.

Trager, W., & Jensen, J. B. (1976). Human malaria parasites in continuous culture. *Science, 193*(4254), 673-675.

Tran, N. T. T., Wang, T.-H., Lin, C.-Y., Tsai, Y.-C., Lai, C.-H., Tai, Y., & Yung, B., YM. (2011). Direct synthesis of rev peptide-conjugated gold nanoparticles and their application in cancer therapeutics. *Bioconjugate Chemistry, 22*(7), 1394-1401.

Tremblay, T., Bergeron, C., Gagnon, D., Bérubé, C., Voyer, N., Richard, D., & Giguère, D. (2023). Squaramide Tethered Clindamycin, Chloroquine, and Mortiamide Hybrids: Design, Synthesis, and Antimalarial Activity. *ACS Medicinal Chemistry Letters, 14*(2), 217-222.

Tsutsumi, H., Ohkusa, H., Park, H., Takahashi, T., Yuasa, H., & Mihara, H. (2012). Gold nanoparticles conjugated with monosaccharide-modified peptide for lectin detection. *Bioorganic & medicinal chemistry letters, 22*(22), 6825-6827.

Turkevich, J., Stevenson, P. C., & Hillier, J. (1951). A study of the nucleation and growth processes in the synthesis of colloidal gold. *Discussions of the Faraday Society, 11*, 55-75.

Ventola, C. L. (2015). The antibiotic resistance crisis: part 1: causes and threats. *Pharmacy and therapeutics, 40*(4), 277.

Verma, A., Uzun, O., Hu, Y., Hu, Y., Han, H.-S., Watson, N., . . . Stellacci, F. (2008). Surface-structure-regulated cell-membrane penetration by monolayer-protected nanoparticles. *Nature materials, 7*(7), 588-595.

Vongvanich, N., Kittakoop, P., Isaka, M., Trakulnaleamsai, S., Vimuttipong, S., Tanticharoen, M., & Thebtaranonth, Y. (2002). Hirsutellide a, a new antimycobacterial cyclohexadepsipeptide from the entomopathogenic fungus hirsutella k obayasii. *Journal of natural products, 65*(9), 1346-1348.

Zipperer, A., Konnerth, M. C., Laux, C., Berscheid, A., Janek, D., Weidenmaier, C., . . . Marschal, M. (2016). Human commensals producing a novel antibiotic impair pathogen colonization. *Nature, 535*(7613), 511-516.

Zong, J., Cobb, S. L., & Cameron, N. R. (2017). Peptide-functionalized gold nanoparticles: versatile biomaterials for diagnostic and therapeutic applications. *Biomaterials science, 5*(5), 872-886.

APPENDICES

APPENDIX A

High performance liquid chromatography condition

Table A1

The conditions of high performance liquid chromatography

	Method 1	Method 2
Column	Finepak SIL C18T-5, 5 μm, C18, 300 °A column (4.6 mm. × 250 mm)	COSMOSIL 5C4-AR-300 5 μm, C4, 300 °A column (4.6 mm. × 150 mm)
Injection volume	10 μL	10 mL
Flow rate	1.0 mL/min	3 mL
Run time	45 min	90 min
Gradient	10%-100% B in 35 min	30%-100% B in 65 min
Mobile phase	A : 0.01% formic acid in H_2O B : 0.01% formic acid in ACN	A : 0.01% formic acid in H_2O B : 0.01% formic acid in MeOH
Detection	UV 220 and 280 nm	UV 215 and 280 nm
Instrument	PU-4180, Jasco UV-4070 UV/Vis detector	PU-4086-Binary pump, Jasco UV-4075 UV/Vis detector

APPENDIX B

Nuclear magnetic resonance spectrum

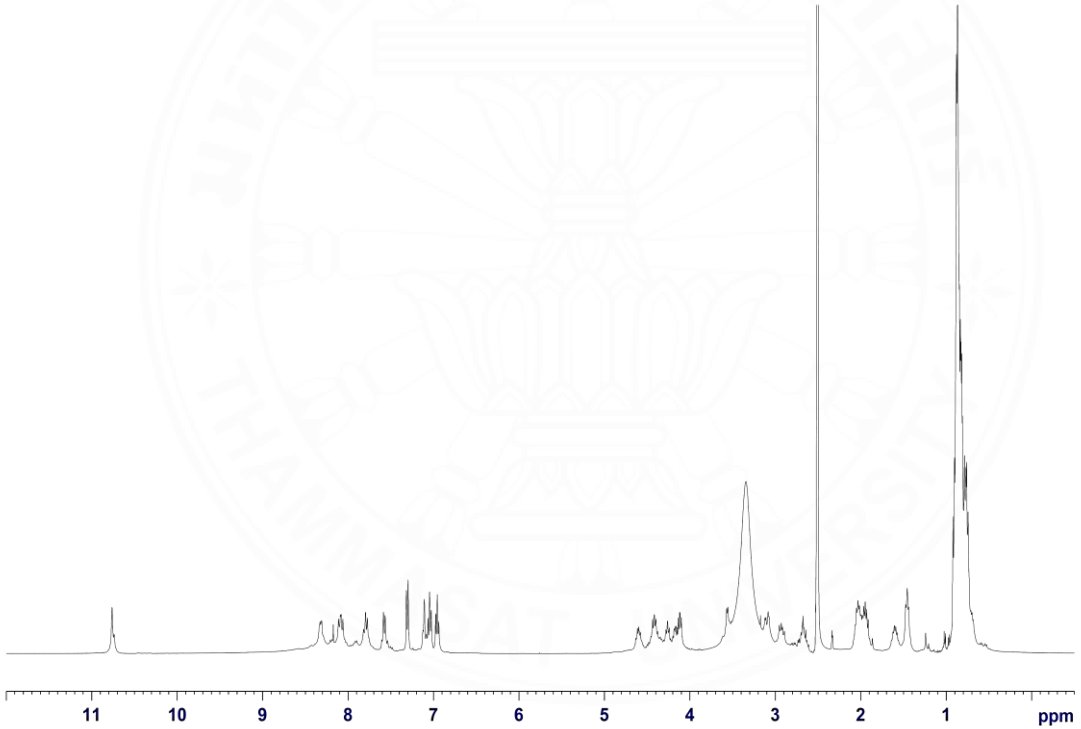

Figure B1 ^{1}H-NMR spectrum of linear thiol-incorporated (**1** and **2)** in DMSO-d_6

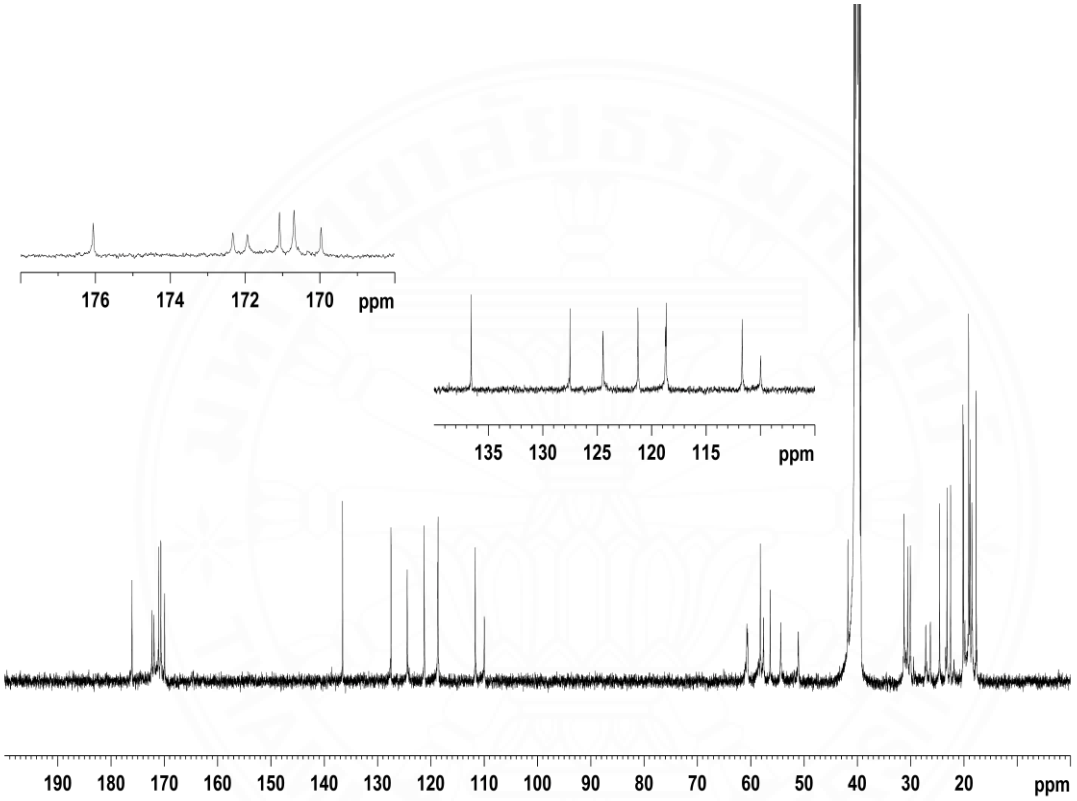

Figure B2 ^{13}C-NMR spectrum of linear thiol-incorporated (**1** and **2)** in DMSO-d_6

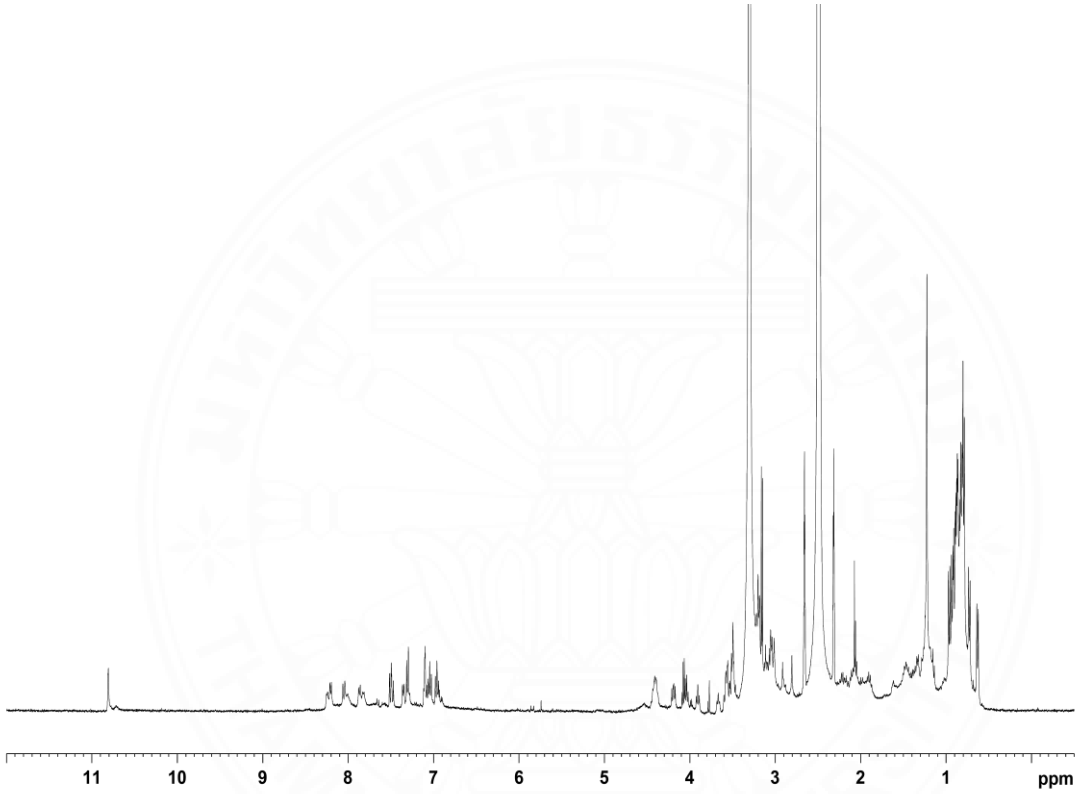

Figure B3 ^{1}H-NMR spectrum of cyclic thiol-incorporated (**3** and **4)** in DMSO-d_6

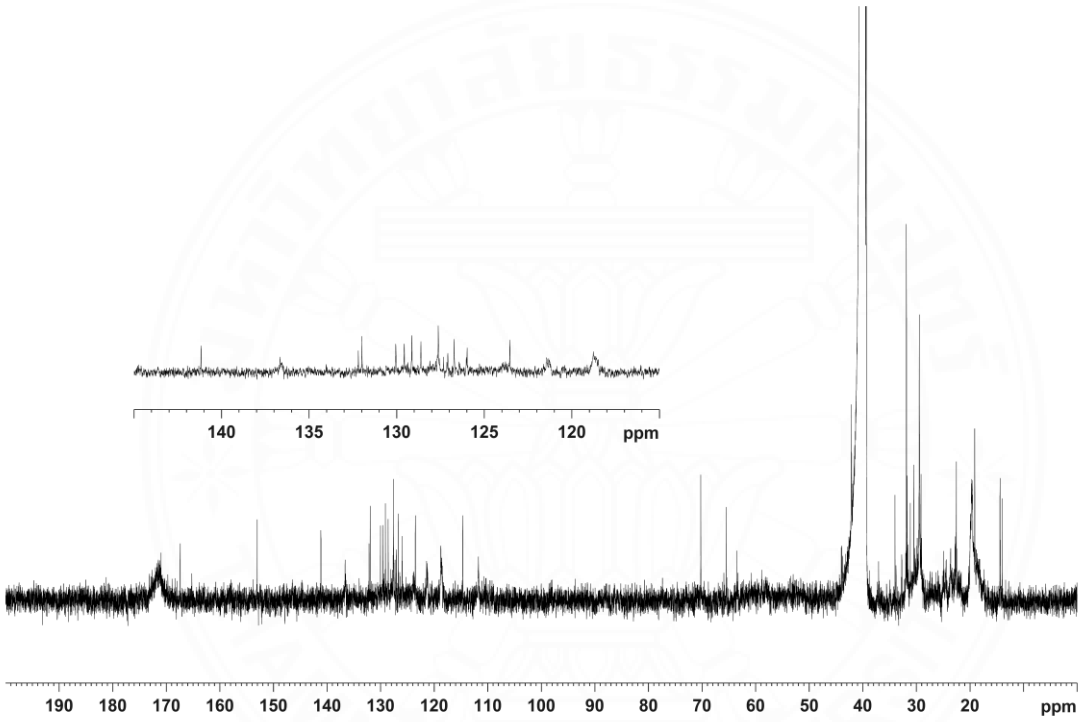

Figure B4 ^{13}C-NMR spectrum of cyclic thiol-incorporated (**3** and **4)** in DMSO-d_6

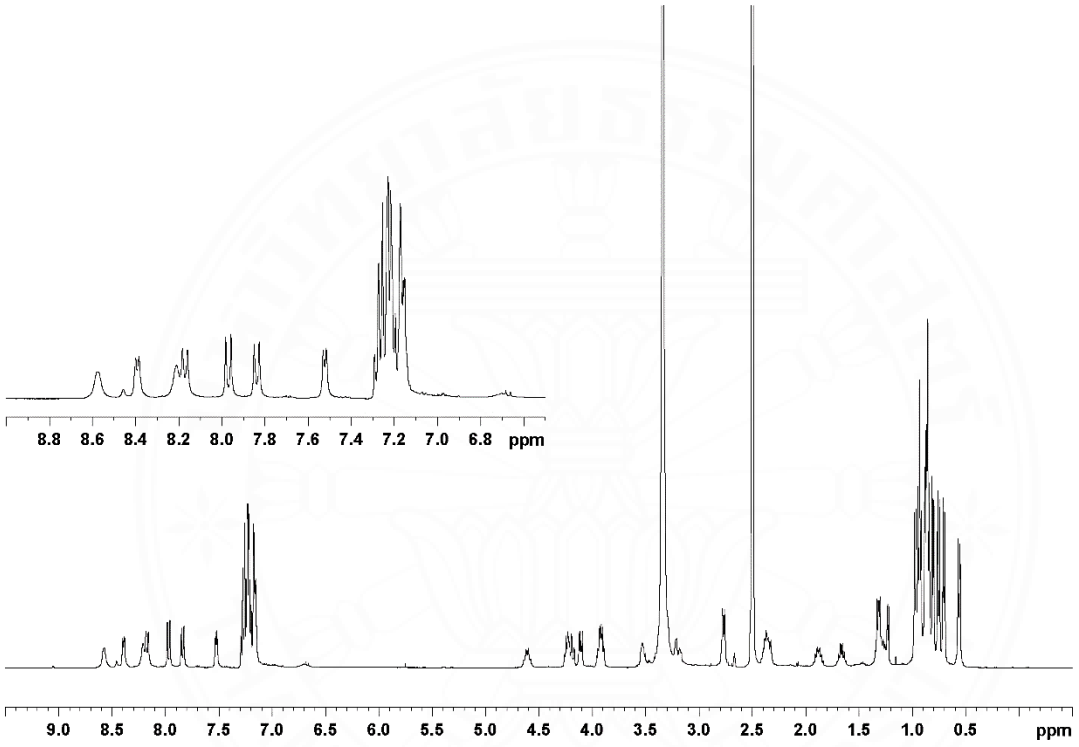

Figure B6 ^{1}H-NMR spectrum of linear re-engineered mortiamide (**9** and **10)** in DMSO-d_6

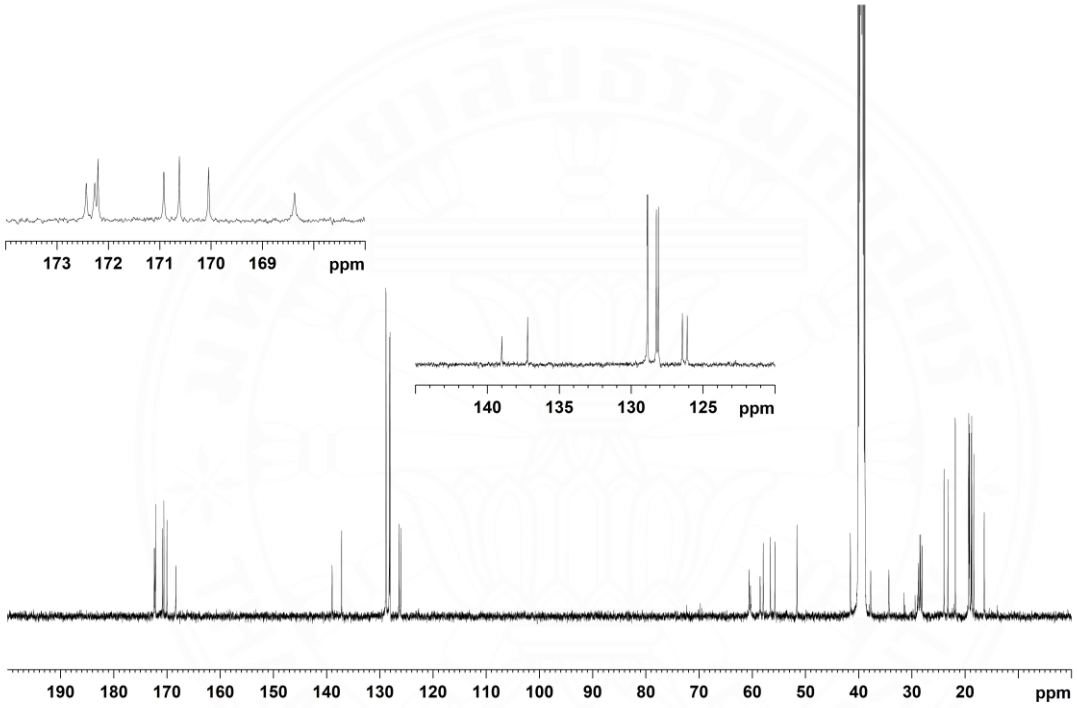

Figure B7 ^{13}C-NMR spectrum of linear re-engineered mortiamide (**10)** in DMSO-d_6

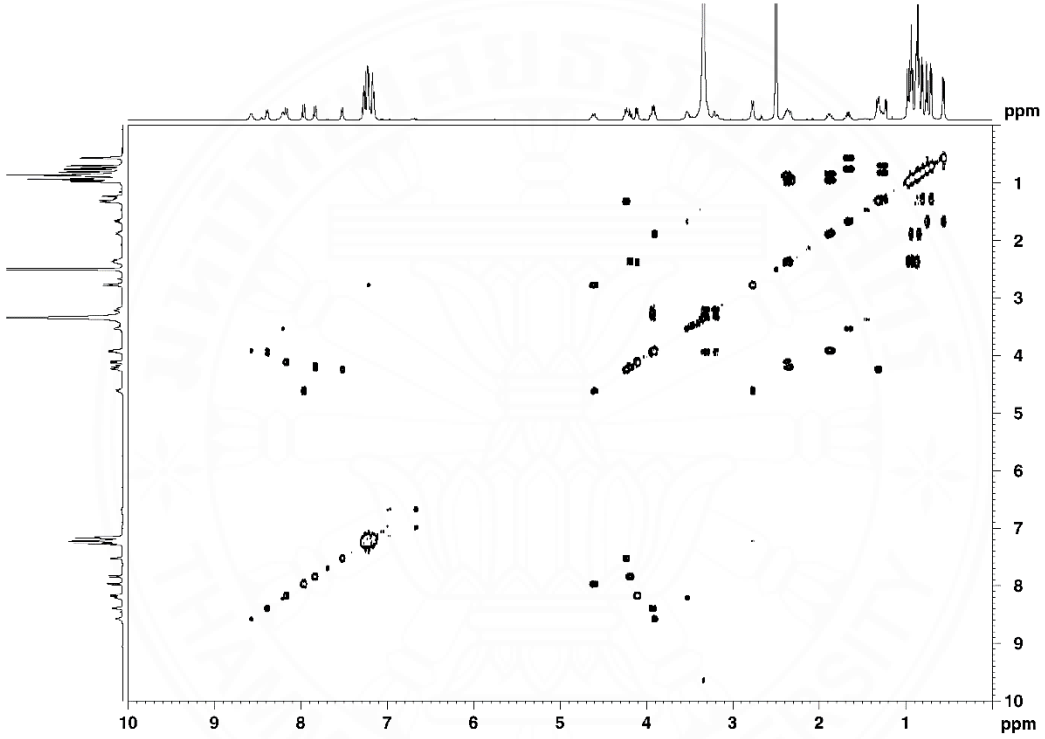

Figure B8 ^{1}H-^{1}H COSY spectrum of linear re-engineered mortiamide (**10)** in DMSO-d_6

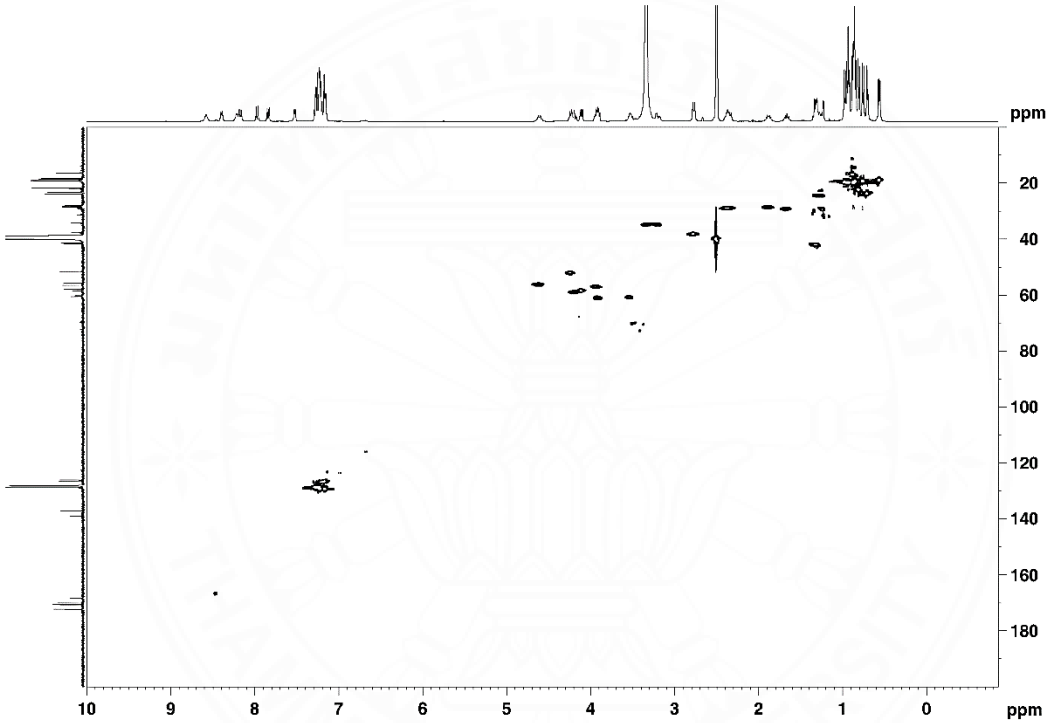

Figure B9 HSQC spectrum of linear re-engineered mortiamide (**10)** in DMSO-d_6

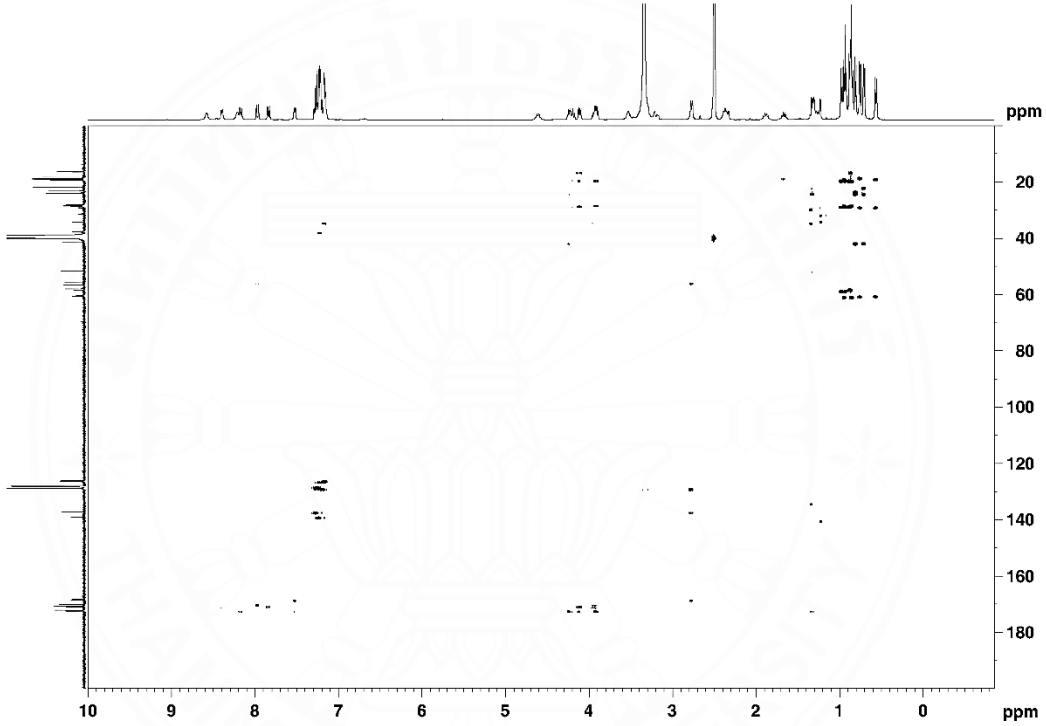

Figure B10 HMBC spectrum of linear re-engineered mortiamide (**10)** in DMSO-d_6

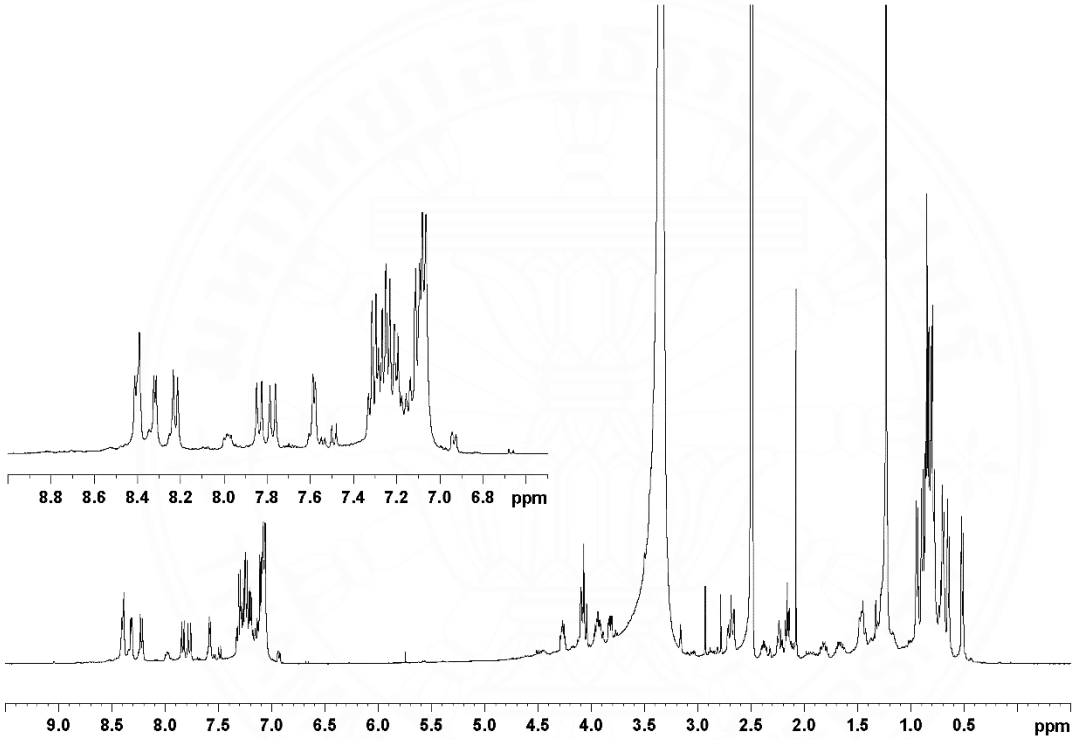

Figure B11 ^{1}H-NMR spectrum of cyclic re-engineered mortiamide (**12)** in DMSO-d_6

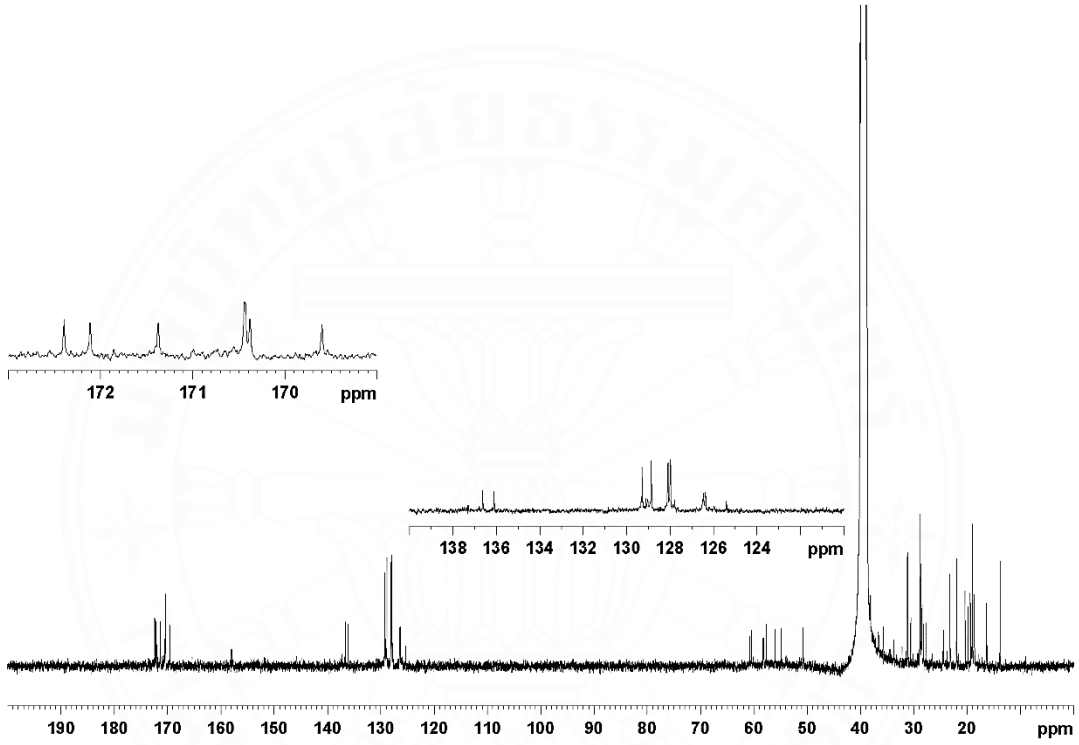

Figure B12 ^{13}C-NMR spectrum of cyclic re-engineered mortiamide (**12)** in DMSO-d_6

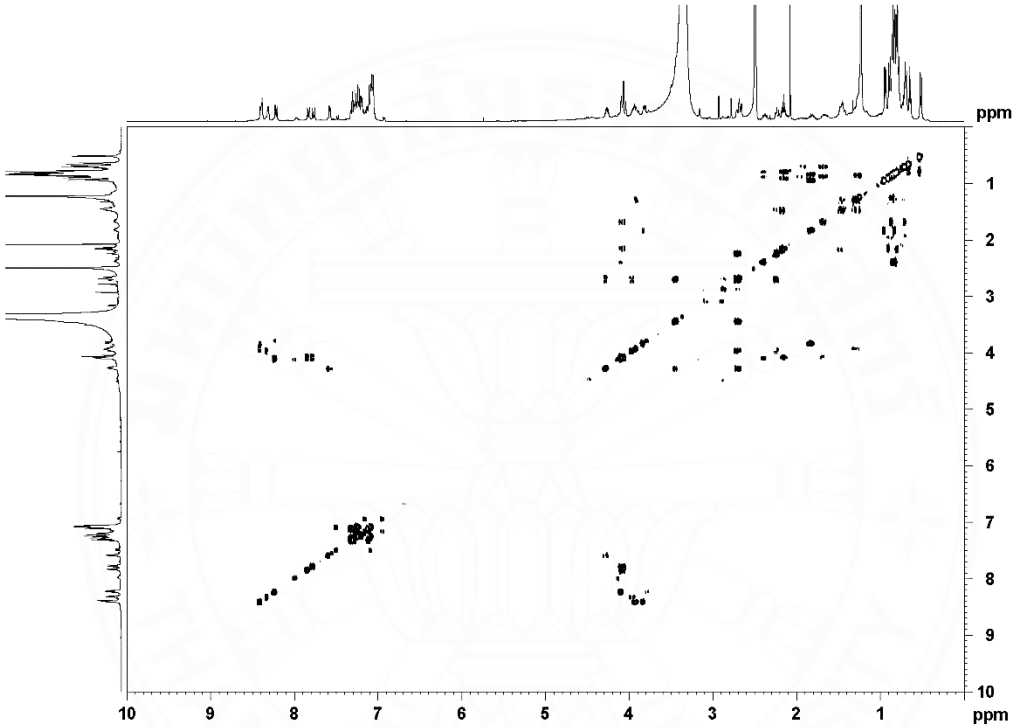

Figure B13 ^{1}H-^{1}H COSY spectrum of cyclic re-engineered mortiamide (**12)** in DMSO-d_6

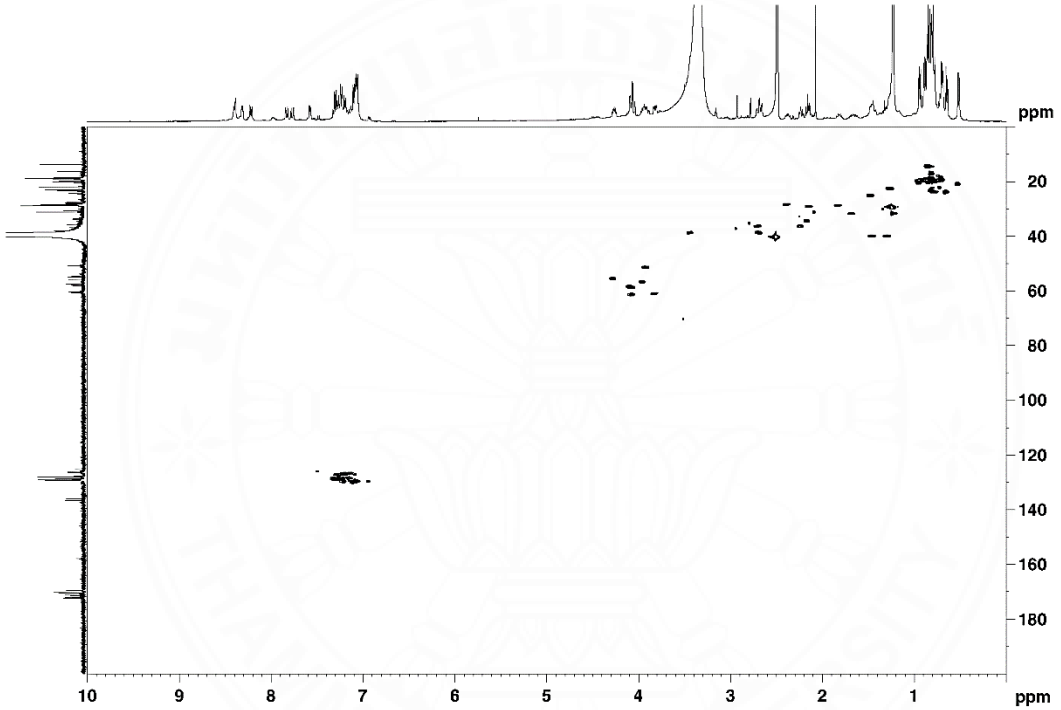

Figure B14 HSQC spectrum of cyclic re-engineered mortiamide (**12)** in DMSO-d_6

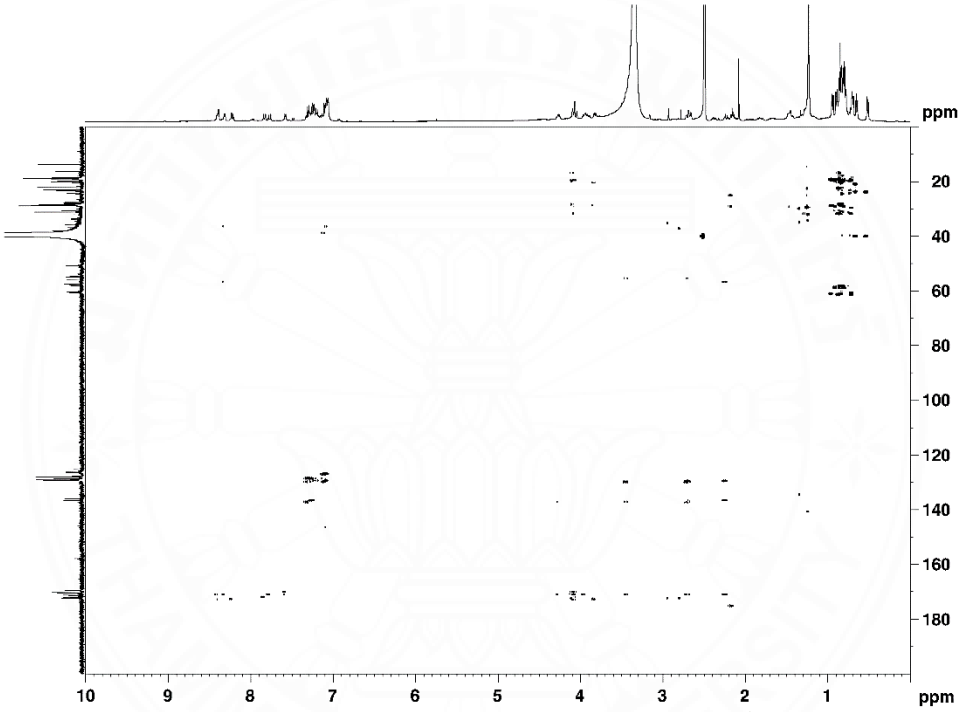

Figure B15 HMBC spectrum of cyclic re-engineered mortiamide (**12)** in DMSO-d_6

APPENDIX C

Mass spectrum

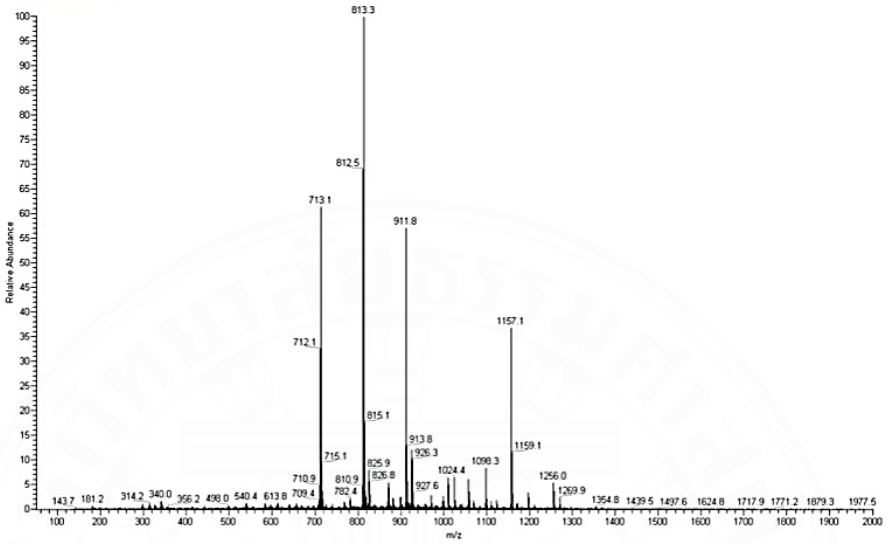

Figure C1 Negative mode mass spectrum of H-Val-Leu-Trp(Boc)-Val-Cys(Trt)-Val-Val-OH Found 1157.1 $[M+H]^-$ Calculated 1158.62 $[M]^+$

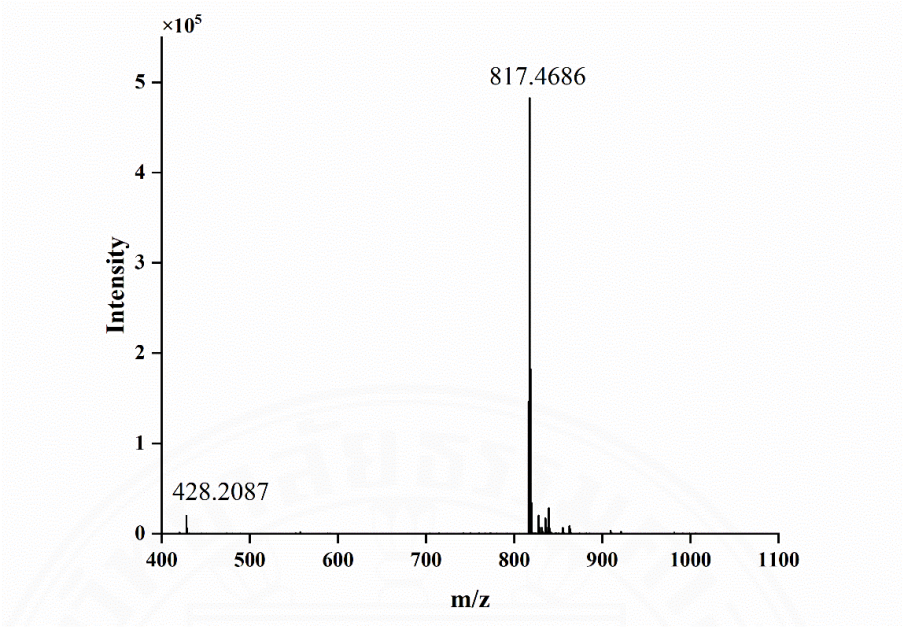

Figure C2 Positive mode mass spectrum of linear thiol-incorporated peptides **(1** and **2**) Found 428.2087 $[M+Na+H]^{2+}$ and 817.4686 $[M+H]^{+}$; Calculated 816.46 $[M]^{+}$

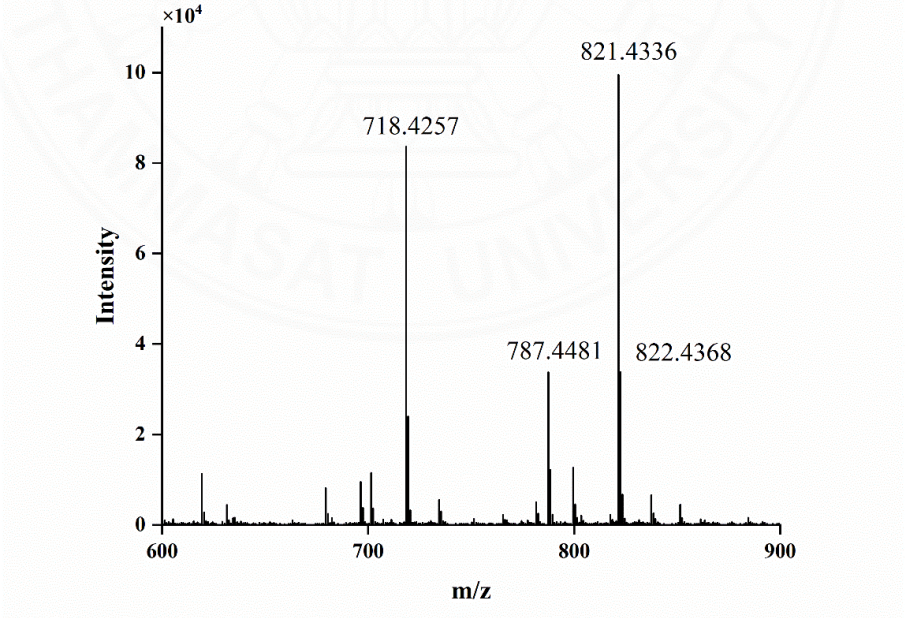

Figure C3 Positive mode mass spectrum of cyclic thiol-incorporated peptides (**3** and **4**) Found 821.4336 $[M+Na]^{+}$; Calculated 798.45 $[M]^{+}$

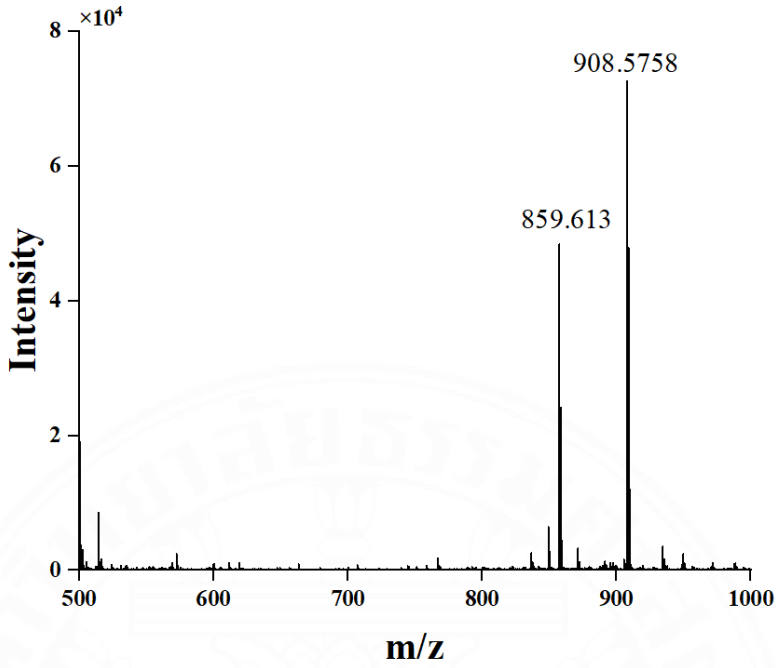

Figure C4 Positive mode mass spectrum of linear re-engineered mortiamide peptides (**9** and **10**) Found 908.5758 $[M+Na]^+$; Calculated 821.51 $[M]^+$

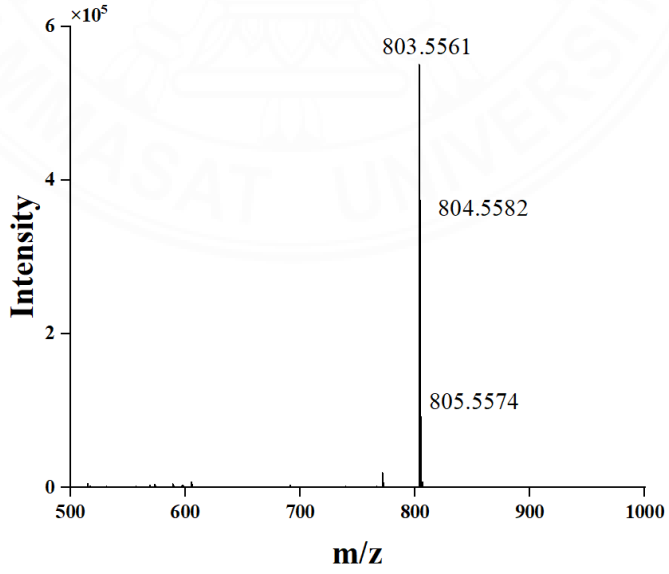

Figure C5 Positive mode mass spectrum of cyclic re-engineered mortiamide peptides (**11** and **12**) Found 804.5582 $[M+H]^+$; Calculated 803.49 $[M]^+$

APPENDIX D

High performance liquid chromatography chrmatogram

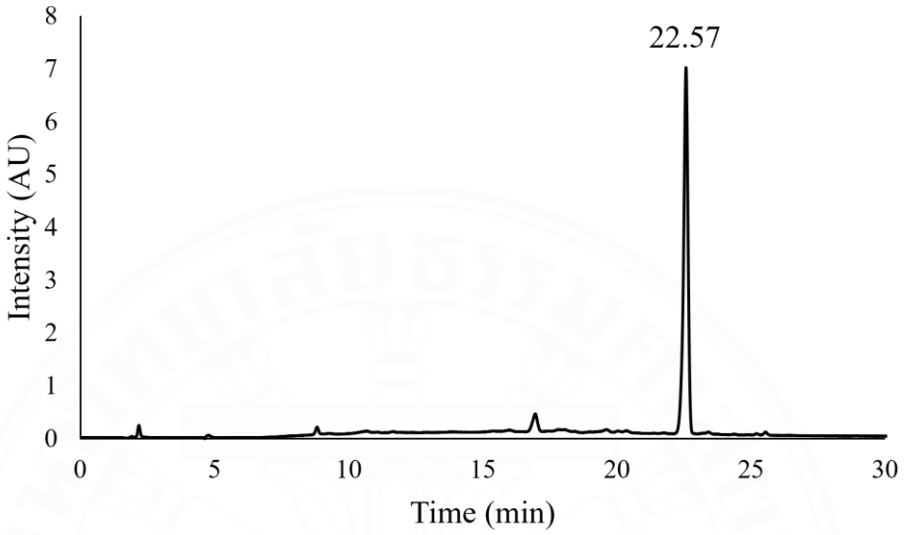

Figure D1 HPLC chromatogram of H-Val-Leu-Trp(Boc)-Val-Cys(Trt)-Val-Val-OH

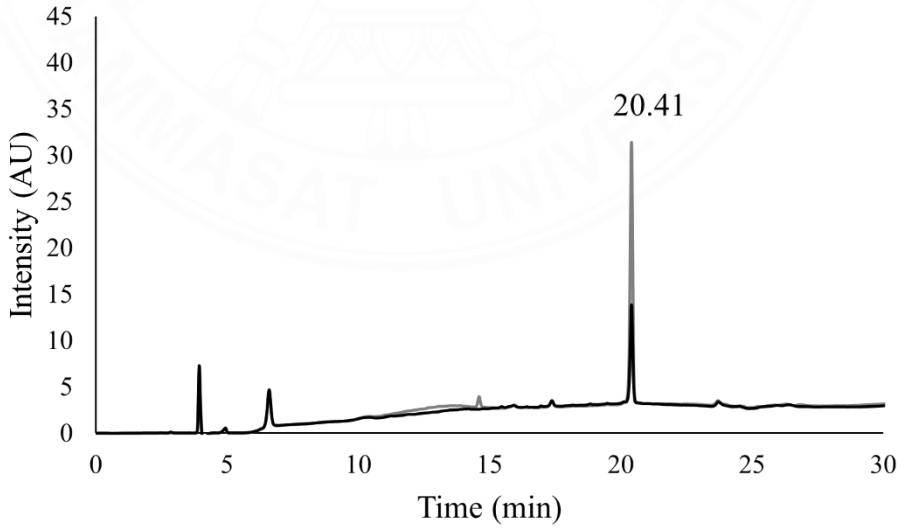

Figure D2 HPLC chromatogram of linear thiol-incorporated peptides (**1**) (black) and (**2**) (grey)

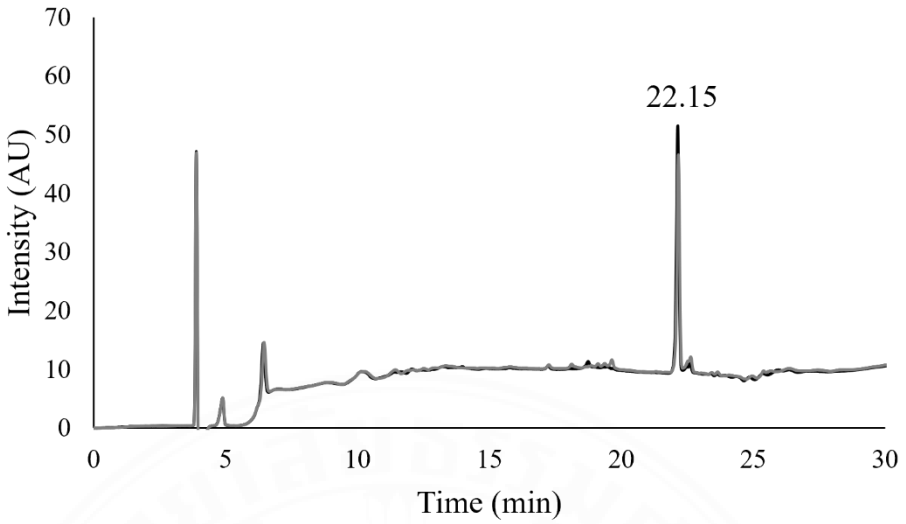

Figure D3 HPLC chromatogram of cyclic thiol-incorporated peptides **(1)** (black) and (**2**) (grey)

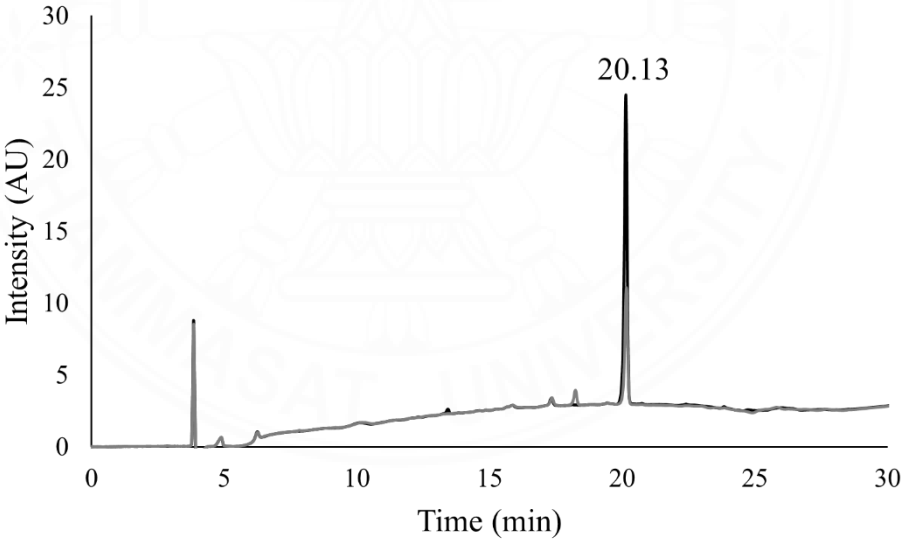

Figure D4 HPLC chromatogram of linear re-engineered mortiamide peptides (**9**) (black) and (**10**) (grey)

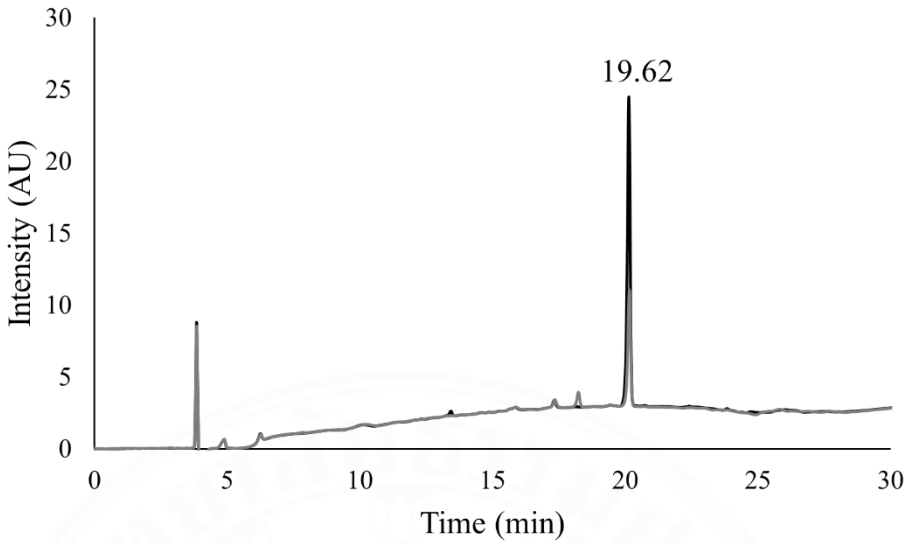

Figure D5 HPLC chromatogram of cyclic re-engineered mortiamide peptides (**11**) (black) and (**12**) (grey)

BIOGRAPHY

Name	Nattamon Trirattanaporn
Educational Attainment	2015-2019: Degree of Bachelor of Science in Chemistry, Thammasat University
Scholarship	2019-2023: The talent student to study graduate program in Faculty of Science and Technology Thammasat University, Contract No. TB 21/2019
Publications	2023: The 12th Rajamangala University of Technology International Conference (RMUT 2023)
Conference	2020: Pure and Applied Chemistry International Conference 2020 (PACCON 2020) 2022: Pure and Applied Chemistry International Conference 2022 (PACCON 2022) 2023: The 12th Rajamangala University of Technology International Conference (RMUT 2023)